

5-9-2016

Applications of nanoporous gold monoliths as substrates for the capture and release of lectins and glycoproteins

Allan Jonson Alla

University of Missouri-St. Louis, ajakd7@mail.umsl.edu

Follow this and additional works at: <https://irl.umsl.edu/dissertation>



Part of the [Chemistry Commons](#)

Recommended Citation

Alla, Allan Jonson, "Applications of nanoporous gold monoliths as substrates for the capture and release of lectins and glycoproteins" (2016). *Dissertations*. 114.

<https://irl.umsl.edu/dissertation/114>

This Dissertation is brought to you for free and open access by the UMSL Graduate Works at IRL @ UMSL. It has been accepted for inclusion in Dissertations by an authorized administrator of IRL @ UMSL. For more information, please contact marvinh@umsl.edu.

Applications of nanoporous gold monoliths as substrates for the capture and
release of lectins and glycoproteins

by

Allan J. Alla

M.S. Chemistry - Graduate, University of Missouri-St. Louis, 2014
B.S. Chemical Engineering - Undergraduate,
University of the Philippines-Los Baños, 2007

A Dissertation

Submitted to the Graduate School of the

University of Missouri-St. Louis
in partial fulfillment of the requirements for the degree

Doctor of Philosophy in Chemistry

May 2016

Advisory Committee

Chair and Advisor: Keith J. Stine, Ph.D.
Alexei V. Demchenko, Ph.D.
Michael R. Nichols, Ph.D.
Chung F. Wong, Ph.D.

ABSTRACT

Applications of nanoporous gold monoliths as substrates for the capture and release of lectins and glycoproteins

May 2016

Allan J. Alla, MS, University of Missouri-St. Louis, MO, USA

Chair and Advisor: Prof. Keith J. Stine

Nanoporous gold (np-Au) monoliths are a free-standing nanostructured material with typical pore dimensions in the tens of nanometers range. The microstructure of np-Au resembles those of macroporous monolithic materials being used in chromatographic separations. The surfaces of np-Au monoliths were modified via flow methods with different ligands to develop affinity substrates for separations. A carbohydrate-modified np-Au monolith was prepared by immobilizing thiolated saccharides and further used to separate lectins. The np-Au monolith surface was also functionalized with self-assembled monolayers (SAMs) of α -lipoic acid (LA) followed by activation of carboxyl terminal groups to create amine reactive esters. Concanavalin A (Con A) was then covalently immobilized to develop a substrate for extraction of glycoprotein from a mixture. Likewise, aminophenylboronic acid was immobilized to develop a substrate that was tested for pH-dependent capture and release of *cis-diol* containing molecules. Preservation of SAMs and immobilized ligands were possibly due to the in situ surface modification of np-Au monoliths that limited the possible damage and degradation of molecules on the surface.

Selectivity of the developed substrates was enhanced by capping the unreacted functional groups or by incorporation of protein resistant spacers to limit the non-specific adsorption of unwanted molecules. The loading and surface coverage of molecules on np-Au monolith surface were determined by thermogravimetric analysis (TGA) and by an in situ solution depletion method. TGA was able to quantify the amount of loading based from the mass loss after the pyrolysis of modified np-Au monoliths. The in situ solution depletion method estimates the amount of loading by the difference in the initial and final concentration of a circulating solution monitored by a UV detector.

This research aims to introduce np-Au monolith as an addition to the materials being used as substrates in chromatographic separation and extraction. The chemical stability, simple but reproducible preparation, high surface-to-volume ratio and availability of wide variety of Au surface functionalization are the features of np-Au monolith that could complement the limitations of the existing materials used in separations. The focus of this research is on the separation of lectins and glycoproteins, which is an important step towards an effective glycan analysis in glycomics.

DEDICATION

TO MY FAMILY

ACKNOWLEDGEMENTS

I would like to thank my research advisor Prof. Keith J. Stine for allowing me to work in his laboratory, providing all my needs in doing my research and with all his support. I appreciate the opportunities he provided that help me to improve my research skills. I will be forever grateful to the University of Missouri-St. Louis (UMSL) Department of Chemistry and Biochemistry for giving me this education and for the teaching and research experiences. I would also like to thank the members of the dissertation committee Prof. Alexei V. Demchenko, Prof. Michael R. Nichols and Prof. Chung F. Wong for the time and support they gave during my graduate study. To them and to all other professors in UMSL Department of Chemistry and Biochemistry for sharing their knowledge.

I am also grateful to UMSL Center for Nanoscience especially to Dr. David Osborn for assisting me in using the instruments. I would also like to thank the people who I worked with in the Prof. Stine laboratory – Dr. Jay K. Bhattarai, Dr. Yih Horng Tan, Dr. Abeera Sharma, Dr. Binod Pandey, Mr. Vasily Mikhaylov, Mr. Dharmendra Neupane, Mr. Felipe B. d'Andrea, Mr. Jared A. Cooper, Mr. Gajan Kumar, Ms. Israa Diab, Ms. Ibtisam Al-badri, Ms. Fawziah Alshehri, Mr. Rajesh Dimal, Mr. Truan Le, Mr. Ani Gururaj, Mr. Timothy Santos, Ms. Anseh Babaei, and Ms. Taylor Laramie.

To my family and friends for the love, my father Mr. Senando A. Alla, my mother Mrs. Elvira J. Alla, my grandmother Mrs. Anicia A. Alla, my sister Ledelyn, my brothers Lizander and Lester, and to all my nephews and nieces. I would also like to thank Mr. Irwin Uminga and Dr. Maria Udan-Johns for their assistance that help me to acquire this opportunity. And to God be the glory.

TABLE OF CONTENTS

ABSTRACT	i
DEDICATION	iv
ACKNOWLEDGEMENTS	v
TABLE OF CONTENTS	vi
LIST OF ABBREVIATIONS	viii
LIST OF FIGURES	x
LIST OF TABLES	xv
CHAPTER I: Introduction	1
1.1. Overview	1
1.2. Nanoporous gold	2
1.3. Macroporous monolithic materials	7
1.4. Glycans and glycomics	8
1.5. Chromatographic separation of glycans	12
1.6. Lectin-carbohydrate interactions	17
1.7. Boronic acid-carbohydrate interactions	21
1.8. Self-assembled monolayers on gold surface	22
CHAPTER II: Materials and methods	26
2.1. Reagents	26
2.2. Apparatus	27
2.3. Preparation of np-Au monoliths	28
2.4. Characterization of np-Au monoliths	29
2.5. Preparation of solutions	29
2.5.1. Preparation of solution of thiolated compounds	29
2.5.2. Preparation of protein solutions	30
2.5.3. Preparation of boronic acid solutions	30
2.6. Surface modification of np-Au by flow method	31
2.6.1. Preparation of carbohydrate-modified np-Au monoliths	31
2.6.2. Preparation of Con A-modified np-Au monoliths	31
2.6.3. Preparation of boronic acid-modified np-Au monoliths	32
2.7. Characterization of loading and surface coverage by thermogravimetric analysis	32
2.8. Estimation of theoretical surface coverage of molecules on np-Au surfaces	33
2.9. Characterization of loading by in-situ solution depletion method	34
2.10. Separation of Con A from its mixture with SBA	35
2.11. Elution of captured Ova	35
2.12. Trypsin digestion of protein	35
2.13. SDS-PAGE analysis	35
2.13.1. Extraction of Ova using Con A-modified np-Au monoliths	36
2.13.2. Characterization of glycopeptide extraction using boronic acid-modified np-Au monolith	37
2.14. Preparation of borohydride bath	37

215. Electroless deposition of Au and Au-Ag alloy	37
2.16. Data analysis	38
CHAPTER III. Carbohydrate-modified nanoporous gold monolith as affinity support material for the separation of lectins	39
3.1. Introduction	39
3.2. Results and discussion	41
3.2.1. Characterization of np-Au monoliths	41
3.2.2. Lectin-carbohydrate interactions on np-Au monolith characterized by thermogravimetric analysis	43
3.2.3. Preliminary assessment of flow system in determining loading and surface coverage of molecules on np-Au monoliths by in-situ solution depletion methods	45
3.2.4. Preparation of carbohydrate-modified np-Au monoliths	48
3.2.5. Characterization of capture of Con A using ManPEG SAM-modified np-Au monolith	50
3.2.6. Elution of captured Con A by ManPEG SAM-modified np-Au monolith	52
3.2.7. Capture and elution of Con A using ManPEG SAM-modified np-Au monoliths	55
3.2.8. Separation of Con A from its mixture with SBA	56
3.3. Conclusion	58
CHAPTER IV. Selective capture of glycoproteins using lectin-modified nanoporous gold monolith	61
4.1. Introduction	61
4.2. Results and discussion	65
4.2.1. Preparation of Con A-modified np-Au monoliths	65
4.2.2. Determination of surface coverage of LA and Con A molecules on np-Au monoliths using thermogravimetric analysis	68
4.2.3. In situ solution depletion method using UV detection in determining surface coverage of molecules on np-Au monolith	73
4.2.4. Characterization of selective capture of Ova using Con A-modified np-Au monoliths	75
4.2.5. Extraction of Ova from a mixture using Con A-modified np-Au monolith	80
4.2.6. Elution of captured Ova	82
4.3. Conclusion	83
CHAPTER V. Boronic acid-modified nanoporous gold monolith for extraction of glycopeptides from trypsin-digested glycoproteins	85
5.1. Introduction	85
5.2. Results and discussion	90
5.2.1. Preparation of boronic acid-modified np-Au monoliths	90
5.2.2. Characterization of pH-dependent capture and release by boronic acid-modified np-Au monolith of <i>cis</i> -diol containing compound	92
5.2.3. SDS-PAGE gel profile of trypsin digested Ova and characterization of its glycopeptide extraction using boronic acid modified np-Au monoliths	93

5.3. Conclusion	95
CHAPTER VI. Methods in electroless deposition of Au and Au-Ag alloy	98
6.1. Introduction	98
6.2. Results and discussion	100
6.2.1. Electroless deposition of Au	100
6.2.2. Electroless deposition of Au-Ag alloy	105
6.3. Conclusion	108
REFERENCES	110

LIST OF ABBREVIATIONS

2-AA	2-aminobenzoic acid
2-AB	2-aminobenzamide
2-AP	2-aminopyridine
ACN	Acetonitrile
AFM	Atomic force microscopy
AMMP	α -methyl mannopyranoside
APBA	3-aminophenylboronic acid
AUC	Area under the curve
AuNP	Gold nanoparticle
BET	Brunauer–Emmett–Teller
BJH	Barrett–Joyner–Halenda
BSA	Bovine serum albumin
C ₁₈ -SH	Octadecanethiol
CE	Capillary electrophoresis
CEC	Capillary electrochromatography
CHN analysis	Carbon-Hydrogen-Nitrogen analysis
Con A	Concanavalin A
Cyt C	Cytochrome C
DMTMM	4-(4,6-dimethoxy-1,3,5-triazin-2-yl)-4-methylmorpholinium chloride
DTSP	3,3'-dithiodipropionic acid di(N-hydroxysuccinimide ester)
ECL	<i>Erythrina cristagalli</i> lectin
EDC or EDAC	1-Ethyl-3-[3-dimethylaminopropyl]carbodiimide hydrochloride
EDS	Energy dispersive X-ray spectroscopy
ELISA	Enzyme-linked immunosorbent assay
Elu	Elution
FITC	Fluorescein isothiocyanate
GalPEG SAM	Self-assembled monolayer of 12-mercaptododecyl β -D-galactopyranoside and ether terminated methyl-PEG ₄ -thiol
GNP	Gold nanoparticle
HILIC	Hydrophilic interaction liquid chromatography
HO-PEG ₂ -SH	8-mercapto-3, 6-dioxaoctanol
IUPAC	International Union of Pure and Applied Chemistry
K _d	Dissociation constants
LA	Lipoic acid
LA SAM	Self-assembled monolayer of lipoic acid
LAC	Lectin affinity chromatography

LC	Liquid chromatography
ManPEG SAM	Self-assembled monolayer of 12-mercaptododecyl α -D-mannopyranoside and ether terminated methyl-PEG ₄ -thiol
MS	Mass spectrometry
MT(PEG) ₄	Ether terminated methyl-PEG ₄ -thiol
NHS	<i>N</i> -hydroxysuccinimide
NMR	Nuclear magnetic resonance
Np-Au	Nanoporous gold
Ova	Ovalbumin
PDB I.D.	Protein data bank identification
PEG	Polyethylene glycol
PNA	Peanut agglutinin
PTFE	Polytetrafluoroethylene
RP-LC	Reverse-phase liquid chromatography
RT	Room temperature
SAM	Self-assembled monolayer
SBA	Soybean agglutinin
S _{BET}	BET specific surface area
SDS-PAGE	Sodium dodecyl sulfate polyacrylamide gel electrophoresis
SEM	Scanning electron microscopy
TEM	Transmission electron microscopy
TFA	Trifluoroacetate
TGA	Thermogravimetric analysis
Tris	Tris(hydroxymethyl)aminomethane
UV-vis	Ultraviolet-visible
α Man-C12-SH	12-mercaptododecyl α -D-mannopyranoside
β Gal-C12-SH	12-mercaptododecyl β -D-galactopyranoside

LIST OF FIGURES

Figure 1.1. SEM image of the microstructure of np-Au monolith showing the interconnected ligaments with gaps of 50-200 nm. Scale bar is 0.2 μm .	4
Figure 1.2. Mechanism of np-Au formation by dealloying. Dealloying process is diffusion and clustering of Au atoms while dissolving of less noble metals.	5
Figure. 1.3. N-linked and O-linked glycans covalently attached to N of Asn or to O of Ser/Thr, respectively. Linking of glycans to form glycoprotein occurs during glycosylation, a post-translational modification of proteins.	10
Figure 1.4. The challenges in glycomics: complex and heterogeneous structure of glycans due to variable monosaccharide composition, branching, isomeric forms, multiple glycosylation sites of glycoconjugates and presence of sialic acids.	12
Figure 1.5. General workflow of glycomics. Preparative methods such as separation, isolation, digestion, glycan release, derivatization/permethylation and enrichment are necessary to achieve an effective MS analysis of glycans from a limited and very complex biological sample.	13
Figure 1.6. Different modes of separation based on the interactions of glycans in the mobile phase to the ligands immobilized in the stationary phase. The separation is due to the extent of hydrophobic, polar or electrostatic interactions; or via affinity of glycans to lectins and boronic acids.	15
Figure 1.7. Crystal structures of Con A-dimannose and PNA- Gal β 1-3Gal complexes. Con A and PNA are both C-type lectins that binding to carbohydrates depend on Ca $^{2+}$ through direct metal-coordination. Loss of metal ions results in local conformational changes <i>i.e.</i> <i>cis-trans</i> isomerization of peptide bonds that destroys the functionality of the carbohydrate binding site.	20
Figure 1.8. Binding of boronic acid to cis-diols of carbohydrates. The binding is covalent forming five or six-membered cyclic esters in basic conditions but reversible and dissociates in acidic conditions.	22
Figure 1.9. Preparation of self-assembled monolayers of thiolated compound on Au surface. The procedure is usually done by	23

incubating the substrate on 1-10 mM dilute ethanol solution of thiolated compound at room temperature.

Figure 1.10. Schematic representation of modification of self-assembled monolayer (SAM) on np-Au surface. (A) Making a mixed SAM by incorporating protein-resistant thiolated polyethylene glycol (PEG). (B) Activation of carboxylic acid functional group of lipoic acid to form reactive ester for protein covalent immobilization. 25

Figure 3.1. Preparation and characterization of np-Au monolith. (A) Dealloying of precursor alloy plate (42% Au, 20% Ag, 38% Cu) in nitric acid at room temperature to produce np-Au monolith. SEM images of the top and side views of the exterior and the interior portion of an 8 mm × 8 mm × 0.50 mm np-Au monolith. All scale bars are 0.5 μm except for the side view (left image) which is 500 μm. (B) Pore size distribution obtained by Barrett–Joyner–Halenda (BJH) analysis of the adsorption branch of the isotherm. (C) EDS spectra of np-Au monolith (at 15 kV). 42

Figure 3.2. Flow system set-up consists of pump, UV detector-data logger system, and flow tube connected in series. Np-Au monoliths were placed in between of spacers and perpendicular to the flow. The working volume is 1.5 mL at 0.5 mL min⁻¹. UV reading acquisition is at 1 Hz. 46

Figure 3.3. Loading of lipoic acid molecules on np-Au monolith surface by flow through method monitored by a UV detector. (A) UV-vis scan of 1 mM LA solution in ethanol showing a maximum absorbance at 330 nm. (B) Experimental determination of ϵ_{330} of LA solution that is equal to 0.1617 mM⁻¹ cm⁻¹, which is the slope of the linear regression of analytical concentration versus absorbance plot. (C) Loading curve of LA on np-Au monolith as recorded by a UV detector at 330 nm. (D) Calibration curve of analytical concentration versus UV detector-data logger reading to obtain a factor of 0.0502 mM⁻¹ to convert data logger reading to concentration. 48

Figure 3.4. (A) Thiolated compounds (12-mercaptododecyl α -D-mannopyranoside (α Man-C12-SH), 12-mercaptododecyl β -D-galactopyranoside (β Gal-C12-SH), and thiolated methyl-polyethylene glycol MT(PEG)₄) used in preparing carbohydrate-modified np-Au monoliths. (B) TGA thermograms for determination of loading of carbohydrate SAMs on np-Au monolith. The temperature was ramped at 20 °C min⁻¹. 49

Figure 3.5. Loading of Con A molecules on bare and SAM-modified np-Au monolith surface by flow through method monitored by a UV 51

detector. (A) UV-vis scan of 1 μM Con A solution in loading buffer (Tris-NaCl) showing a maximum absorbance at 280 nm. (B) Calibration curve of analytical concentration versus UV detector-data logger reading to obtain a factor of $0.0329 \mu\text{M}^{-1}$ to convert data logger reading to concentration. (C) Loading curves of Con A on bare and SAM-modified np-Au monoliths as recorded by a UV detector at 280 nm.

Figure 3.6. TGA thermograms showing the capture and elution of Con A using ManPEG SAM-modified np-Au monoliths by using (A) 0.10 M α -methyl mannopyranoside [3], (B) 0.50 M mannose, and (C) 0.80 M urea. The temperature was ramped at $20 \text{ }^\circ\text{C min}^{-1}$. 54

Figure 3.7. In-situ monitoring of capture and elution of Con A using ManPEG SAM-modified np-Au monolith substrate. The A_{280} readings were acquired at 1 Hz. The circulation of Con A solution was stopped when there were no more decrease or increase in A_{280} reading. 55

Figure 3.8. Separation of Con A from SBA using ManPEG SAM-modified np-Au monolith. (A) UV-vis scan of Con A-FITC and SBA alone and their equimolar mixture. (B) UV-vis scan of the Con A-FITC – SBA mixture before and after circulation through ManPEG SAM-modified np-Au monoliths. (C) Chromatogram of washing and elution of captured Con A using 2 mL 0.10 M α -methyl mannopyranoside detected by UV spectrophotometer at 280 nm at 1 Hz. 57

Figure. 4.1. (A) Schematic diagram of flow system set-up consists of pump, UV detector-data logger system, and flow cell connected in series. np-Au monoliths were placed in between of spacers and perpendicular to the flow. The working volume is 3 mL at 0.5 mL min^{-1} . UV reading acquisition is at 1 Hz. (B) Schematic representation of preparation of Con A-modified np-Au monolith done by in-situ flow method surface modification. 67

Figure 4.2. TGA thermograms of LA, DMTMM and protein powder. LA and DMTMM were completely decomposed at $400 \text{ }^\circ\text{C}$. Proteins, on the other hand, were not completely decomposed even until $1050 \text{ }^\circ\text{C}$. Ash residue were left on the weighing pan after the pyrolysis. The temperature was ramped at $20 \text{ }^\circ\text{C min}^{-1}$. 69

Figure 4.3. TGA thermograms for determination of LA loading and stability on np-Au monolith. The temperature was ramped at $20 \text{ }^\circ\text{C min}^{-1}$. 70

Figure 4.4. TGA thermograms for determination of Con A loading and stability on SAM-modified np-Au monolith. The temperature was ramped at 20 °C min ⁻¹ .	72
Figure 4.5. Loading curve of (A) LA on np-Au monolith and (B) Con A on SAM-modified np-Au monolith as recorded by a UV detector at 330 and 280 nm, respectively.	75
Figure 4.6. TGA thermograms showing the capture of OVA and BSA using Con A-modified np-Au monolith without the capping procedure. The temperature was ramped at 20 °C min ⁻¹ .	77
Figure 4.7. TGA thermograms showing the (A) effect of adding the capping procedure, i.e., immobilization of Con A to the esters of SAM-modified np-Au monolith was restricted by the capping procedure, (B) capture of OVA and BSA using Con A-modified np-Au monolith with capping procedure. The temperature was ramped at 20 °C min ⁻¹ .	79
Figure 4.8. Characterization of extraction of OVA from a mixture with BSA using Con A-modified np-Au monoliths. (A) Schematic diagram of the procedure, (B) SDS-PAGE of 20 μM BSA (66.4 kDa) and 20 μM OVA (44.3 kDa) and of the aliquots obtained at the end of each 30 min cycle of circulation of 1:3 molar mixture of OVA and BSA through an increasing number of Con A-modified np-Au monoliths.	82
Figure 4.9. Chromatogram generated by flowing 2 mL 1 μM OVA solution through the flow cell monitored at 280 nm (A) without np-Au monolith and (B) with Con A-modified np-Au monolith followed by elution using 2 mL 0.1 M α-methyl mannopyranoside (AMMP).	83
Figure 5.1. Schematic representation of the preparation of boronic acid-modified np-Au monolith.	91
Figure 5.2. Characterization of loading of APBA on SAM-modified np-Au monolith using in-situ solution depletion method. (A) UV-vis scan of 1 mM APBA in 60% acetonitrile solvent. (B) Loading curve of APBA on LA SAM-modified np-Au monolith monitored as recorded by a UV detector at 300 nm.	92
Figure 5.3. In-situ characterization of release in acidic condition of captured adenosine and deoxyadenosine. (A) UV-vis scan of adenosine and deoxyadenosine in phosphate buffer 8.5. (B) Elution curve of adenosine and deoxyadenosine from boronic acid-modified np-Au monolith as recorded by a UV detector at 260 nm.	93

Figure 5.4. SDS-PAGE of (A) intact 1 mg mL ⁻¹ OVA and HRP and digested with 40 and 80 µg mL ⁻¹ trypsin, (B) trypsin digested OVA before and after circulation through boronic acid modified np-Au monoliths and elution buffer acetate buffer 2.7.	95
Figure 6.1. (A) Electroless plating set-up. (B) Schematic representation of the preparation of gold sputtered substrate for autocatalytic electroless deposition.	101
Figure 6.2. SEM images of electrolessly plated Au with different plating temperature. Scale bars are 5 µm, 0.5 µm and 0.2 µm in the first, second and last column panels, respectively.	102
Figure 6.3. SEM images of electrolessly plated Au with different plating time at 80 °C. Scale bars are 5 µm, 0.5 µm and 0.2 µm in the first, second and last column panels, respectively.	103
Figure 6.4. SEM images of electrolessly plated gold at 97 °C for 5 min with reduced KOH concentration. Scale bars are 5 µm, 0.5 µm and 0.2 µm in the first, second and last row panels, respectively.	104
Figure 6.5. SEM images of electrolessly plated Au-Ag alloy at 80 °C for 5 min. Scale bars are 5 µm, 0.5 µm and 0.2 µm in the first, second and last row panels, respectively.	106
Figure 6.6. SEM images and EDS spectra (insets) of electrolessly plated Au-Ag alloy with varying Au:Ag composition ratio at 80 °C for 5 min. Scale bars are in 1 µm.	107

LIST OF TABLES

Table 3.1. Surface coverages of Con A on bare and SAM-modified np-Au monoliths.	52
Table 4.1. CHN analysis of the ash obtained after the pyrolysis of lyophilized Con A powder up to 1050 °C.	69
Table 4.2. TGA analysis data from pyrolysis of SAM- and activated SAM-modified np-Au monoliths.	71
Table 4.3. TGA analysis data from pyrolysis of Con A-modified np-Au.	72
Table 4.4. TGA analysis data from pyrolysis of Con A-modified np-Au monoliths with captured OVA or BSA without capping procedure.	78
Table 4.5. TGA analysis data from pyrolysis of Con A-modified np-Au monoliths with captured OVA or BSA with capping procedure.	80
Table 5.1. Monolithic enzyme reactor columns used in digestion and deglycosylation of glycoproteins and glycopeptides.	87
Table 5.2. Summary of research works that use monolithic materials modified with boronic acids used in separation, enrichment and analysis of glycans, glycoproteins and glycopeptides	88
Table 6.1. Recipe in preparing borohydride bath for electroless deposition of Au.	100
Table 6.2. Recipe in preparing borohydride bath for electroless deposition of Au-Ag alloy.	105

CHAPTER I: INTRODUCTION

1.1. Overview

This research has the objective of studying the potential of surface-modified nanoporous gold (np-Au) as affinity substrate in chromatographic separation and extraction of lectins and glycoproteins. To attain this goal, different methods were developed to characterize the loading of thiolated compounds to form self-assembled monolayers (SAMs) on np-Au surfaces, to activate and preserve the loaded SAMs, and subsequent loading of ligands to be used in capturing lectins, glycoproteins or glycopeptides, modification of the immobilized affinity ligands to reduce non-specific adsorption of proteins by capping the unreacted activated functional groups or by incorporating thiolated protein-resistant spacers, selective capture of target analytes to isolate, and the release of the captured analytes by elution. The surface-modified np-Au monolith is free-standing, has pore sizes within the IUPAC definition of macropore range and these pore sizes can be tuned by thermal annealing, can be cut into different sizes keeping its “one-piece” porous form, is thermally and chemically stable and has easy yet reproducible method of preparation. The np-Au substrate is developed to be an affinity substrate in separation of lectins and glycoproteins, which could be a significant preparative tool in glycomics.

Chapter I is the introduction that discusses the properties and significance of np-Au among the other widely studied nanostructured materials, the importance of chromatographic separation in glycomics, why glycans are important, and interactions of glycans with lectins and boronic acid that are utilized in this study to develop np-Au affinity substrate. In Chapter II, the

materials and methods in this study are detailed. Chapter III describes the work in developing carbohydrate-modified np-Au monolith for separation of lectins. Works in developing lectin-modified np-Au monolith for selective capture of glycoproteins are presented in Chapter IV. In Chapter V, the works in using boronic acids as ligands in extracting glycopeptides from a trypsin digest glycoprotein are discussed. Lastly, in Chapter VI, an electroless method of deposition of a form of nanoporous gold is described.

1.2. Nanoporous gold

Gold is the most noble of all metals. Though it forms very stable alloys with many other metals, it is chemically inert towards atoms or molecules at the interface with a gas or a liquid [1]. Np-Au is a nanostructured material produced by removing the less noble metal(s) from a low carat gold alloy. The removal could be done commonly by selective dissolution [2], wherein the alloy is immersed in concentrated nitric acid at room temperature. The procedure is also called dealloying or leaching. Therefore, the precursor alloy could be a binary or ternary gold alloy that has at least one less noble metal. Some examples of these alloys are Au-Ag [3], Au-Cu [4], and Au-Zn [5]. In research laboratories, different ways of making precursor gold alloys have been developed. Np-Au film was fabricated by electrodeposition of Au-Zn alloy at gold wires followed by subsequent electrochemical dealloying of Zn [5]. Np-Au electrodes have been prepared by electroplating Au-Ag alloy on a gold wire followed by dealloying in a HNO_3 [6]. Np-Au leaf electrode film was prepared by attaching the white gold leaf onto a 1,6-hexanedithiol-modified gold support

followed by dealloying [7]. The most practical and inexpensive production of np-Au is by dealloying of commercially available ~100 nm thick white gold leaf ($\text{Au}_{35}\text{Ag}_{65}$, 50/50 by weight). Dealloying of this very fragile material can be done by floating it upon 70 vol % HNO_3 at room temperature for 5 min [8]. np-Au monoliths used in this study was prepared by dealloying commercially available 0.25 mm and 0.50 mm thick 10 carat yellow gold sheets (41.7% Au, 20.3% Ag, and 38% Cu) [9]. Development of fabrication methods that can control the morphology, sizes and thickness of np-Au have been also reported. Preparation by substrate-conformal imprint lithography, dewetting and dealloying were used to produce a perfectly ordered 2-dimensional arrays of np-Au nanoparticles. This method was able to control the particle size, particle spacing, ligament size or pore size of the np-Au nanoparticles [10]. All the preparation methods of np-Au mentioned above required a dealloying process. Recently last year, a method has been reported that did not require dealloying but formed a free-standing nanoporous single crystal of gold by growing it from a liquid phase during self-forming eutectic decomposition. The method did not require cutting from the bulk piece and shape can be controlled by the original droplets wetting properties [11].

The microstructure of np-Au has interconnected bicontinuous ligaments forming gaps that are called pore sizes in the range of 10-100 nm (Figure 1.1). It was in 1963 that the microstructures of dealloyed gold alloy (Au-Cu) was first observed using transmission electron microscopy (TEM). It was described as a localized pitting or tubular form initiated at grain boundaries and antiphase boundary junctions [12]. Different models and mechanisms were proposed to explain the corrosion observed during the dealloying of the gold alloy. An

ordering-reordering model used Au-Ag and Au-Cu alloys and suggested that the dealloying process starts with the formation of island nuclei that form growing gold layer. The island nuclei eventually try to merge and form connected structure, enclosing channels and pits [13]. The disordering process was observed to be dependent on the rate at which the Ag atoms are dissolved and so on the composition of the alloy, strength of the acid being used and time of exposure [14]. It was proposed that surface diffusion of gold during the process is important; such that in the dealloying of Au-Ag alloy, residual gold atoms reform into gold-rich islands after the dissolution of Ag exposing the inner Ag atoms to a corrosive environment in a layer-by-layer manner [15].

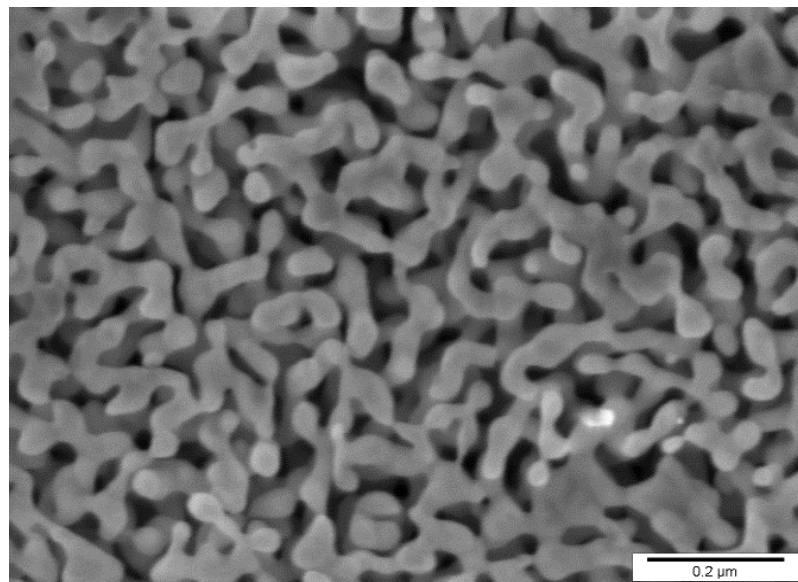


Figure 1.1. SEM image of the microstructure of np-Au monolith showing the interconnected ligaments with gaps of 50-200 nm. Scale bar is 0.2 μm .

Nanoporosity of np-Au was explained by Erlebacher and coworkers in 2001 in his model based on experiments and theoretical simulation of alloy dissolution using a kinetic Monte Carlo method (Figure 1.2). Three-dimensional

nanopores are suggested to form due to diffusive redistribution of components on a crystal lattice. Upon dealloying, a new gold cluster nucleates once a new pit with sufficient depth is formed. Small new pits with smaller surface area are formed from parent pores which continue through the inside of the bulk to increase their surface area. Formation of new clusters and pits repeats until a full three-dimensional nanoporous structure is formed [16]. It was proposed that the significant factors in np-Au formation are Au fractions, the chemical potentials for the acid ions and the vacancy concentrations [17]. In summary, the mechanism of dealloying process could be considered as diffusion and clustering of Au atoms and dissolving of less noble metals like Ag [18].

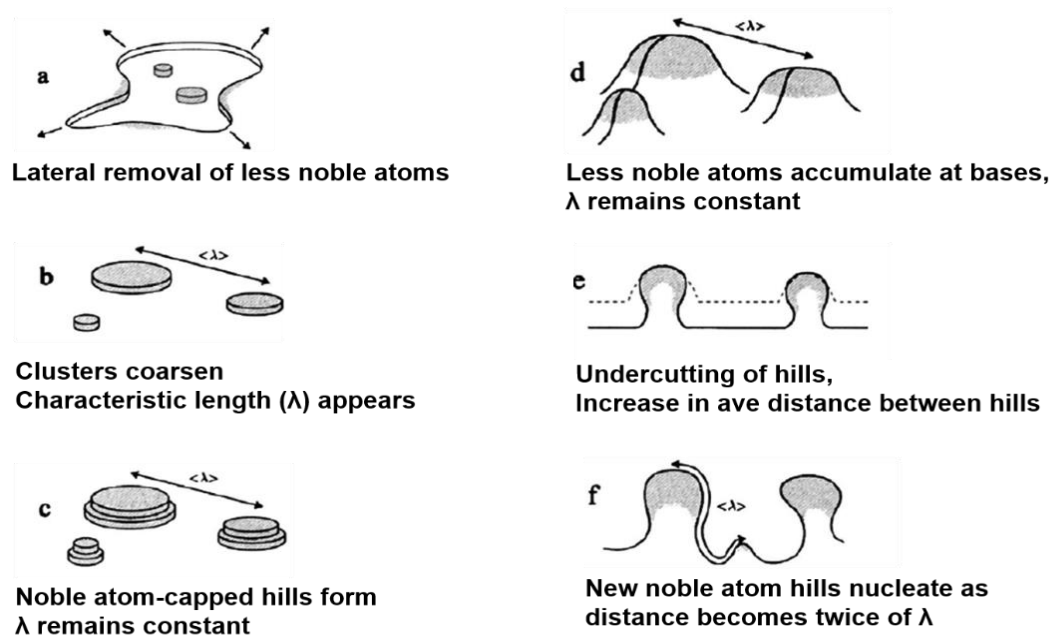


Figure 1.2. Mechanism of np-Au formation by dealloying [19]. Dealloying process is diffusion and clustering of Au atoms while dissolving of less noble metals.

Nanostructured materials or those that have structural elements dimension between 1 to 100 nm range have been studied and developed in a wide variety of applications because of their enhanced chemistry, much higher surface area and better stability compared to their bulk counterparts [20]. For example, the high surface-to-volume ratios of transition metal nanoparticles have been utilized for catalysis. Surface atoms of these materials are so active that their properties could be changed by size and shape [21]. Specific examples are the gold nanoparticles (AuNPs) also called as gold colloids that are currently being used in catalysis and biology, and characterized as the most stable metal nanoparticles [22]. For example, AuNPs were modified by linking to mercaptoalkyloligonucleotide to perform a highly selective, colorimetric polynucleotide detection method. AuNPs have absorption across most of the visible region. In this study, detection was accomplished because of the interparticle distance-dependent color change i.e., turns red when the distance is greater than the average particle diameter otherwise turns blue [23]. Gold nanostructures reported are nanorods, nanospheres, nanoshells, and nanocages. The variation of shape and structure of these materials enable tuning of its surface plasmon resonance peaks from the visible to near infrared region and can be used in bioassay applications [24]. Nanostructured Au electrodes, due to their electrochemical characteristics, have been used as sensing devices. These materials can be either architecture or arrays patterned on the surface that creates conductive particles that could be porous, high surface-area electrodes [25]. In this study, the nanostructured gold material used is the np-Au. As described above, np-Au is a highly porous material and therefore of much higher surface area as compared to a non-porous form of Au.

Np-Au is being developed in different applications such as bio- and chemical detection, electrochemistry, catalysis, energy storage, and solid support synthesis. This study is focused on the application of np-Au in capture and release of proteins, specifically in chromatographic separation and extraction of lectins and glycoproteins. Np-Au could be in different forms such as np-Au wires [6] and np-Au thin film [26]. In this study, the monolithic form of np-Au is used. This np-Au material has microstructures similar to the macroporous monolithic polymers being used in chromatographic separations.

1.3. Macroporous monolithic materials

Under the International Union of Pure and Applied Chemistry (IUPAC) definition, 'macropore' range is typically 50 nm and greater [27]. Macroporous monolithic materials have large interconnected pores or channels that allow high flow rates at low pressure. Due to the continuous effort to improve methods for faster and more efficient separations, biocatalysis and related applications, monolithic materials being used in preparing chromatographic separation columns were invented and are being developed. Monolithic materials are considered as the new generation of column materials that are being used in designing efficient enzyme reactors and separation columns due to their continuous porous morphology and increases permeability with low back pressure that enhances the catalysis and separation processes. The story of developing these monolithic materials started with columns packed with uniformly sized porous particles that appear to have large interstitial spaces. These types of columns facilitate separation mainly based on diffusion of

solutes from a more concentrated mobile phase to the stagnant phase inside the pores. Fluid carrying the solute tends to flow through the void spaces not reaching most of the surface inside the pores. Reducing the sizes of these particles is an option to diminish the functionless voids; however, packing of smaller particles reduces the permeability of the column developing high back pressure during the separation. Finally, a sophisticated design of an integrated and continuous network of flow-through pores was introduced forming a “one-piece” porous material currently called a “monolithic column” [28-30]. Monolithic columns are known to have these distinct and advantageous characteristics: (1) easy fabrication; (2) versatility for a variety of surface chemistries; and (3) good permeability that allows fast convective mass transfer with low backpressure even at high flow rates.

1.4. Glycans and glycomics

Glycans, also called as carbohydrates or as oligosaccharides, are structures of monosaccharides connected to each other in linear or branched arrangements. The synthesis of glycans does not follow a repetitive pattern of steps like that found for polypeptides and polynucleotides. Additionally, the compositions, configurations, and linkages vary from one glycan to another. For these reasons, glycan structures are known to be complex and heterogeneous and this allows for their widely diverse biological functions [31]. Glycans are usually exposed at the cell surface as part of the glycoconjugates such as glycoproteins, glycopeptides, proteoglycans, glycolipids and lipopolysaccharides, where they are covalently attached. Therefore, they serve as recognition armies of the cell and mediate as receptors to pathogens and

other cells. Glycans could also serve as biological process modulators, for example as on-off switches of the function of the protein to which it is attached. Attachment of glycans to proteins occurs during glycosylation, a post-translational modification of proteins. The linkage is covalent and the most prevalent are either through N of asparagine (Asn) called *N*-glycosylation or through O of serine (Ser) or threonine (Thr) called *O*-glycosylation (Figure 1.3). *N*-linked glycans have a common core oligosaccharide $\text{Man}_3\text{GlcNAc}_2$. *O*-linked glycans, on the other hand, do not. The attached glycans influenced the biological functions and structure of the glycosylated proteins. Therefore aberrant glycosylation is correlated to several mammalian diseases such as cancer [32]. Aberrant glycosylation is usually caused by different factors in the cell environment that interfere the process such as changes in the expression levels of enzymes e.g., glycosyltransferases and glycosidases, and the availability of the precursor monosaccharides. An example is the observed increase in sialidase activity of plasma membrane-associated ganglioside sialidase (NEU3) in the serum patients with prostate cancer [33]. Sialidase has been known to catalyze the removal of sialic acid residues from the glycans of glycoconjugates. Other alterations in glycan structures that are correlated with diseases are increased glycan branching [34], incomplete glycosylation [35], and changes in the extent of fucosylation of glycans in specific glycosylation sites of glycoproteins [36].

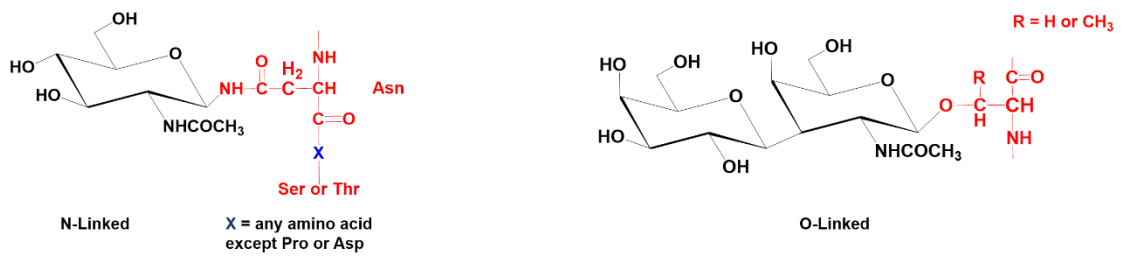


Figure 1.3. *N*-linked and *O*-linked glycans covalently attached to N of Asn or to O of Ser/Thr, respectively. Linking of glycans to form glycoprotein occurs during glycosylation, a post-translational modification of proteins.

One great importance of glycans, for example those in glycoproteins, are their use as disease biomarkers. As mentioned above, the enzymes responsible for the production and modification of glycans on glycoproteins are being upregulated or downregulated and cause aberrant glycosylation and alterations of glycan structure and lead to diseases. Due to these events, healthy cells are being converted to diseased cells and can progress within the tissue. Circulating blood and other fluids being exposed to these diseased tissues can carry these membrane-bound and secreted glycoproteins as potential biomarkers. For this reason, glycans of glycoproteins, the protein backbone that contains glycosylation sites and the glycoproteins as a whole become targets for detection for subsequent qualitative and quantitative analysis and identification strategies. Comparison of the analysis of the glycoproteins derived from healthy and diseased biological samples is the most common approach for the discovery of disease biomarkers that can be helpful in the diagnosis, monitoring and prognosis of several diseases [37]. In 1969, high molecular weight membrane glycoproteins were detected in virus-

transformed mouse fibroblasts, which were absent in their normal counterparts [38]. Glycans have several advantages over proteins as disease markers since disease states can affect glycan synthesis more significantly than that of the protein synthesis itself, and then glycan quantification can be simpler because of its smaller size [39]. Characterization of these glycans, especially in glycoproteins, could be helpful in therapeutic development and in elucidation of biological processes.

Glycomics is the study of glycans' structures and biological functions, whether free glycans or in glycoconjugates. The current approach in glycomics is the structural characterization of glycans and deglycosylated proteins that provide "marks" to locate the glycosylation sites. The challenge in current glycomics is the complex and heterogeneous structure of glycans. Complexity is due to the (1) variable composition, (2) branching, (3) isomeric forms, (4) multiple glycosylation sites, and (5) presence of terminal units such as sialic acids [40] (Figure 1.4). Another challenge in glycomics is the very low ratio of glycans and glycopeptides to other components in complex biological samples and glycan pools. These difficulties can be aided by the preparative methods that may include separation and isolation, digestion and glycan release, derivatization or permethylation of glycans and enrichment prior to MS analysis. Chromatographic separation is one very useful tool in preparative methods in glycomics.

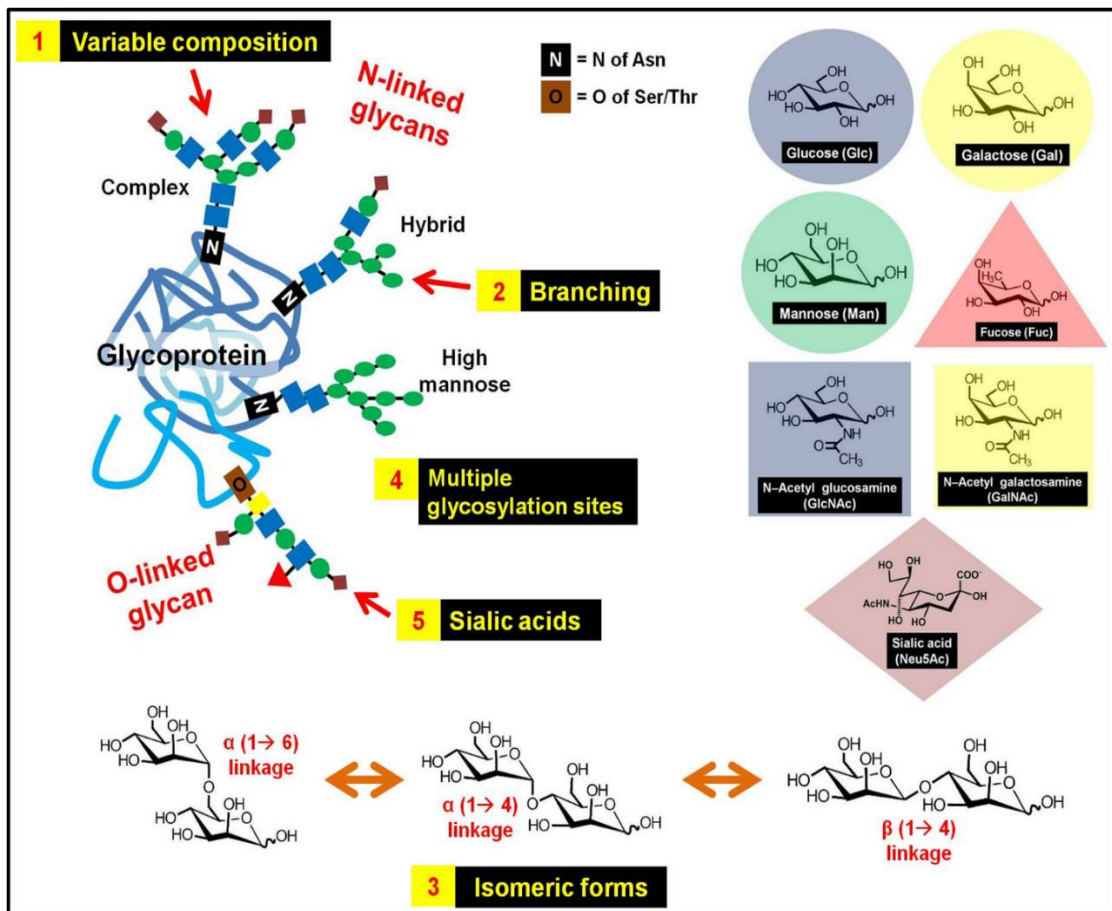


Figure 1.4. The challenges in glycomics: complex and heterogeneous structure of glycans due to variable monosaccharide composition, branching, isomeric forms, multiple glycosylation sites of glycoconjugates and presence of sialic acids.

1.5. Chromatographic separations of glycans

A series of preparative and enrichment methods are usually necessary prior to MS analysis of glycans and glycopeptides. These methods may include but not limited to separation, extraction, and isolation from interferences in the sample such as non-glycosylated proteins, reagents, enzymes and cell lysate residues. These methods reduce the complexity of the sample, increase the

abundance of glycopeptides and glycans, and minimize ionization suppression, thus far considered as the limiting steps of successful glycan analysis. In the general workflow of glycomics these methods are incorporated prior to MS analysis (Figure 1.5). Along with classical methods in separation and isolation of glycoproteins such as sodium dodecyl sulfate polyacrylamide gel electrophoresis (SDS-PAGE), chromatographic separation methods such as liquid chromatography (LC) is the best choice in tandem with MS analysis [41]. In some cases, derivatization of glycans is necessary to resolve the limitation of sensitivity of MS detection. Labeling glycans with 2-aminobenzamide (2-AB) is an example of glycan derivatization [42].

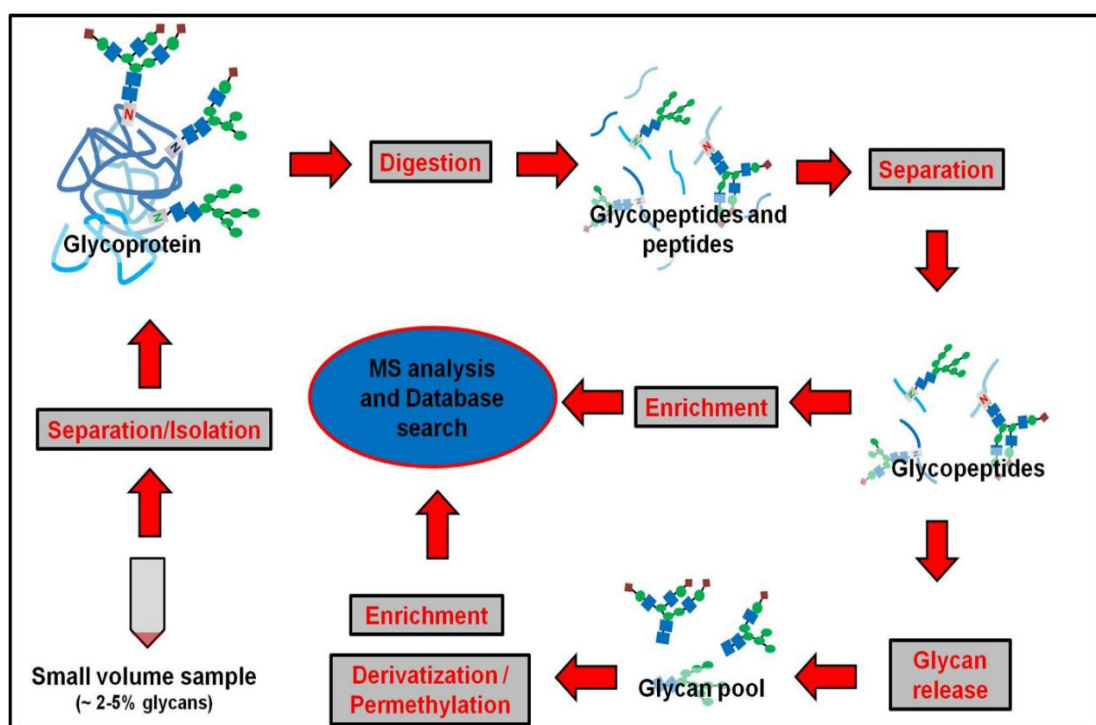


Figure 1.5. General workflow of glycomics. Preparative methods such as separation, isolation, digestion, glycan release, derivatization/permethylation and enrichment are necessary to achieve an effective MS analysis of glycans from a limited and very complex biological sample.

Monolithic materials have been utilized in creating columns for chromatographic separation processes. Chromatographic separation is a method of isolating the wanted or unwanted components from a mixture in the mobile phase when being captured by the stationary phase. Separation in LC is due to the difference in the extent of interactions of the solutes in the mobile phase to the functionalized stationary phase. In glycomics, the functionalization of stationary phase could be done by immobilizing different ligands that the stationary solid support could capture the glycans rather than the other components in its mixture. The type of bound ligands dictates the mode of separation of glycans, which differ from each other by their interactions with the target glycans. The different modes of separation of glycans are (1) interactions between hydrophobic surface and hydrophobic labels of derivatized glycans, (2) H-bonding between the neutral polar surface and OH groups of glycans, (3) electrostatic interactions between charged (cationic) surface and negatively charged ionized glycans, anionic terminal sialic acids or labels of derivatized glycans, and (4) affinity between immobilized lectins and its complementary glycan structure or between boronic acids on the surface and *cis-diols* of glycans (Figure 1.6). The mobile phase should give an appropriate environment to the glycans by tuning its pH, ionic strength, and organic solvent content.

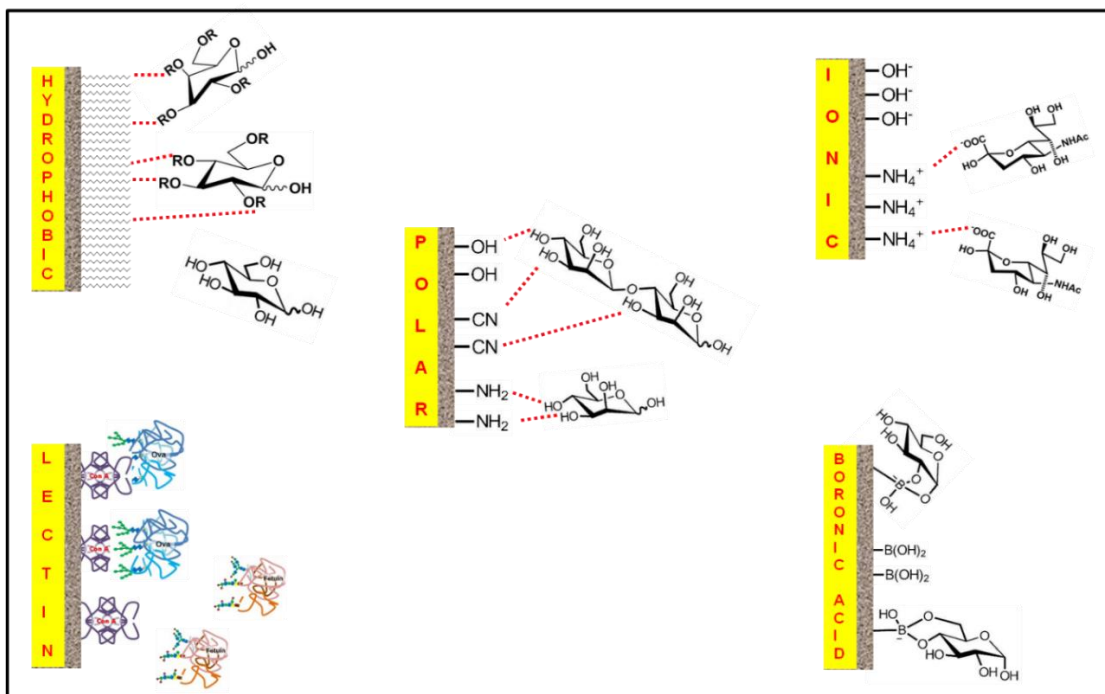


Figure 1.6. Different modes of separation based on the interactions of glycans in the mobile phase to the ligands immobilized in the stationary phase. The separation is due to the extent of hydrophobic, polar or electrostatic interactions; or via affinity of glycans to lectins and boronic acids.

Reverse-phase separation (RP-LC) uses a hydrophobic stationary phase and a polar mobile phase to separate glycans by the differences in the extent of hydrophobic interactions. Underivatized glycans (neutral glycans) are retained very weakly on the commonly used C18 stationary phase. Therefore, use of small molecular tags such as 2-AB, 2-aminopyridine (2-AP), and 2-aminobenzoic acid (2-AA) amongst many others to modify glycans yield enhanced separation or increase the signal for fluorescence detection [43]. A potential advantage of RP-LC is that the solvent used (water + organic solvent + acid) is compatible with mass spectrometry analysis [44]. Polar mode or normal phase mode of separations involves H-bonding and dipole-dipole

interactions between polar stationary phase and OH groups of neutral glycans. In this method, the mobile phase is less polar than the stationary phase. Therefore, less polar glycans are eluted first and separation is achieved based on differences in glycan hydrophilicity. Polar stationary phase may contain amino-, cyano-, amido-, or diol- functional groups. A popular example of polar mode separation of glycans is the zwitterionic-hydrophilic interaction liquid chromatography (HILIC) [45]. The electrostatic mode of glycan separation is affected by the electrostatic attraction and repulsion between the glycan and the stationary phase. The pH of the mobile phase influences the separation as it can modify the charge of the glycan-containing glycoproteins based on their isoelectric point. Glycans are weak acids and are deprotonated at very high pH (>12) and become negatively charged. High-performance anion-exchange chromatographic separation of underivatized weakly acidic glycans used an amine-functionalized polymeric monolithic column at high pH [46]. Affinity mode of separation involves reversible interactions between matrix-bound ligands and specific sites of the glycans. The purified glycan is recovered from the matrix by rinsing with the competitive ligands of higher affinity or alteration of the elution buffer i.e., change in pH, ionic strength, or dwell time. The two most popular ligands used in affinity mode separation of glycans are lectins and boronic acids. In this study, the interactions of glycans or glycoproteins with lectins and boronic acids are used to develop np-Au substrate for isolation of glycoproteins.

1.6. Lectin-carbohydrate interactions

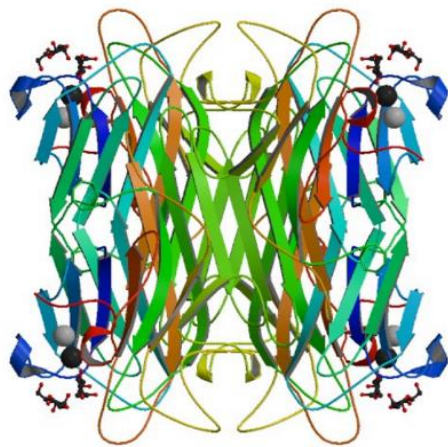
Lectins are proteins that interact non-covalently with carbohydrates and have no catalytic activity like enzymes and are not produced by the immune response like antibodies [47]. They exist in almost all forms of life ranging from viruses through bacteria and plants to animals. Their interactions with carbohydrates is of high interest in research due to their role in cell-cell recognition and as useful tools in studying glycoforms in solution and on cell surfaces [48]. Lectins are polyvalent, thus they have at least two carbohydrate binding sites. In vitro studies show that due to polyvalency, lectins can cross-link between cells resulting to cell-agglutination and subsequently to precipitation, and can be inhibited by the carbohydrate for which the lectin is specific [49]. Lectins are usually less expensive and can be better characterized with respect to binding specificity than monoclonal antibodies [50]. Lectins are also abundant in nature, and can be found in plant seeds and tissues.

Lectins are classified by their sequence similarity and structural organization. *Lis* and *Sharon* came up with five groups according to the monosaccharide for which the lectin exhibits the highest affinity: (1) mannose, (2) galactose/*N*-acetylgalactosamine, (3) *N*-acetylglucosamine, (4) fucose, and (5) *N*-acetylneuraminic acid [51]. Current primary and 3D structures of lectins are stored in a database and accessible on the World Wide Web at <http://lectin3d.cermav.cnrs.fr/>. Lectins interact with carbohydrates at their binding sites. 3D structures confirm that members of each lectin group have conserved residues at the core of its carbohydrate binding site that provide H-bonding to sugars and this core is flanked by two variable loops that provide additional *van der Waals* and H-bond interactions that determine specificity

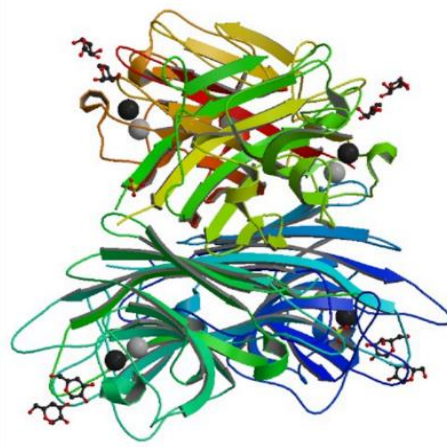
[52]. Weis reviewed the structural basis for carbohydrate-lectin interactions and recognition [53]. Interactions are primarily due to cooperative H-bonding wherein a hydroxyl group acts simultaneously as H-bond donor and acceptor. Water molecules may also mediate H-bonds between sugar and proteins. Polar groups also provide electrostatic stabilization while sugars' non-polar patches formed by aliphatic protons and carbons stack with tryptophan and phenylalanine residues of lectins creating non-polar interactions. Interactions of C-type lectins, or those that depend on divalent cation Ca^{2+} , are through direct metal-coordination, wherein loss of metal ions results in local conformational changes *i.e.* *cis-trans* isomerization of peptide bonds that destroys the functionality of the carbohydrate binding site [52]. Legume lectins use the divalent cation Ca^{2+} together with transition metal cation Mn^{2+} to indirectly interact by stabilizing the binding site and fixing the positions of amino acids [53]. Unlike enzymes and transport proteins, lectins' carbohydrate binding sites are shallow and at the surface of the protein and exposed to solvent. They bind to monosaccharide reversibly and have dissociation constants (K_d) in the millimolar range, and lower for oligosaccharides [51]. Lectin-carbohydrate binding sites are also small, and that makes them attractive for investigation due to their simplicity and they can be a general model in studying protein-carbohydrate interactions. Due to their high specificity towards carbohydrates, it has been demonstrated and proven that lectins are useful tools in glycomics [54]. Lectins have been used in screening of biological samples to analyze the structures of different glycoforms. Lectins can induce agglutination in blood cells, and thus are useful tools in the study of blood group classification. And in

the developing trend of high-throughput technologies, lectin microarrays were invented for fast, easier and more efficient ways of glycomics analysis [55].

The most studied lectin is the Concanavalin A (Con A), which is a C-type lectin from *Canavalia ensiformis* (Jack bean) seeds. Con A binds to α -mannose and α -glucose sugar units of glycans [56]. Specifically, Con A has been reported to bind to high-mannose [57] and trimannoside cores of complex type N-linked glycans [58]. Con A exists as a homotetramer in solution at pH 7.0 and as a dimer at pH 5.0 [59]; each subunit is a single polypeptide chain of 231 amino acids [60]. In a crystallography study, the location of the carbohydrate binding site of Con A is found to be in a deep cavity that is more than 20 Å from the Mn^{2+} and Ca^{2+} ions [61]. Peanut agglutinin (PNA) is another C-type lectin derived from a legume seed but the specificity is toward terminal β -D-galactosyl residues [62]. PNA has 236 amino acid residues in which the sequence is identical to Con A metal binding site and the hydrophobic pocket. Unlike with the Con A, the carbohydrate binding site of PNA was found to be more open cleft [63]. This variation in structure of the carbohydrate-binding domain could explain the difference in specificities of Con A and PNA (Figure 1.7).



PDB: 1I3H
Concanavalin A-dimannose structure



PDB: 2DV9
Peanut lectin- Galβ1-3Gal structure

Figure 1.7. Crystal structures of Con A-dimannose [64] and PNA- Galβ1-3Gal [65] complexes. Con A and PNA are both C-type lectins that binding to carbohydrates depend on Ca^{2+} through direct metal-coordination. Loss of metal ions results in local conformational changes *i.e.* *cis-trans* isomerization of peptide bonds that destroys the functionality of the carbohydrate binding site.

The specificity and reversibility of lectin-carbohydrate interactions are reasons why both lectins and carbohydrates are being used as ligands in chromatographic separations to isolate carbohydrates and lectins, respectively. Lectins are the ligands in lectin affinity chromatography (LAC). LAC is the most useful and efficient mode of separation of glycoproteins [66]. Multi-lectin affinity columns were developed using different lectins for comprehensive capture of serum glycoproteins [67]. The weak binding between lectin and carbohydrate can be utilized to afford elution of the bound target lectins or glycoproteins using carbohydrate ligands. The release of captured molecules is due to the competition between the carbohydrates in solution and immobilized carbohydrate for the binding site of lectin. Elution of captured lectin can be done

using various elution techniques like using a much higher concentration of mannose [68], methyl mannopyranoside [69] or urea [70].

1.7. Boronic acid-carbohydrate interactions

Lectin-affinity separation is a highly selective method but appears primarily limited to N- and O-linked glycoproteins [71]. C-mannosylation at tryptophan, more recently discovered, has been found not to be recognized by mannose-binding lectins [72]. Another approach that is getting huge attention recently is the affinity separation using boronic acids. Boronic acids form stronger covalent bonds rather than non-covalent interactions with *cis-diol*-containing molecules such as RNA, nucleosides, glycans, glycoproteins and glycopeptides. The binding is reversible and pH-dependent, *i.e.*, it forms five or six-membered cyclic esters in basic conditions and dissociates when the conditions are switched to acidic (Figure 1.8). Acids such as formic acid and acetic acid are commonly used as the eluting mobile phase. Boronic acids as ligands are found in applications such as sensing, separation and self-assembly. The use of boronate functionalized monolithic stationary phases in separation of *cis-diol* containing molecules has been reviewed [73,74]. Boronate affinity will not be specific to glycans or glycoproteins and will bind other *cis-diol* containing molecules in a sample. If a boronate affinity column has hydrophobic character, then reversed phase non-specific interactions can degrade the performance [75]. Standard boronate affinity methods usually require the use of pH > 8–9 for capture (above the pK_a of the boronic acid), and this may degrade certain targets. However, sialic acids are known to bind strongly to boronic acid at pH

$< pK_a$ of the boronic acid. Recent efforts have focused on lowering the pH required for glycan capture using modified boronic acids and different binding modes [76].

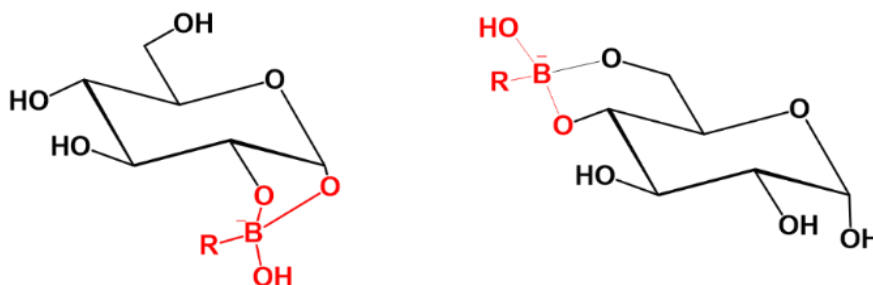


Figure 1.8. Binding of boronic acid to *cis-diols* of carbohydrates. The binding is covalent forming five or six-membered cyclic esters in basic conditions but reversible and dissociates in acidic conditions.

1.8. Self-assembled monolayers on gold surface

Surface of substrates such as metals, mica, glass and silicon wafers can be modified by forming self-assembled monolayers (SAMs) through spontaneous adsorption of surfactant from a liquid or vapor phase. Surfactants such as thiols, disulfides, sulfides, silanes, alkynes and alkenes have a head group at one end that has specific affinity to the substrate and a functional group on the other end that can be used to immobilize or resist biomolecules [77]. Therefore, SAM formation can be defined as a method of functionalization of the substrate wherein the surface is modified in order to present functional groups, which are supported by well-defined and organized organic assemblies. The most common way of preparing SAMs on substrates like gold is by incubating the clean substrate in a dilute (1-10 mM) ethanolic solution of

thiols for 12-18 h at room temperature [78] (Figure 1.9). Choice of solvent, immersion time, temperature, concentration of adsorbate and chain length can affect the structure and rate of formation of SAMs onto the substrate. Composition of the surface can be made more defined by mixing molecular structures to form mixed SAMs. One example is co-adsorption from solutions containing mixtures of thiols ($RSH + R'SH$). Another method of modifying the preformed SAMs is the use of activators for further immobilization of biomolecules. 1-Ethyl-3-[3-dimethylaminopropyl] carbodiimide hydrochloride (EDC or EDAC) and *N*-hydroxysuccinimide (NHS), for example, can be used to activate the carboxylic acid functional group to a reactive ester for subsequent amide bond formation with amino groups of protein residues such as lysines [79].

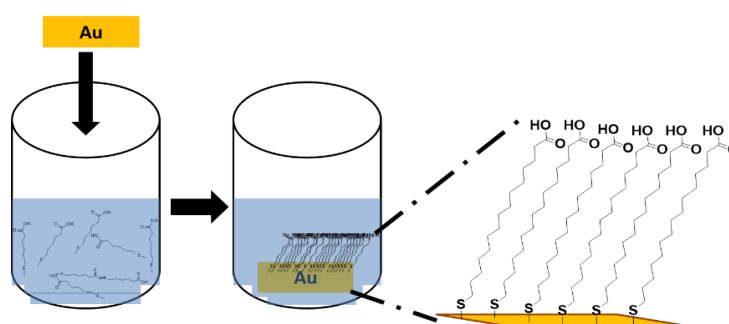


Figure 1.9. Preparation of self-assembled monolayers of thiolated compound on Au surface. The procedure is usually done by incubating the substrate on 1-10 mM dilute ethanol solution of thiolated compound at room temperature.

The significance of nanostructured gold materials such as AuNP, Au films, Au nanostructure including np-Au in various applications such as affinity

biosensors [80], biocatalysis [81], and affinity separation [82] is due to their frequently reported use as substrates for SAM formation. In one study, gold particles (3.5 μm) coated with octadecanethiol were used as stationary phase in reversed-phase separation of polyaromatic hydrocarbons [83]. In another study, gold foils modified with SAM of dithiobis-(succinimidylpropionate) were used to immobilize Con A to create a lectin probe to concentrate carbohydrate-containing samples that were analyzed at low levels [84,85]. In yet another study, monolithic surface coated with 20 nm gold nanoparticles assembled 3,3'-dithiodipropionic acid di(N-hydroxysuccinimide ester) (DTSP) were used to immobilize *Erythrinacristagalli* lectin (ECL) for extraction of galactose-specific proteins [86]. In this study, thiolated carbohydrates such as $\alpha\text{Man-C12-SH}$ and $\beta\text{Gal-C12-SH}$ were used. Protein resistant thiolated spacer $\text{CH}_3\text{-PEG}_4\text{-SH}$ was incorporated to form mixed SAMs that reduced the non-specific adsorption of protein to the np-Au surface (Figure 1.10A). To immobilize covalently the ligand lectin, lipoic acid (LA) was used. LA is a yellow, sulfurous fatty acid compound with its head group consisting of two sulfur atoms connected by a disulfide bond in its oxidized form [87]. This carboxylic acid terminal functional group tends to be exposed when sulfur atoms selectively bind to gold surface through SAM formation. The procedure of SAM formation of LA to functionalize gold surfaces has already been established [88,89]. To facilitate immobilization of lectin, further activation of the carboxylic acids of LA—via esterification with 4-(4,6-dimethoxy-1,3,5-triazin-2-yl)-4-methylmorpholinium chloride (DMTMM) is needed (Figure 1.10B). DMTMM is a water-soluble, white-powdery coupling reagent of carboxylic acids and amines [90,91].

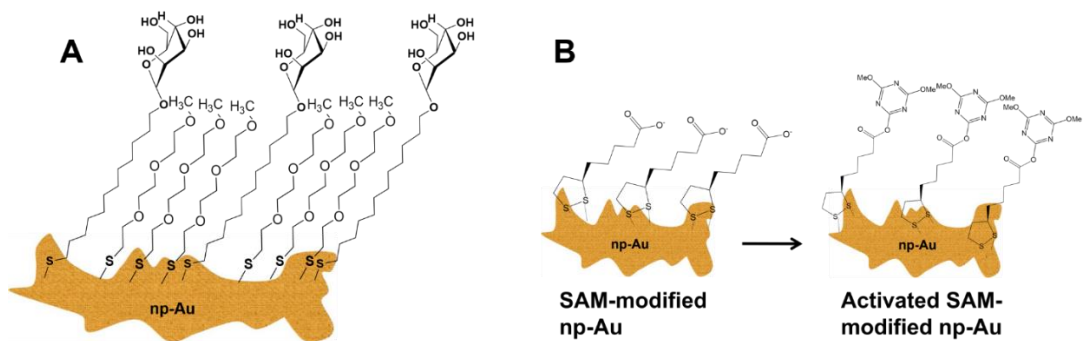


Figure 1.10. Schematic representation of modification of self-assembled monolayer (SAM) on np-Au surface. (A) Making a mixed SAM by incorporating protein-resistant thiolated polyethylene glycol (PEG). (B) Activation of carboxylic acid functional group of lipoic acid to form reactive ester for protein covalent immobilization.

CHAPTER II: MATERIALS AND METHODS

2.1. Reagents

Ten carat yellow gold plates were purchased from Hoover and Strong, Richmond, Virginia, USA. Trace metal grade nitric acid was purchased from Fisher Scientific, Pittsburgh, Philadelphia, USA. Lyophilized powder of unconjugated and FITC conjugate Concanavalin A from *Canavalia ensiformis* (Jack Bean) of $\geq 95.0\%$ purity, albumin from chicken egg white (ovalbumin) of $\geq 98\%$ purity, lectin from *Arachis hypogaea* (peanut), peroxidase from horseradish, bovine serum albumin of $\geq 98\%$ purity, trypsin from bovine pancreas, HPLC grade ethanol, α -lipoic acid, 4-(4,6-dimethoxy-1,3,5-triazin-2-yl)-4-methylmorpholinium chloride, tris(hydroxymethyl)aminomethane (Trizma® base and Trizma® hydrochloride), 2-aminophenylboronic acid, adenosine, 2'-deoxyadenosine monohydrate, sodium chloride (NaCl), calcium chloride dihydrate ($\text{CaCl}_2 \cdot 2\text{H}_2\text{O}$), manganese(II) chloride tetrahydrate ($\text{MnCl}_2 \cdot 4\text{H}_2\text{O}$), potassium phosphate dibasic (K_2HPO_4), potassium dihydrogen phosphate (KH_2PO_4), α -methyl mannopyranoside, D-mannose, urea, sodium hydroxide (NaOH), glycine, HPLC grade methanol, potassium dicyanoaurate(I) ($\text{KAu}(\text{CN})_2$), potassium dicyanoargentate, sodium borohydride (NaBH_4), and potassium hydroxide (KOH) were all purchased from Sigma Aldrich, St. Louis, Missouri, USA. Ether terminated methyl-PEG₄-thiol (MT(PEG)₄), sulfuric acid (H_2SO_4), 30% hydrogen peroxide (H_2O_2), pre-mixed Laemmli sample buffer, 2-mercaptoethanol, trace metal grade acetic acid, and Page Ruler Plus prestained protein ladders were all purchased from Thermo Scientific, Illinois, USA. Soybean agglutinin (SBA) was purchased from Vector Laboratories, Burlingame, California, USA. One hundred percent ethanol was purchased

from Decon Laboratories, Inc., Pennsylvania, USA. Sodium dodecyl sulfate (SDS) and Coomassie Brilliant Blue R250 were purchased from Bio-Rad Laboratories, Inc., Richmond, California, USA. Milli-Q water (18.2 M Ω .cm at 25 °C) was prepared using a Simplicity UV system from Millipore Corporation, Boston, USA. All chemicals, reagents and proteins were used as received. Thiolated mannoside (α Man-C12-SH) and thiolated galactoside (β Gal-C12-SH) were synthesized in the GlycoWorld (Prof. Alexei V. Demchenko laboratory) and were used as received.

2.2. Apparatus

The flow cell system consisted of a home-made flow tube or Teflon flow cell, C-FLEX or PTFE tubing (Masterflex, Cole-Parmer Instrument Company, Illinois, USA), peristaltic pump (Model 77390-00, Cole-Parmer Instrument Company, Illinois, USA), UV–visible spectrophotometer (Model SPD-10A, SHIMADZU Scientific Instruments, Inc., Columbia, Maryland, USA) and data logger (Model USB 1608-G, Measurement Computing, Norton, Maryland, USA). Scanning electron microscopy (SEM) and energy dispersive X-ray spectroscopy (EDS) was done using JEOL JSM-6320F field emission SEM (JEOL USA, Inc., California, USA). Surface area and pore size analysis were done using a Beckman Coulter SA-3100 Gas Adsorption Surface Area and Pore Size Analyzer (Beckman Coulter, Inc. California, USA), with stated resolution of $>0.01 \text{ m}^2 \text{ g}^{-1}$. A standard BET sample holder (3cc RapiTube, model number 7215 006B, Beckman Coulter, Inc. California, USA) was used to hold the np-Au samples. Thermogravimetric analysis was done using a Q500 Thermogravimetric Analyzer (TA Instruments, Delaware, USA). UV–vis scans

and absorbance readings were done using a Varian Cary 50 UV–vis spectrometer (Varian Australia Pty Ltd., Victoria, Australia) and Suprasil quartz spectrophotometer cuvette with ten millimeter light path and volume capacity of three milliliters (model number 14-385-902C, Fischer Scientific, Pittsburgh, Pennsylvania, USA). Mini-PROTEAN pre-casted 4-20% polyacrylamide gel was used for SDS-PAGE in a Mini-PROTEAN Tetra Cell (Bio-Rad Laboratories, Inc., Richmond, California, USA). Electroless deposition used 10 mm dia glass coverslips (Ted Pella, Inc., Redding, California, USA) sputtered with Au using Hummer VI sputter coater (Anatech Ltd, Battle Creek, Michigan, USA).

2.3. Preparation of np-Au monoliths

Commercially available 0.25 mm and 0.50 mm thick ten carat yellow gold plates (41.7% Au, 20.3% Ag, and 38.0% Cu) were cut into the desired dimensions – 6.0 mm × 6.0 mm × 0.25 mm for thermogravimetric characterization, 2.5 mm × 2.5 mm × 0.50 mm (Chapter III and V) or 8.0 mm × 8.0 mm × 0.50 mm (Chapter IV) for solution depletion with UV detection experiments and 2.0 mm × 2.0 mm × 0.25 mm and 4.0 mm × 4.0 mm × 0.50 mm for BET surface area analysis. The cut pieces were then dealloyed by placing them in a concentrated nitric acid (HNO₃) bath for 48 h and replenishing the acid solution after 24 h. (CAUTION!!! HNO₃ is a very strong acid, extra careful handling is advised) A glass holder was used in dealloying to ensure that all the surface of Au alloy plates were exposed to acid. Dealloyed monoliths were then rinsed thoroughly with Milli-Q water to neutral pH followed by rinsing

with ethanol. Np-Au monoliths were dried with N₂ gas and weighed. Np-Au monoliths were kept inside a vacuum desiccator until used.

2.4. Characterization of np-Au monolith

The exterior nanostructure of np-Au monoliths was characterized using SEM. The np-Au monolith was also broken into smaller pieces and the side of a cleaved fragment was imaged using SEM to characterize the interior nanostructure and confirm its nanoporosity. The elemental analysis was done using energy dispersive X-ray spectroscopy (EDS) at 15 kV. The specific surface area (S_{BET}) was determined using the Brunauer–Emmett–Teller (BET) method [9]. Sample size was a minimum of 1 g of np-Au monoliths as required by the instrument for sample with expected specific surface area of 3.0-9.9 m² g⁻¹. The pore volume versus diameter distribution was calculated by analyzing the adsorption branch of the isotherm using the Barrett-Joyner–Halenda (BJH) method [9].

2.5. Preparation of solutions

2.5.1. Preparation of solution of thiolated compounds

All thiolated compound used to form SAMs in this study were dissolved in HPLC grade ethanol. For Chapter III, 5 mM total of mixed α Man-C12-SH (0.10 mole fraction) with CH₃-PEG₄-SH or 5 mM total of mixed β Gal-C12-SH (0.10 mole fraction) with CH₃-PEG₄-SH was used to prepare mannose-PEG SAM (ManPEG SAM)- or galactose-PEG SAM (GalPEG SAM)-modified np-Au

monoliths, respectively. For Chapter IV and V, 1 mM of LA was used to prepare LA SAM-modified np-Au monolith.

2.5.2. Preparation of protein solutions

Lyophilized powder of proteins (lectins: Con A, PNA, SBA; glycoproteins: Ova, HRP; and BSA) were dissolved in binding buffer (10 mM Tris, 0.10 M NaCl, 1 mM CaCl₂, 1 mM MnCl₂ adjusted to pH 7.4). Concentrations of protein solutions were determined using the Beer-Lamberts equation $A_{280} = \epsilon_{280} \times C \times l$, where A_{280} is the absorbance at 280 nm using in UV-vis spectrophotometer (Simple Reads), C is the concentration at μM , l is the 1 cm path length and ϵ_{280} is the extinction coefficient of the protein at 280. ϵ_{280} values of proteins were calculated as the weighted sum of the ϵ_{280} values of Trp, Tyr and Cys using the proposed equation: $\epsilon_{280} (\text{M}^{-1} \text{cm}^{-1}) = \text{no. of Tryptophan} \times 5500 + \text{no. of Tyrosine} \times 1490 + \text{no. of Cysteines} \times 125$ [92]. The values were as follows: ϵ_{280} (Con A) = $0.129720 \mu\text{M}^{-1} \text{cm}^{-1}$ [92], ϵ_{280} (PNA) = $0.129720 \mu\text{M}^{-1} \text{cm}^{-1}$, ϵ_{280} (SBA) = $0.153600 \mu\text{M}^{-1} \text{cm}^{-1}$, ϵ_{280} (Ova) = $0.031525 \mu\text{M}^{-1} \text{cm}^{-1}$ [92]; and ϵ_{280} (BSA) = $0.042925 \mu\text{M}^{-1} \text{cm}^{-1}$ [92]. The protein solutions were immediately used after preparation.

2.5.3. Preparation of boronic acid solutions

3-aminophenylboronic acid (APBA) was dissolved in 60% (v/v) acetonitrile aqueous solution.

2.6. Surface modification of np-Au by flow method

Surface modification of np-Au was done by flow through method at 0.5 mL min⁻¹. Np-Au monoliths were placed inside the flow tube or flow cell perpendicular to the flow sandwiched by Teflon spacers. The sequence of solutions circulated through the SAM-modified np-Au monoliths are discussed below. The working volume was 1.5 mL using flow tube (Chapter III and V) or 3.0 mL using flow cell (Chapter IV). For flow through process that require detection, UV detector was set to the desired wavelength, zeroed using the reading for the solvent, and then tubing was emptied first and blown through with air to dry prior to circulation of solutions. Circulation of solutions were stopped when there was no increase or decrease observed in the absorbance reading.

2.6.1. Preparation of carbohydrate-modified np-Au monoliths

To prepare carbohydrate-modified np-Au monoliths, surface modification was done by flowing through these solutions in this sequence: ethanol wash (10 min) → circulation of 5 mM of mixed SAM solution (thiolated carbohydrate and PEG) (6 h) → ethanol wash (10 min) → Milli-Q water wash (10 min) → loading buffer wash (10 min).

2.6.2. Preparation of Con A-modified np-Au monoliths

To prepare Con A-modified np-Au monoliths, surface modification was done by flowing through these solutions in this sequence: ethanol wash (10

min) → circulation of 1 mM LA solution (3 h) → ethanol wash (10 min) → Milli-Q water wash (10 min) → circulation of 10 mM of DMTMM solution (30 min) → Milli-Q water wash (10 min) → circulation of 1 % (v/v) ethanolamine solution (30 min) → loading buffer wash (10 min) → circulation of 6 μM Con A solution (2 h) → loading buffer wash (10 min).

2.6.3. Preparation of boronic acid-modified np-Au monoliths

To prepare boronic acid-modified np-Au monoliths, surface modification was done by flowing through these solutions in this sequence: ethanol wash (10 min) → circulation of 1 mM LA solution (3 h) → ethanol wash (10 min) → Milli-Q water wash (10 min) → circulation of 10 mM of DMTMM solution (30 min) → Milli-Q water wash (10 min) → circulation of 1 % (v/v) ethanolamine solution (30 min) → 60% (v/v) acetonitrile wash (10 min) → circulation of 10 mM APBA solution (3 h) → loading buffer wash (10 min).

2.7. Characterization of loading and surface coverage by thermogravimetric analysis

Modified np-Au monoliths were air-dried then placed in a platinum weighing pan and heated inside the thermogravimetric analyzer from room temperature to 600 °C at a ramping rate of 20 °C min⁻¹. The carrier gas used was nitrogen, which was held at a flow rate of 40 mL min⁻¹. Prior to initiating the temperature ramp, N₂ gas was allowed to flow through the sample for 5–10 min. Initial mass, mass losses and weight change percent were obtained from the analysis. Surface coverage of the molecules on np-Au monolith surface was

calculated based on the net mass loss that was normalized to BET surface areas.

$$\text{Weight change \%} = \frac{\text{initial mass} - \text{final mass}}{\text{initial mass}} \times 100$$

$$\text{Surface coverage} \left(\frac{\text{molecules}}{\text{m}^2 \text{ np Au}} \right) = \frac{\frac{\text{mg loss} \times 6.02 \times 10^{23}}{\text{MW} \times 1000}}{\text{initial np Au mass} \times \text{BET surface area}}$$

In Chapter IV, powdered samples were also analyzed with TGA using the same condition but with scanning up to 1050 °C. Ash residues left in the pan after pyrolysis of proteins were sent to Atlantic Microlab, Inc. (Norcross, Georgia, USA) for CHN analysis.

2.8. Estimation of theoretical surface coverage of molecules on np-Au surface

Theoretical surface coverage of molecules was estimated by calculating the minimum and maximum expected numbers of molecules per m² of np-Au monolith. Minimum and maximum surface area of molecule was based on the smallest and largest area obtained using the dimensions of the unit cell based on the crystal structure reported of the molecule. For example, the reported crystal structure unit cell dimensions of LA are: a = 11.744 Å, b = 9.895 Å, c = 9.246 Å, where there were four LA molecules per unit cell [93]. Therefore, the three possible surface area of one LA molecule are 0.91, 1.09, and 1.16 nm² and the a complete and ordered coverage of LA molecules on Au surface would be in the range of 3.45 × 10¹⁸ – 4.40 × 10¹⁸ molecules m⁻². Similarly for Con A

molecule, the maximum possible surface coverage is estimated as 1.29×10^{16} – 1.82×10^{16} molecules m^{-2} assuming that Con A molecules lay flat and that they pack side-by-side. This is based on the unit cell dimensions of tetrameric Con A (PDB ID: 3CNA) $a = 63.15 \text{ \AA}$, $b = 86.91 \text{ \AA}$, $c = 89.25 \text{ \AA}$ [60] and assuming three possible surface areas per molecule of 54.8, 56.4 and 77.6 nm^2 .

2.9. Characterization of loading by in situ solution depletion method

The amount of molecules loaded on np-Au monoliths were estimated by determining the difference between the final and initial concentration (ΔC) of the circulating solution monitored by UV detector. UV detector absorbance readings were acquired and recorded at the frequency of 1 Hz (1 reading per second). Data logger readings were converted to concentrations by using a factor obtained from the slope of the linear regression of calibration curve (analytical concentrations vs. absorbance plot). The factors are: LA ($\lambda_{max}=330 \text{ nm}$) = 0.0502 mM^{-1} , Con A ($\lambda_{max}=280 \text{ nm}$) = 0.0329 , APBA ($\lambda_{max}=300 \text{ nm}$) = 0.217 mM^{-1} , adenosine ($\lambda_{max}=260 \text{ nm}$) = 2.980 mM^{-1} , and deoxyadenosine ($\lambda_{max}=260 \text{ nm}$) = 2.850 .

Loading was estimated by:

$$\frac{\text{molecules}}{m^2 \text{ np Au}} = \frac{\Delta C \times \text{volume of circulating volume} \times (6.02 \times 10^{23})}{\text{mass of np Au} \times \text{BET surface area}}$$

2.10. Separation of Con A from its mixture with SBA

A 1.5 mL mixture of 10 μ M Con A and 10 μ M SBA was circulated through ManPEG SAM-modified np-Au monoliths until saturation was observed as monitored by a UV detector at 280 nm. UV-vis scans of the Con A-SBA solution before and after the circulation were obtained using a UV-vis spectrophotometer. Afterwards, the np-Au monoliths were washed for 10 min. A 2 mL of elution buffer (0.10 M α -methyl mannopyranoside dissolved in loading buffer) was flowed through while monitoring at 495 nm followed by washing again with the loading buffer.

2.11. Elution of captured Ova

Capture and elution was characterized by flowing through np-Au monoliths at 0.5 mL min⁻¹ a series of solution: loading buffer \rightarrow 2 mL of Ova solution \rightarrow loading buffer \rightarrow 2 mL elution buffer \rightarrow loading buffer. Elution buffer is 0.1 M α -methyl mannopyranoside dissolved in loading buffer. The A_{280} of the solution flowing through was recorded at 1 Hz.

2.12. Trypsin digestion of protein

Digestion of Ova, HRP and BSA was done by mixing equal volume of 2 mg mL⁻¹ protein and 80 μ g mL⁻¹ trypsin, each dissolved in 50 mM ammonium bicarbonate followed by incubation at 37 °C for 16 h.

2.13. SDS-PAGE analysis

SDS-PAGE analysis was done using a precast 4-20% polyacrylamide gel. The sample to be analyzed and sample buffer (20:1 Laemmli: β -mercaptoethanol) were mixed in 1:1 volume ratio. The mixture was heated using a hot water bath at 97 °C for 5 minutes and cooled down afterwards. 15 μ L of each sample mixture and molecular weight ladder were loaded into the wells of the polyacrylamide gel placed in a cassette. The cassette was then placed inside the Biorad Mini-Protean Tetra Cell and run with a running buffer (25 mM Tris, 192 mM Glycine, 0.1% SDS adjusted to pH 8.3) at 120 V. The electrophoresis was stopped when the sample reached approximately 1 cm from the bottom of the gel. The gel was taken out of the cassette and washed with Milli-Q water and placed in a staining container. The gel was immersed in a staining solution (250 mg per 100 mL of Brilliant Blue R250 dissolved in aqueous solution of 40% methanol, 7% acetic acid) overnight. The gel was de-stained using de-staining solution (aqueous solution of 40% methanol, 7% acetic acid). The gel were finally rinsed with Milli-Q water, placed in between of two transparent films, and scanned using a desktop scanner.

2.13.1. Extraction of Ova from a mixture using Con A-modified np-Au monoliths

A batch of 8 pieces of Con A-modified np-Au monoliths was prepared. At the end of each 30 min cycle of circulation of 5 μ M Ova and 15 μ M BSA mixture, an aliquot was taken and kept. Two monoliths were initially used and

after each cycle, the number of substrates was increased by adding two more monoliths. The aliquots of protein mixture were analyzed through SDS-PAGE.

2.13.2. Characterization of glycopeptide extraction using boronic acid-modified np-Au monoliths

A batch of boronic acid-modified np-Au monoliths was prepared. Trypsin digested Ova in phosphate buffer pH 8.5 was circulated through these monoliths until saturation monitored by a UV detector at 280 nm. The monoliths were washed for 10 min prior to circulation of acetate buffer pH 2.7. Aliquots of the digested solution before and after circulation and of the elution buffer were run and analyzed by SDS-PAGE.

2.14. Preparation of borohydride baths

The recipe of borohydride baths was based from the reported literature [94]. The $\text{KAu}(\text{CN})_2$ and/or $\text{KAg}(\text{CN})_2$ were dissolved separately from $\text{NaCN}+\text{KOH}+\text{NaBH}_4$ solution. The solvent used was Milli-Q water. The solutions were mixed together and stored in a dark bottle.

2.15. Electroless deposition of Au and Au-Ag alloy

The substrate 1 cm diameter glass coverslips were cleaned with piranha solution (3:1 mixture of concentrated H_2SO_4 :30% H_2O_2 ; CAUTION!!! Piranha solution is highly corrosive and an extremely powerful oxidizer, extra careful handling is advised) and rinsed with Milli-Q water followed by ethanol. Cleaned glass plates were incubated in 5 mM APTES solution in ethanol overnight

followed by washing with ethanol. The substrates were then dried inside the oven for 30 mins at 70 °C. The APTES-modified glass plates were gold-sputtered for 50 s at 10 mA, 60 millitorr. The sputtered glass plates were then electrolessly deposited with Au or Au-Ag alloy.

Electroless deposition was done using 500 µL of borohydride bath. The bath was placed in 5 mL beaker and then put in a hot water bath pre-heated at desired temperature. The gold-sputtered glass plate was immersed in the borohydride bath to start the plating. The temperature was kept during plating and monitored using the attached thermometer. After the desired plating time, the plated glass plate was removed from the bath and washed with Milli-Q water and ethanol. The washed plated substrates were dried inside a vacuum desiccator. The microstructure and elemental analysis of the plated Au or Au-Ag film was characterized using SEM and EDS spectroscopy, respectively.

2.16. Data analysis

All data calculations and graphing were done using Sigma Plot 12.0. Analysis of protein gel band sizes and intensities was done using ImageJ (imagej.nih.gov/ij/). Calculation of area under the curve (AUC) was done using GraphPad Prism 6.07.

CHAPTER III. Carbohydrate-modified nanoporous gold monolith as affinity support material for the separation of lectins

3.1. Introduction

Lectins are proteins derived from plants or animals that contain carbohydrate-binding domains that can selectively recognize specific carbohydrate structures. Procedures and tools to capture, screen and separate lectins are important in the on-going development of glycomics. Also known as glycans, these carbohydrates are attached to proteins, lipids or to other carbohydrates to form glycoconjugates. Glycoproteins, the most studied glycoconjugate, have glycans being covalently attached during glycosylation. As mentioned above that during this process, some glycan structures and composition could be altered and were found related to mammalian diseases such as cancer. Therefore, glycomics has a true importance in medical research, and one of the most utilized tools in this field are lectins [95].

Purification of low abundant proteins are significant steps in proteomics [96]. The whole protein purification process consist of series of separation and detection methods. In purification of proteins extracted from plants, the process usually commences with the precipitation and chromatography techniques, which are actually the limiting steps [97]. Purification of lectins is important prior to investigating its specificity and possible use in screening carbohydrates. Purified lectins are useful in glycoassays such as lectin microarrays [98]. The main challenge in purification of proteins is its relatively low abundance in a very complex environment. Complexity is due to the variation in sizes and charges of the components in the sample. In addition to this is the requirement

of retaining the biochemical and biological activity of the protein after the purification method.

Along with the development of novel separation methods of proteins is the invention and innovation of materials that could be used as column materials, extraction media or stationary phases in chromatographic separations. These materials are expected to have high retention, selectivity and stability to be useful in a separation process. Generally, a good substrate should have minimal non-specific interactions with proteins, and be mechanically and chemically stable to conditions used during capture and elution of the analyte, have fairly uniform accessible area for the entry and exit of large macromolecules, and be rigid [99]. The conventional materials being used in separation of proteins are porous particulate media that could be placed inside a column. Then monolithic materials have been discovered and showed faster and more efficient separations due to their porosity, highly permeable “no-discontinuity” surface and ease, economical and reproducible preparation [100]. These separation materials are usually made of organic polymers and inorganic silica. Recently, different inorganic materials have been reported [101]. Chromatographic macroporous monoliths are best characterized by large pores for convection and a connected network of shorter, smaller pores for diffusion [102]. Macroporous materials are suitable chromatographic substrates in applications employing liquid flow-through immobilization of ligands and subsequent binding of biomolecules [103]. Monolithic form of np-Au has three-dimensional, connective macroporous structure, pores ranging from 10 to 100 nanometers and therefore suitable for liquid flow-through and also leave adequate space for immobilization of ligands and subsequent binding of

biomolecules [104]. In addition, biocompatibility of np-Au monolith makes it suitable in protein separations [105].

3.2. Results and discussion

3.2.1. Characterization of np-Au monoliths

Our lab previously reported the preparation of np-Au monoliths by selective dissolution of commercially available gold alloy plates in nitric acid [106], and these were then surface modified with C₁₈-SH [9]. Scanning electron microscope (SEM) images of the dealloyed 8 mm × 8 mm × 0.5 mm np-Au monoliths revealed interconnected ligaments and pores both in the exterior and interior of the monolith (Figure 3.1A). Pore size distribution using Barrett–Joyner–Halenda (BJH) analysis of the adsorption branch resulted in a pore diameter range of predominantly 80–120 nm (Figure 3.1B) and thus the material would be considered as macroporous by the IUPAC definition (> 50 nm). Through analysis using the Brunauer–Emmett–Teller (BET) method, the specific surface area of the monoliths was determined to be $6.9 \pm 0.5 \text{ m}^2 \text{ g}^{-1}$ (n = 3). Dealloying of the alloy plate with a calculated geometric surface area of $1.44 \times 10^{-4} \text{ m}^2$, increased the surface area by 8,403× producing a np-Au monolith with a mass of 175 mg and a surface area of 1.21 m². Elemental analysis of the np-Au monolith using EDS showed a composition of almost 99% gold after the dealloying process (Figure 3.1C). Characterization of cleaved np-Au monoliths modified with proteins via flow method using tapping mode atomic force microscopy (AFM) revealed immobilization of significant amount of proteins in the interior of the monolith [106]. The average pore size of these np-

Au monoliths was controllable by thermal annealing, i.e., the porosity of all free standing np-Au structures decreases as the heat treatment temperature increases [9]. Our lab also developed an electrochemical method of annealing np-Au by potential cycling in the paper “Electrochemical annealing of nanoporous gold by application of cyclic potential sweeps” published in 2015 in Nanotechnology [107].

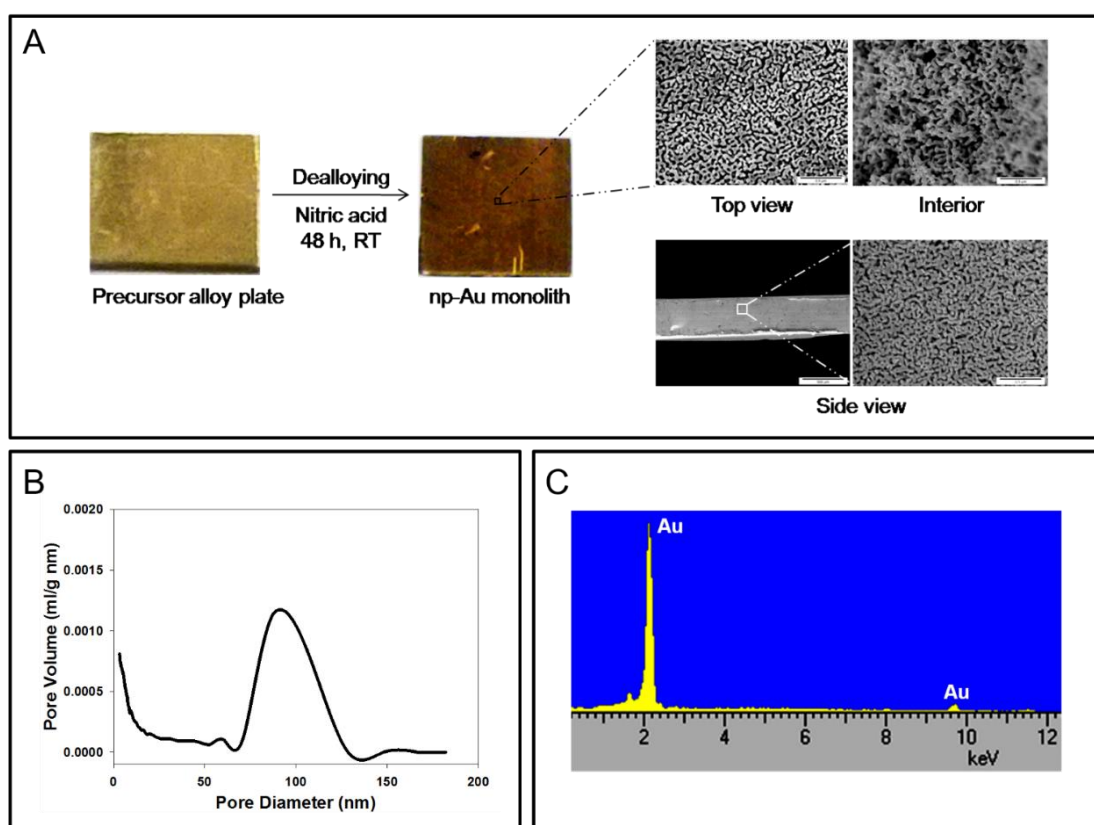


Figure 3.1. Preparation and characterization of np-Au monolith. (A) Dealloying of precursor alloy plate (42% Au, 20% Ag, 38% Cu) in nitric acid at room temperature to produce np-Au monolith. SEM images of the top and side views of the exterior and the interior portion of an 8 mm × 8 mm × 0.50 mm np-Au monolith. All scale bars are 0.5 μm except for the side view (left image) which

is 500 μm . (B) Pore size distribution obtained by Barrett–Joyner–Halenda (BJH) analysis of the adsorption branch of the isotherm. (C) EDS spectra of np-Au monolith (at 15 kV).

3.2.2. Lectin-carbohydrate interactions on np-Au monolith characterized by thermogravimetric analysis

Our lab reported in 2013 in *New Journal of Chemistry* on “Lectin-carbohydrate interactions on nanoporous gold monoliths” [108]. In this reported study, we used thermogravimetric analysis (TGA) in determining the amount of loading of thiolated carbohydrate molecules on np-Au monolith. Subsequent loadings of lectin bound to the immobilized carbohydrate ligand were also assessed using TGA. TGA is a destructive analytical method, which allows for quantitative measurement of the change or rate of change in the weight of a material as a function of temperature or time. TGA has been used to quantify the loading of dodecanethiol monolayers formed on gold nanoparticles [109]. TGA has also been used to determine the temperature stability of the octadecylamine monolayer coating gold nanoparticles [110]. Our lab has previously reported the use of TGA to analyze the one-step decomposition of octadecanethiol on np-Au [9]. Key results this reported study that motivated the current study are:

- Np-Au monoliths were successfully modified by flow-through method confirmed by the mass losses obtained from TGA analysis, therefore quantification of molecules loaded into the monoliths was possible to determine.

- Loading kinetics of 8-mercaptooctyl α -D-mannopyranoside (α -Man-C₈-SH) on np-Au monoliths characterized by TGA showed two stages: (1) a very fast chemisorption step and (2) a slower assembly step. Using flow-through method, saturation of loading was first observed after 6 h modification.
- Modification of np-Au monolith surface with mixed SAMs of 8-mercaptooctyl α -Man-C₈-SH and 8-mercapto-3, 6-dioxaoctanol (HO-PEG₂-SH) showed minimal non-specific binding of Con A, i.e., reduced the possible binding of Con A onto bare np-Au surface. Using mixed SAMs of α -Man-C₈-SH with octadecanethiol (C₁₈-SH) showed significant non-specific adsorption of Con A.
- Mannose-presenting SAMs in np-Au retained selectivity for Con A, evidenced by the greater mass loss due to subsequent loading of Con A as compared with PNA or IgG.
- Comparing different mole fractions of α -Man-C₈-SH in the mixed SAMs solutions of α -Man-C₈-SH and HO-PEG₂-SH showed 0.10 mole fraction as the greatest Con A loading possibly due to a surface density of mannose created on the np-Au surface that is more conducive to polyvalent interactions and enhanced lectin binding.
- Flowing a solution of methyl α -D-mannopyranoside through the np-Au monolith eluted the captured Con A molecules by mannose ligands in the SAM.

The study proposed that monitoring the capture and elution of lectins using a UV detector at 280 nm could provide an in situ characterization of the loading of the lectin to and release from carbohydrate-modified np-Au monoliths. The

absorbance at 280 nm (A_{280}) of proteins was due to the tryptophan (Trp) and tyrosine (Tyr) residues and to the disulphide bonds formed between cysteine residues of the peptides to form cystine residues (Cys). Tetrameric Con A has 16 tryptophan (Trp) and 28 tyrosine (Tyr) residues [111].

3.2.3. Preliminary assessment of flow system in determining loading and surface coverage of molecules on np-Au monoliths by in situ solution depletion method

The flow cell system used in this study consisted of a flow tube connected in series with peristaltic pump and UV-visible spectrophotometer (UV-vis detector) by polytetrafluoroethylene (PTFE) tubing (Figure 3.2). The UV-vis detector was connected to a data logger with a USB port terminal cable readily available to be attached to a laptop. The flow tube is made of a 1.5 in 3 mm ID long PTFE tubing with customized Teflon spacers arranged inside perpendicularly to the flow. The $2.5 \text{ mm} \times 2.5 \text{ mm} \times 0.50 \text{ mm}^3$ np-Au monoliths were placed in between of the spacers to provide steady and full-surface access to the flowing through solution (Figure 3.2).

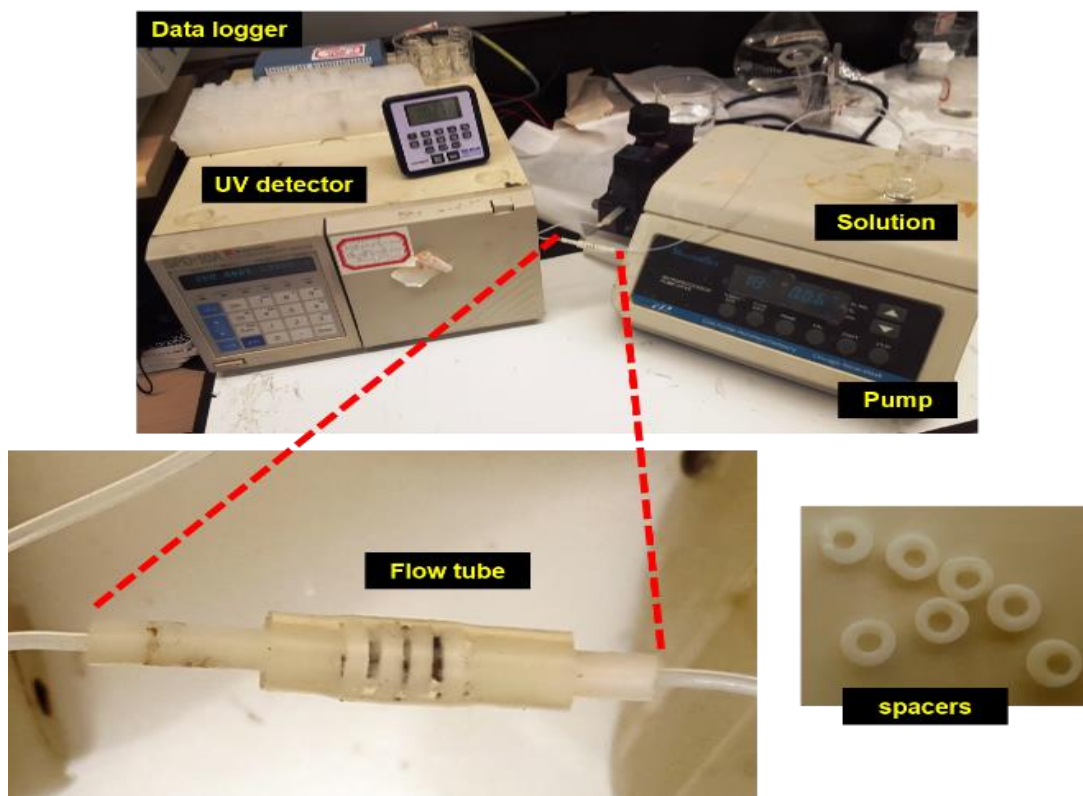


Figure 3.2. Flow system set-up consists of pump, UV detector-data logger system, and flow tube connected in series. Np-Au monoliths were placed in between of spacers and perpendicular to the flow. The working volume is 1.5 mL at 0.5 mL min^{-1} . UV reading acquisition is at 1 Hz.

To evaluate the method of monitoring the absorbance of circulating solution, a thiolated compound that has observable maximum absorbance was used. By doing a UV-vis scan of lipoic acid (LA) solution in ethanol, a maximum absorbance at 330 nm (λ_{max}) were observed (Figure 3.3A). This should be due to the strained five-membered cyclic disulfide structure of LA [112]. Different analytical concentrations of LA solution was plotted versus their respective absorbance at 330 (A_{330}) (Figure 3.3B). Concentration and A_{330} of LA solution have good linear correlation for the range of concentration up to 4 mM. From

this plot, an experimental extinction coefficient (ϵ_{330}) was determined from the slope of the linear regression fit to the plot, and the value was $0.1617 \text{ mM}^{-1} \text{ cm}^{-1}$. A 2 mL volume of 1 mM LA solution was flowed through a 70 mg np-Au until saturation was observed (Figure 3.3C). Saturation means there is no longer any change in the UV detector reading of the circulating solution. UV readings were multiplied by a numerical factor 0.0502 obtained from the calibration curve, i.e., the slope of the linear regression fit to the plot of different analytical concentration of LA solutions versus UV detector readings at 330 nm (Figure 3.3D). The loading of LA molecules on this np-Au was assessed by the difference of the final from the initial concentration of the circulating 1.5 mL LA solution and was determined to be 5.11×10^{17} molecules LA. Surface coverage of LA molecules on this np-Au monolith (see Section 2.10) was determined to be 1.06×10^{18} molecules m^{-2} np-Au. Based on theoretical estimates (see Section 2.8), a 70 mg np-Au could have maximum surface coverage within the range of 1.78×10^{18} - 2.28×10^{18} molecules m^{-2} np-Au. The observed surface coverage suggests that the LA molecules assembled in a disorderly fashion on np-Au monolith surface with possible incompleteness of coverage. Reported surface coverages of LA on flat gold surfaces are $3.00 \times 10^{-10} \text{ mol cm}^{-2}$ (1.81×10^{18} molecules m^{-2}) [113], $3.50 \times 10^{-10} \text{ mol cm}^{-2}$ (2.11×10^{18} molecules m^{-2}) [114] and $2.42 \times 10^{-10} \text{ mol cm}^{-2}$ (1.46×10^{18} molecules m^{-2}) [6].

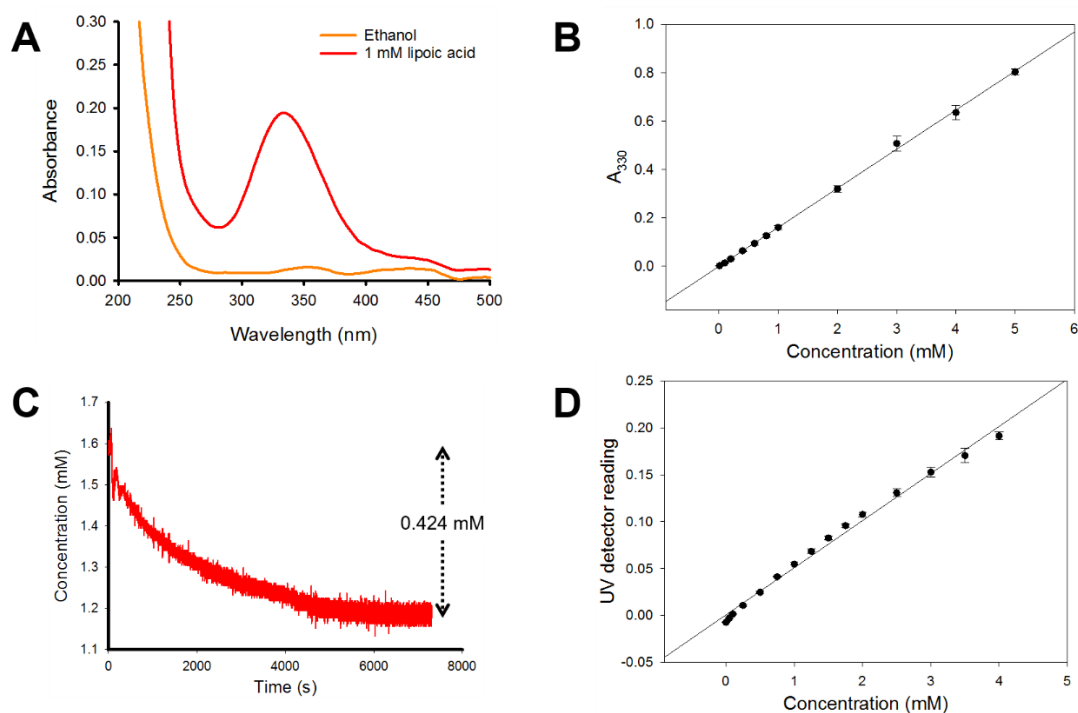


Figure 3.3. Loading of lipioic acid molecules on np-Au monolith surface by flow through method monitored by a UV detector. (A) UV-vis scan of 1 mM LA solution in ethanol showing a maximum absorbance at 330 nm. (B) Experimental determination of ϵ_{330} of LA solution that is equal to $0.1617 \text{ mM}^{-1} \text{ cm}^{-1}$, which is the slope of the linear regression of analytical concentration versus absorbance plot. (C) Loading curve of LA on np-Au monolith as recorded by a UV detector at 330 nm. (D) Calibration curve of analytical concentration versus UV detector-data logger reading to obtain a factor of 0.0502 mM^{-1} to convert data logger reading to concentration.

3.2.4. Preparation of carbohydrate-modified np-Au monoliths

Two different carbohydrate-modified np-Au monolith were prepared for this study. One is modified with mannose-containing thiolated compound $\alpha\text{Man-C}_{12}\text{-SH}$ (refer to as ManPEG SAM) and the other is with galactose-containing

galactopyranoside (β Gal-C12-SH), and thiolated methyl-polyethylene glycol MT(PEG)₄ used in preparing carbohydrate-modified np-Au monoliths. (B) TGA thermograms for determination of loading of carbohydrate SAMs on np-Au monolith. The temperature was ramped at 20 °C min⁻¹.

3.2.5. Characterization of capture of Con A using ManPEG SAM-modified np-Au monolith

The loading of Con A molecules into SAM-modified np-Au monolith, was characterized by the in situ solution depletion method. The change in concentration of the circulating Con A solution was observed at $\lambda_{\text{max}} = 280$ nm (Figure 3.6A); the absorbance was due to the tryptophan (Trp) and tyrosine (Tyr) residues and to the disulphide bonds formed between cysteine residues of the peptides to form cystine residues (Cys). Tetrameric Con A has 16 tryptophan (Trp) and 28 tryrosine (Tyr) residues [111]. All the data logger readings were converted to concentrations by multiplying by a factor 0.0329 μM^{-1} obtained from the calibration curve (Figure 3.6B). A 1 μM Con A solution in binding buffer was circulated through flow tube without np-Au monolith as negative control and those containing bare np-Au, PEG SAM-modified np-Au monolith (no carbohydrate), GalPEG SAM-modified np-Au mono ManPEG SAM-modified np-Au monolith (Figure 3.6C). The mass of one-piece np-Au monoliths used was in the range of 34 to 40 mg per piece. The observed surface coverages are summarized in Table 3.1. The low binding of Con A towards PEG SAM-modified np-Au monolith showed the capability of these PEG molecules to resist protein adsorption and therefore being suitable for use as

spacers to reduce non-specific adsorption. The lower loading of Con A to GalPEG SAM-modified than ManPEG SAM-modified np-Au monolith suggest specificity of Con A towards mannose ligands on np-Au surface. However, the relatively higher than desirable amount of Con A loading on GalPEG SAM should be further investigated. A higher mass of np-Au monolith (2-3x more) or a higher concentration of Con A solution (up to 6 μM) could be used to create a more pronounced depletion of the solution concentration. The decrease in loading of Con A when the np-Au surface was modified with ManPEG SAM (reduced by half compared to bare np-Au) showed specific binding of Con A to the formed SAM.

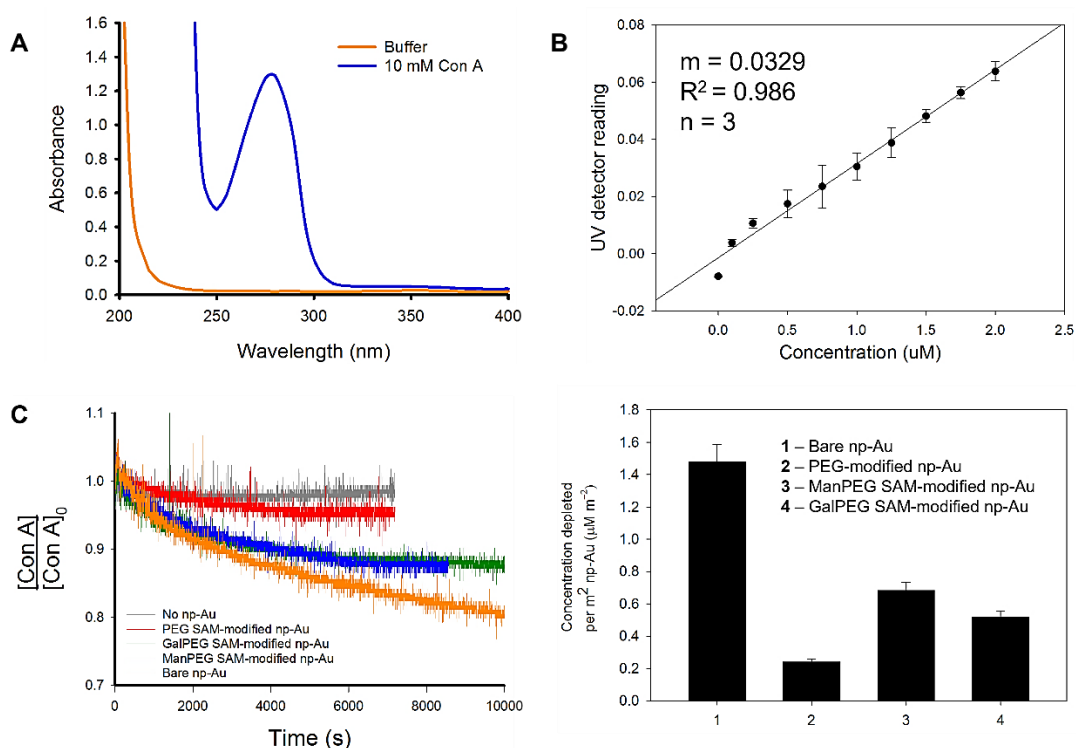


Figure 3.5. Loading of Con A molecules on bare and SAM-modified np-Au monolith surface by flow through method monitored by a UV detector. (A) UV-vis scan of 1 μM Con A solution in loading buffer (Tris-NaCl pH 7.4) showing a maximum absorbance at 280 nm. (B) Calibration curve of analytical

concentration versus UV detector-data logger reading to obtain a factor of $0.0329 \mu\text{M}^{-1}$ to convert data logger reading to concentration. (C) Loading curves of Con A on bare and SAM-modified np-Au monoliths as recorded by a UV detector at 280 nm.

Table 3.1. Surface coverages of Con A on bare and SAM-modified np-Au monoliths.

	Surface coverage (molecules Con A m^{-2} np-Au)
Bare np-Au	1.34×10^{15}
PEG SAM-modified np-Au	2.18×10^{14}
ManPEG SAM-modified np-Au	6.17×10^{14}
GalPEG SAM-modified np-Au	4.67×10^{14}

All surface modification of np-Au monoliths were done by flow-through method for at least 6 h for SAMs and until saturation for Con A. It is also worth reporting the observation that during the preliminary study where np-Au monolith was modified by incubation into solutions instead of flow-through method, and then transferred to the flow tube for further use as substrate, there were less or almost no Con A loading observed. In situ modification of np-Au monolith from SAM formation to immobilizing ligand could preserve the SAM on the np-Au monolith and limit the possible damage or degradation of SAM molecules on np-Au surface.

3.2.6. Elution of captured Con A by ManPEG SAM-modified np-Au monolith

Thermogravimetric analysis was done to characterize the release of captured Con A from the substrate modified by 1:3 molar ratio of α Man-C₁₂-SH:CH₃-PEG₄-SH. Con A is a lectin that has specificity to α -mannose and α -glucose sugar units of glycans. Therefore, the binding can be reversed by exposure to a high concentration of mannose [115] and α -methyl mannopyranoside [69] monosaccharides being used as components of an eluting solution. Urea has also demonstrated a very effective elution capability with the consequence of denaturing the protein analyte [70]. In our previous study it was determined that 0.10 M α -methyl mannopyranoside solution was able to elute ~80% of the captured Con A (Figure 3.6A). Further in this study, 0.50 M mannose solution and 0.80 M urea solution were able to elute ~51% and 90% of the bound Con A, respectively (Figure 3.6B and C).

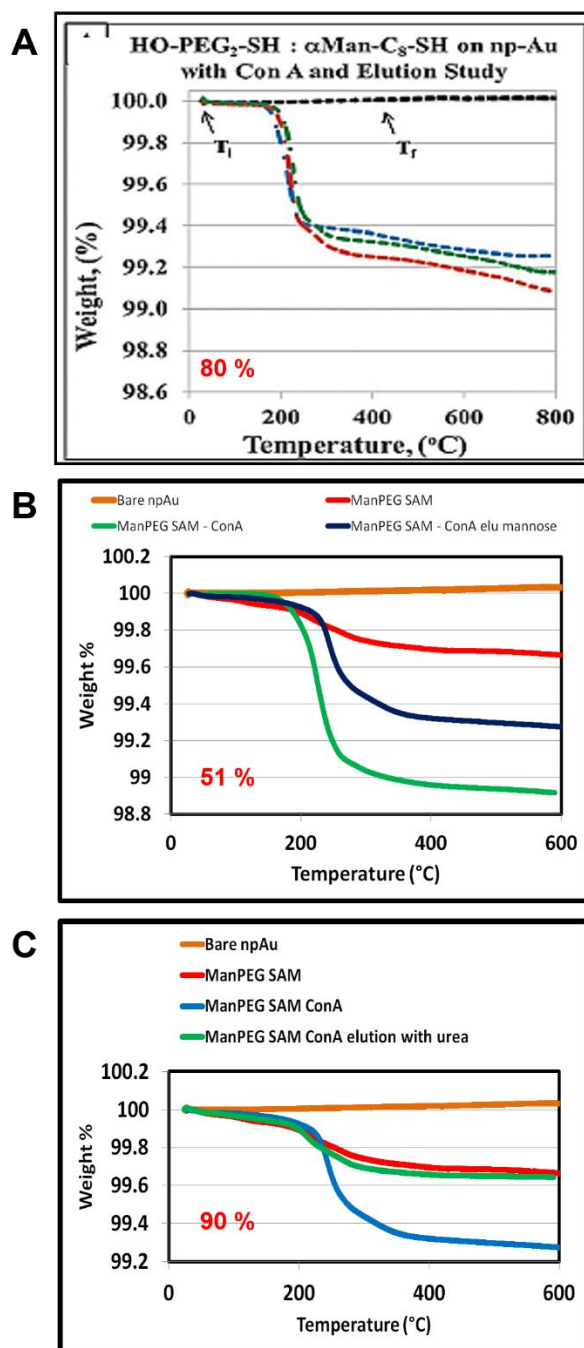


Figure 3.6. TGA thermograms showing the capture and elution of Con A using ManPEG SAM-modified np-Au monoliths by using (A) 0.010 M α -methyl mannopyranoside [108], (B) 0.50 M mannose, and (C) 0.80 M urea. The temperature was ramped at 20 °C min⁻¹.

3.2.7. Capture and elution of Con A using ManPEG SAM-modified np-Au monoliths

A simultaneous capture and elution of Con A was carried out using in situ prepared ManPEG SAM-modified np-Au monoliths. The change in concentration of the circulating solution was monitored and recorded until no change was observed. The concentration of Con A solution was depleted by $0.271 \mu\text{M}$ for a circulation of almost 3 h. The depletion was fast for the first 30 min and gradually decreasing in rate until saturation was reached. The substrate was washed by buffer for 10 min and the elution buffer containing 0.10 M α -methyl mannopyranoside was circulated. The elution solution attained a final concentration of $0.255 \mu\text{M}$. The working volume for both loading and elution was 1.5 mL . Therefore, this run eluted almost 94% of the captured Con A. The elution procedure took 1.5 h to reach saturation. In situ monitoring using a UV detector allowed optimized capture and elution of analyte to separate (Figure 3.7). Increasing the flow rate in elution process could enhance the turn-out at shorter period of time.

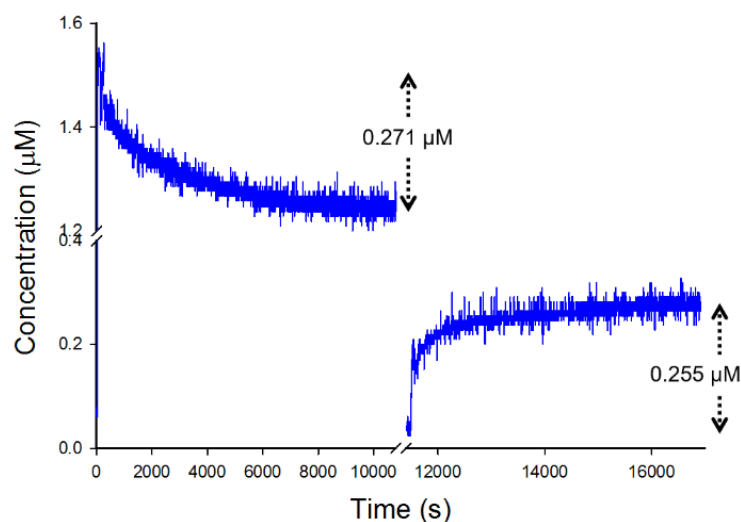


Figure 3.7. In situ monitoring of capture and elution of Con A using ManPEG SAM-modified np-Au monolith substrate. The A_{280} readings were acquired at 1 Hz. The circulation of Con A solution was stopped when there were no more decrease or increase in A_{280} reading.

3.2.8. Separation of Con A from its mixture with SBA

To test these developed carbohydrate-modified np-Au monoliths in separation of lectins, ManPEG SAM-modified monoliths were used to specifically capture Con A from its mixture with soybean agglutinin (SBA). SBA, like Con A, is a homotetramer lectin with molecular weight of 120 kDa [116]. Immunochemical studies of SBA determined its specificity to terminal α -linked 2-acetamido-2-deoxy-D-galactopyranosyl or to α - or β -D-galactopyranosyl residues [117]. The monosaccharide inhibitor of binding are acetyl-n-galactosamine and to a lesser extent by D-galactose. Unfolding studies of SBA and Con A showed higher conformational stability of SBA than Con A and was determined to be largely due to the substantial differences in their degrees of subunit interactions [118]. To characterize the separation, we used fluorescein isothiocyanate (FITC)-conjugated Con A that has two prominent maximum absorbance at 280 nm (A_{280}) and 495 nm (A_{495}) (Figure 3.8A). SBA, on the other hand, only showed maximum absorbance A_{280} . A 10 μ M equimolar solution of FITC-Con A and SBA were circulated through the ManPEG SAM-modified np-Au monoliths until saturation monitored at 280 nm. The UV-vis scan of the solution after the circulation was obtained and there was a decrease in both A_{280} and A_{495} of the solution (Figure 3.8B). After washing, the flow tube

was placed before the detector, and monitored the A_{495} of flowing through solution. The sequence of the solution being flowed through was: loading buffer → 2 mL 0.10 M α -methyl mannopyranoside in loading buffer → loading buffer. Chromatogram showed initial peak obtained due to the detected non-specifically adsorbed Con A being washed off from the substrate. The next peaks obtained were due to the eluted Con A captured by the mannose-modified np-Au monolith substrate (Figure 3.8C).

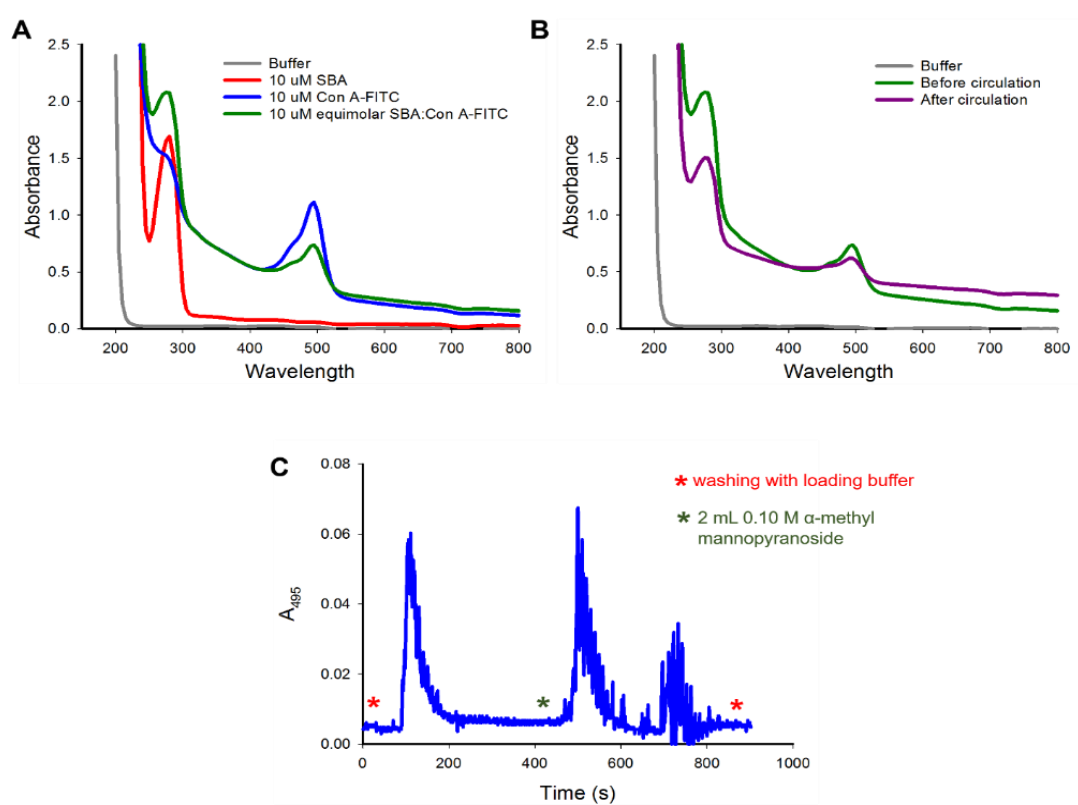


Figure 3.8. Separation of Con A from SBA using ManPEG SAM-modified np-Au monolith. (A) UV-vis scan of Con A-FITC and SBA alone and their equimolar mixture. (B) UV-vis scan of the Con A-FITC – SBA mixture before and after circulation through ManPEG SAM-modified np-Au monoliths. (C) Chromatogram of washing and elution of captured Con A using 2 mL 0.10 M α -

methyl mannopyranoside detected by UV spectrophotometer at 280 nm at 1 Hz.

3.3. Conclusion

There is a need in glycomics for an efficient and effective methods of characterizing new discovered lectins. This is because lectins are very useful tool in glycobiology and glycomics. Lectins are used in enzyme-linked immunosorbent assay (ELISA) measurements of glycan determinants, cell agglutination (blood typing), cell sorting and in glycoconjugate purification. Characterization of lectins involved extraction and purification of lectins, hemagglutination and inhibition assays to determine lectin activity and specificity, determination of the molecular weight and the effect of pH and temperature on protein stability, amino acid analysis, and ligand binding study [119]. Purification steps are considered the limiting steps of the whole process. One of the main focus in developing purification procedures is the materials used in designing separation columns.

The latest development in designing separation columns is the use of monolithic materials. Monolithic materials are single-porous materials that have an interconnected ligament structure that limits the void volume inside the column, thus increasing the efficiency without sacrificing the permeability. The popular materials being used are silica and organic polymers. Innovation of these materials are by modifying the porous monoliths with gold nanoparticles (GNPs) to provide formation of SAMs of functional group-terminated alkanethiols that could be more versatile in separations. For example, separation of short peptides by capillary electrochromatography (CEC) used

GNP-modified porous polymer monoliths that has exchangeable chemistries i.e., varying functionalities such as carboxylic acid, hydroxyl, or amine of the alkanethiols [120]. Replacing inorganic coated columns with inorganic monolithic columns offers greater surface coverage of the inorganic material while maintaining good mass transfer and flow-through properties.

Np-Au monoliths described in this study have “macropores” that can facilitate SAM formation and entry and exit of lectins for the separation. This study extend our previous work in using TGA in the characterization of loading of molecules on the interior and exterior surface of np-Au monolith. The detected significant amount of SAM and lectin molecules loaded into the np-Au monoliths provide the evidence that the inner surfaces were reached using flow-through method of the surface modification. Flow through system that utilizes UV detection facilitates in situ monitoring of loading and could be possibly used in studying the kinetics of lectin binding to carbohydrates immobilized on np-Au surface. Moreover, this method could also maximize the substrate’s affinity ligands during loading and can assure maximum recovery of the captured analyte. The methods developed in this study were optimized based on the properties of the substrate and analyte. For example, the wide difference in melting temperature of Au and molecules such as thiolated compounds and proteins enable the use of TGA. The suggested dilute effective concentration of thiolated compounds to form SAMs on Au surface allowed the in situ characterization of loading of these molecules using even a small piece of substrate down to 34 mg. SAM preservation could also be achieved by doing in situ surface modifications. Np-Au monoliths has versatility to be modified with thiolated compounds that can carry the necessary ligands for separation. In this

case, synthesized thiolated saccharides with a 12-carbon spacer chain length was utilized for lectin capture and release. Specificity was attained due to the known lectin-carbohydrate interactions and optimized compositions of the mixed SAMs. This study exemplifies the use of developed carbohydrate-modified np-Au monoliths in separations.

CHAPTER IV. Selective capture of glycoproteins using lectin-modified nanoporous gold monolith

4.1. Introduction

Glycoproteins have attached oligosaccharide units called glycans, and belong to the collective group known as glycoconjugates. Glycans are synthesized to attach proteins to form glycoprotein in the process of glycosylation. The significance of glycoproteins are related to the aberrant glycosylation, i.e., changes in oligosaccharide structure upon biosynthesis can be related to diseases such as cancer [32]; therefore, glycoproteins are now used as cancer biomarkers [121,122]. As discussed above, the structures of glycans are complex, heterogeneous and isobaric. This poses a challenge in glycomics where elucidation and identification of glycan structure and the glycosylation sites of glycopeptides are required in determining their respective biological functions [123]. Various methods are used in glycan analysis such as mass spectrometry (MS) [124-126], nuclear magnetic resonance (NMR) [127], electrochemistry [128], UV detection of derivatized glycans [129] and fluorescence imaging [130]. Comprehensive glycan analysis using microarrays of lectins [131] and antibodies [132] has also been developed. Prior to analysis, several preparative methods are usually needed that may include separation, isolation and enrichment in order to increase the abundance of glycoproteins, glycopeptides and glycans in complex samples such as serum, plant and cell tissue extracts and cultured cells. Preparative methods in glycomics include sodium dodecyl sulfate polyacrylamide gel electrophoresis (SDS-PAGE) [133], capillary electrophoresis (CE) [134] and chromatographic separation methods

such as liquid chromatography (LC) [135] and capillary electrochromatography (CEC) [136].

One major factor that determines the success and efficiency of chromatographic separation is the optimization of the stationary phases in which different ligands are attached to a matrix or substrate that can selectively capture and isolate target analytes. In separation of intact glycoproteins, a popular and widely used method is lectin affinity chromatography (LAC). Due to the high selectivity of lectins to specific glycan structures, lectins are now used as binding ligands of affinity matrices in purification of glycoproteins and glycopeptides and also in cell separations. To create the stationary phase, lectins are commonly covalently immobilized to the surface [137]. Due to the selectivity of lectins and improved immobilization techniques, LAC is the most useful and efficient mode of separation of glycans and glycoproteins. For example, multi-lectin affinity columns were developed using different lectins for comprehensive capture of serum glycoproteins [138,139].

As discussed above, the current approach in glycomics is the development of more sensitive, efficient, and faster methods of glycan separation and analysis. One specific strategy is the development of new materials to be used in designing separation columns and extraction media. The conventional packed columns with uniform size porous particles have been traditionally used in these chromatographic separations. A new generation of separation media called monolithic materials has become an interesting option due to their design that allows faster, more efficient and versatile separations of glycans, glycopeptides and glycoproteins [140]. Monolithic columns are usually prepared in situ fused with silica capillary tubes by co-polymerization of

cross-linking and functional monomers together with porogens and initiators. Other monoliths are silica-based and prepared via sol-gel synthesis. The applications of these monoliths are exclusive depending on their morphology and structure. They also have respective disadvantages; for example, organic polymer-based monoliths swell in organic solvents whereas silica-based monoliths are limited by their effective pH ranges. Therefore, rather than choosing the material to use in designing chromatographic separation and extraction media, it is important to optimize the nature of ligands bound to the substrate for an efficient, stable and selective capture of target analytes.

Recently, a number of efforts to modify porous polymer monoliths with gold nanoparticles (GNPs) have appeared. The GNPs are either formed in situ or by flowing a GNP dispersion through the monolith whose surface presents amine or thiol groups for binding the GNPs. Porous polymer monoliths modified with GNPs were used for the capture and separation of cysteine containing peptides [141]. These monoliths were then modified with carboxylic acid, hydroxyl, or amine terminated alkanethiols and applied to separate short peptides by capillary electrochromatography [142]. The surface chemistries were shown to be exchangeable by removal using an excess of 2-mercaptoethanol. The monoliths were also shown to separate a mixture of three proteins by nano-HPLC in either reverse phase or ion exchange mode. GNP immobilization onto amine-terminated grafted polymer chains was shown to provide a dense and homogenous coverage [143]. A polymer monolith was decorated with 20 nm gold nanoparticles onto which 3,3'-dithiodipropionic acid di(N-hydroxysuccinimide ester) (DTSP) was assembled and used to immobilize *Erythrina cristagalli* lectin (ECL) for extraction of glycoproteins with terminal

galactose units on their glycans [86]. GNP modified polymer monoliths modified with cysteine were used to separate a mixture of nucleosides in hydrophilic interaction chromatography (HILIC) mode and their modification with polyethyleneimine was used to separate a mixture of di- and tripeptides [144]. GNP decorated monoliths were found most effective for a particle size of 15, 20, or 30 nm when modified with octanethiol or octadecanethiol and used in reverse phase separation of a mixture of three proteins [145]. Strategies using photomasking have been used to create monolith columns with specific segments being GNP modified [146,147]. Application of GNP decorated polymer monoliths for mixed modes of separation by modifying the GNPs with mixture of alkanethiols, ω -mercaptoalkanoic acids, and amine-terminated alkanethiols was demonstrated for a three-protein mixture in reverse phase, cation exchange, anion exchange and mixed modes of separation [148]. GNP decorated polymer monoliths have also been applied in Au driven catalysis [149] and to create a lipase flow through reactor [150].

In this work, monolithic np-Au plates referred to as np-Au monoliths that underwent surface chemical modifications to develop Concanavalin A (Con A)-modified np-Au monolith were prepared and its potential to selectively capture glycoprotein are shown. Np-Au as a material can add to and complement the possibilities described using GNP decorated monoliths, and np-Au is relatively easy to prepare. The surface coverage of SAM and protein molecules prepared by a flow method onto the np-Au monolith was characterized using thermogravimetric analysis (TGA) and an in situ solution depletion method monitored by UV detection. The demonstrated selectivity of the developed Con A-modified np-Au monoliths to the high mannose-containing glycoprotein

ovalbumin (Ova) shows its potential to be further developed as a material for chromatographic extraction of glycoproteins, which is a significant part of glycomics. This work has been published in *Journal of Chromatography A* in 2015 [151].

4.2. Results and discussion

4.2.1. Preparation of Con A-modified np-Au monoliths

The preparation of Con A-modified np-Au monoliths was done under flow conditions, wherein solutions of desired molecules were circulated through the flow cell containing np-Au monoliths. The flow cell system used in this study consisted of a home-made Teflon flow cell, C-FLEX tubing, peristaltic pump, UV-vis spectrophotometer and data logger (Figure 3.1A). Unlike the flow tube, this flow cell system has a working volume of 3 mL. Surface modification started with the formation of α -lipoic acid (LA) SAM in order to functionalize the np-Au monolith surface with carboxylic acid functional groups. The procedure of SAM formation of LA to functionalize gold surfaces has already been established [88,89]. To facilitate immobilization of lectin Con A, we further activated the carboxylic acid groups of LA via their esterification with 4-(4,6-dimethoxy-1,3,5-triazin-2-yl)-4-methylmorpholinium chloride (DMTMM). DMTMM is a water-soluble coupling reagent for activating carboxylic acids for reaction with amines to form amide bonds [90,91]. Con A molecules were immobilized through the replacement of the activated esters on np-Au monolith surface via amide bond formation. Con A, as mentioned above, is a C-type lectin from *Canavalia ensiformis* (Jack bean) seeds that belongs to a general group of lectins which requires Ca^{2+} and/or Mn^{2+} ions for full activation that binds to α -mannose and

α -glucose sugar units of glycans of glycoproteins [152]. Specifically, Con A has been reported to bind to high-mannose [153] and trimannoside cores of complex type N-linked glycans [154] (Figure 3.1B).

A main advantage that we want to showcase in this study is the straightforward and reproducible preparation of the np-Au monoliths introduced here as a new material in chromatographic extraction of glycoproteins. The simple one-step preparation of np-Au monolith via selective dealloying in nitric acid overcomes the multi-step preparation of the reported AuNP-modified monolithic materials to achieve greater surface area [142,155,156]. The rigidity of the np-Au as a material in bioaffinity separations may resolve the issues of swelling in organic solvents of organic polymer materials [157]. The chemical stability of np-Au monolith and its applicability in a wide range of buffers can complement the limitation of silica based materials at high pH [158]. Moreover, the high melting point of np-Au monolith could be promising in beneficial high temperature separation of intact proteins [159]. Preparation of a bimodal np-Au monolith has been reported using a nanocasting method, and such a structure could provide large pores for high permeability and smaller pores to create a higher surface area [160]. Since, annealing was achieved to tune the pore size and morphology of the developed np-Au monolithic plate [9], an np-Au material with highly permeable structure and high loading capacity similar to the reported monolithic columns [161] used in chromatographic analysis and separations could be achieved.

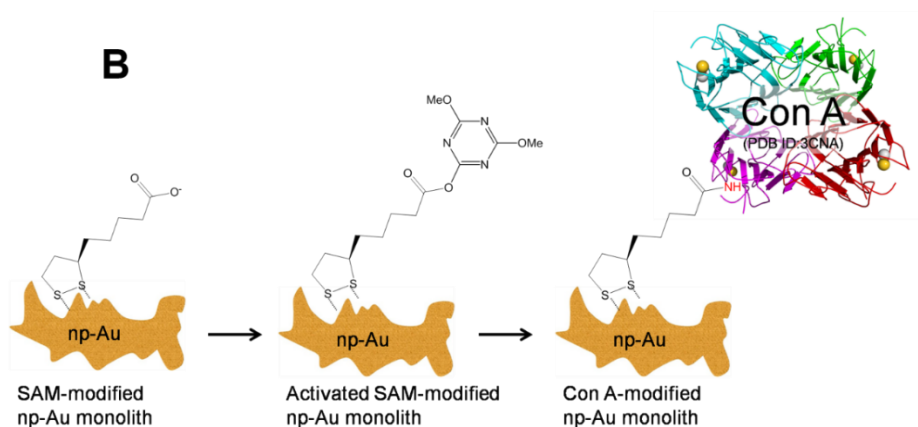
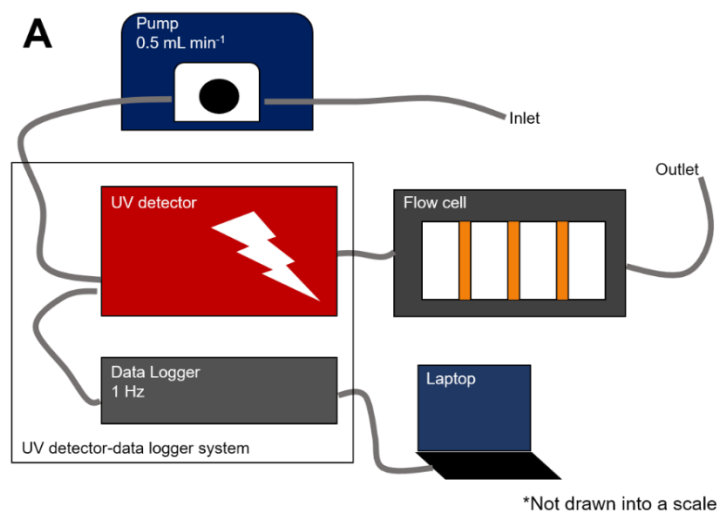


Figure 4.1. (A) Schematic diagram of flow system set-up consists of pump, UV detector-data logger system, and flow cell connected in series. Np-Au monoliths were placed in between of spacers and perpendicular to the flow. The working volume is 3 mL at 0.5 mL min⁻¹. UV reading acquisition is at 1 Hz. (B) Schematic representation of preparation of Con A-modified np-Au monolith done by in situ flow method surface modification.

4.2.2. Determination of surface coverage of LA and Con A molecules on np-Au monoliths using thermogravimetric analysis

We used thermogravimetric analysis (TGA) to characterize the loading of molecules onto the np-Au monoliths. We quantified the amount of molecules loaded onto the np-Au monolith using TGA allowing us to determine the surface coverage of the molecules being immobilized taking into account the specific surface area of the np-Au. We subjected the air-dried modified np-Au monoliths to pyrolytic decomposition in an inert environment while scanning up to 600 °C. At this temperature, both LA and DMTMM molecules were expected to be completely decomposed. Pyrolysis of the LA and DMTMM powders resulted in complete decomposition before the temperature reached 600 °C (Figure 4.2). In contrast, proteins were not completely decomposed and left some solid ash residue on the pan after scanning up to 1050 °C (Figure 4.2). CHN analysis of the residue resulted in 70% C, 2.5% H, 11.8% N with a C:H:N ratio of 35:1:5.5. The result was little changed by holding the temperature at 600 °C for two hours, with the CHN analysis then being 69% C, 2.6% H, and 11.0% N. The lyophilized powder of the protein has a theoretical composition of 46% C, 8% H and 14% N by mass with C:H:N of 5.75:1:1.75 (Table 4.1). Clearly, the residue after the pyrolysis was mostly composed of carbon. Having these results, the mass losses due to proteins were multiplied by factors of 1.20 to determine the total protein mass being loaded into np-Au monolith. TGA was capable of resolving mass losses to 0.1 µg and therefore suited to report loading of micrograms of molecules onto a single np-Au monolith.

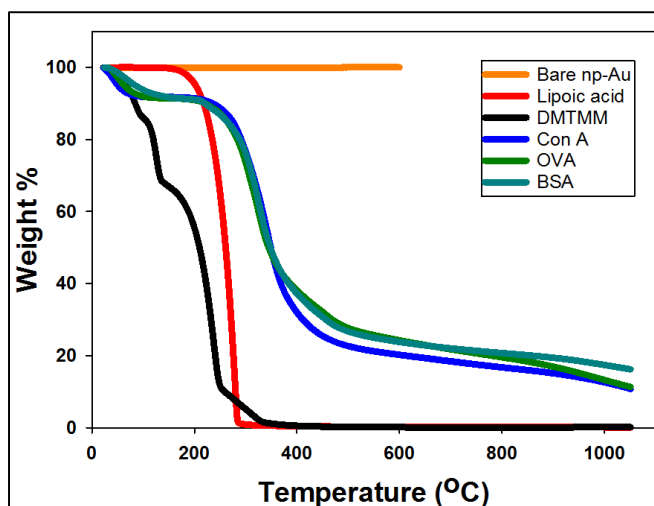


Figure 4.2. TGA thermograms of LA, DMTMM and protein powder. LA and DMTMM were completely decomposed at 400 °C. Proteins, on the other hand, were not completely decomposed even until 1050 °C. Ash residue were left on the weighing pan after the pyrolysis. The temperature was ramped at 20 °C min⁻¹.

Table 4.1. CHN analysis of the ash obtained after the pyrolysis of lyophilized Con A powder up to 1050 °C.

	% C	% H	% N	C:H:N
Theoretical	46.0	8.0	14.0	5.75 : 1.00 : 1.75
Experimental				
TGA analysis up to 1050 °C	70.0	2.5	11.8	28 : 1.00 : 4.72
TGA analysis up to 600 °C, then hold up for 2 h	69.0	2.6	11.0	26.5 : 1.00 : 4.23

The np-Au monolith modified by 1 h of circulation of a 1 mM LA solution in ethanol and referred to here as “SAM-modified np-Au monolith” was subjected to TGA and found to lose 0.30% of its mass during the temperature scan (Figure 4.3). This mass loss corresponded to 0.4485 mg m⁻² of LA self-assembled onto the np-Au monolith surface giving a corresponding surface

coverage of 1.31×10^{18} molecules m^{-2} (Table 4.2). The theoretical estimates of a complete and ordered coverage of LA molecules on a gold surface would have resulted in $3.45 \times 10^{18} - 4.40 \times 10^{18}$ molecules m^{-2} . An additional TGA mass loss of 0.1311 mg m^{-2} . Np-Au was found during the temperature scan of SAM-modified np-Au subjected to DMTMM activation of carboxylic acids to esters and increased the weight change percent to 0.39% (Figure 4.3). We tested the stability of the SAM formed on the np-Au monolith by washing it with binding buffer for another 7 h; the TGA mass loss was 0.41% which was an insignificant change when compared to that for the one washed for only 30 min (0.39%) (Figure 4.3).

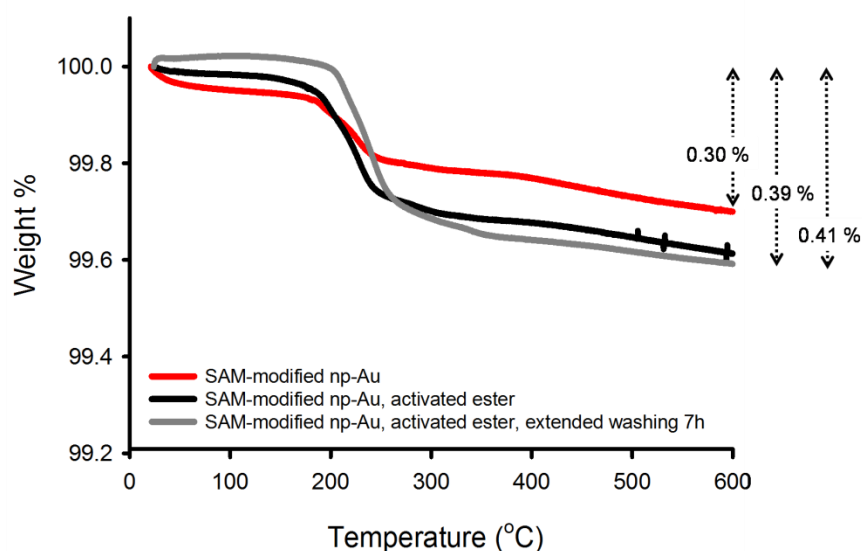


Figure 4.3. TGA thermograms for determination of LA loading and stability on np-Au monolith. The temperature was ramped at $20 \text{ }^\circ\text{C min}^{-1}$.

Table 4.2. TGA analysis data from pyrolysis of SAM- and activated SAM-modified np-Au monoliths.

	Wt. Change (%)	Mass loss (mg m ⁻²)
SAM-modified np-Au	0.30	0.4485 ± 0.0366
SAM-modified np-Au, activated	0.39	0.5796 ± 0.0474
SAM-modified np-Au, activated, (extended washing 7h)	0.41	0.6117 ± 0.0500
Molecules LA immobilized per m ² np-Au	1.31 × 10 ¹⁸	

The SAM-modified and activated np-Au monolith was further modified by 3 h circulation of a 10 µM Con A solution in buffer and referred to here as “Con A-modified np-Au monolith” was also subjected to TGA and found to lose 0.47% of its mass corresponding to an additional 0.3135 mg m⁻² during the temperature scan (Figure 4.4). This mass loss was calculated by subtracting the mass loss of the SAM-modified np-Au monolith from the mass loss found for the Con A-modified np-Au monolith and then multiplying by the factor of 1.2. Therefore, only the mass of Con A molecules being immobilized was accounted for and this resulted in a surface coverage of 1.85 × 10¹⁵ molecules m⁻² (Table 4.3). The maximum possible surface coverage for Con A is estimated as 1.29 × 10¹⁶–1.82 × 10¹⁶ molecules m⁻² based on the unit cell dimensions of tetrameric Con A (PDB ID: 3CNA) a = 63.15 Å, b = 86.91 Å, c = 89.25 Å [162] and assuming three possible surface areas per molecule of 54.8 nm², 56.4 nm² and 77.6 nm² calculated assuming that the Con A molecules lay flat and that they pack side-by-side. The surface coverage of LA and Con A molecules

obtained by TGA suggests partial but extensive surface coverage of Con A molecules on SAM-modified np-Au monoliths. We also tested the stability of immobilized Con A molecules by additional washing with buffer for another 3 h after the immobilization. An insignificant change in mass loss (0.46%) was seen after longer washing of 4 h when compared to the Con A-modified np-Au monolith washed for only 30 min (0.47%) (Figure 4.4). The observed insignificant mass loss suggests that the covalently immobilized Con A remained bound to the surface for at least another 3 h under flow conditions.

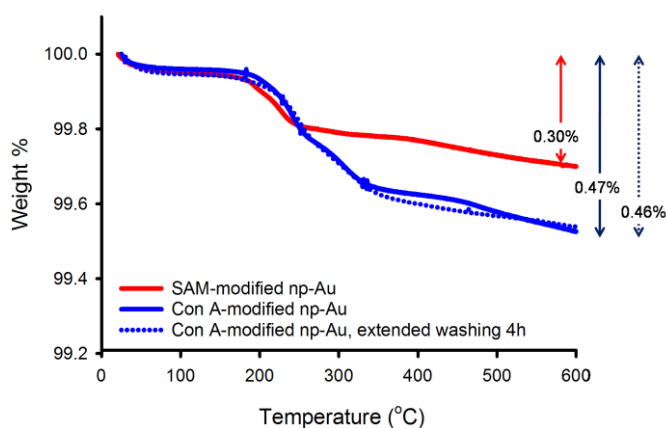


Figure 4.4. TGA thermograms for determination of Con A loading and stability on SAM-modified np-Au monolith. The temperature was ramped at 20 °C min⁻¹.

Table 4.3. TGA analysis data from pyrolysis of Con A-modified np-Au.

	Wt. Change (%)	Mass loss (mg m ⁻²)
SAM-modified np-Au	0.30	0.4485 ± 0.0366
Con A-modified np-Au, activated	0.47	0.7098 ± 0.0580
Con A-modified np-Au, activated, (extended washing 4h)	0.46	0.6920 ± 0.0565
Molecules Con AA immobilized per m ² np-Au	1.85 × 10 ¹⁵	

4.2.3. In situ solution depletion method using UV detection in determining surface coverage of molecules on np-Au monolith

Surface coverage of LA and Con A were also characterized by the developed in situ solution depletion method. Using this non-destructive method, the substrate could possibly be regenerated. Circulation of 3 mL of 1 mM LA solution through 175 mg np-Au monolith resulted in a change of concentration of 0.663 mM; this corresponded to 1.20×10^{18} LA molecules lost from the 3 mL solution (Figure 4.5A). Normalizing this amount of molecules to the calculated 1.21 m² surface area of the np-Au monolith resulted in a surface coverage of 0.989×10^{18} molecules m⁻². The volume of the circulating solution was based on the surface coverage estimated by TGA, assuring that there were enough molecules available in the solution for the np-Au monolith being used. For example, a 175 mg np-Au monolith with surface area of 1.21 m² would have contained 1.66×10^{18} LA molecules on the basis of 1.37×10^{18} molecules m⁻² surface coverage. The 3 mL solution of 1 mM LA contains 1.81×10^{18} LA molecules. Circulation of 3 mL of 6 μM Con A solution on SAM-modified np-Au monolith resulted in a change in concentration of 0.891 μM (Figure 4.5B). This corresponded to 1.61×10^{15} Con A molecules lost from a 3 mL solution. Normalizing to 1.21 m² resulted in coverage of 1.32×10^{15} molecules m⁻². Likewise, 3 mL of 6 μM Con A solution contained 1.08×10^{16} Con A molecules and was sufficient based on the amount of Con A molecules (2.24×10^{15}) using the surface coverage of Con A molecules characterized by TGA. The concentration of 10 μM used in TGA was decreased to 6 μM in this method so the A₂₈₀ readings would not exceed 1.0 and diluted enough to obey the linearity

of absorbance with concentration according to the Beer–Lambert Law. The method using the UV detector was developed to provide a procedure that can determine when to stop the circulation with the assurance that there were no longer available sites on the surface of np-Au available for the immobilization of molecules. The surface coverages found by the thermogravimetric analysis approach are generally larger both for LA and for Con A. TGA quantifies the molecules on the np-Au monolith after washing steps and drying. The solution depletion method, on the other hand, quantifies the molecules by a two-point absorbance difference for a continuously flowing solution. It is possible that additional molecules that are not bound to the surface become trapped inside the monolith when it is removed and subjected to TGA. The possible positive baseline drift of UV detection method could also be responsible for the lower estimation of surface coverage found using this method [163].

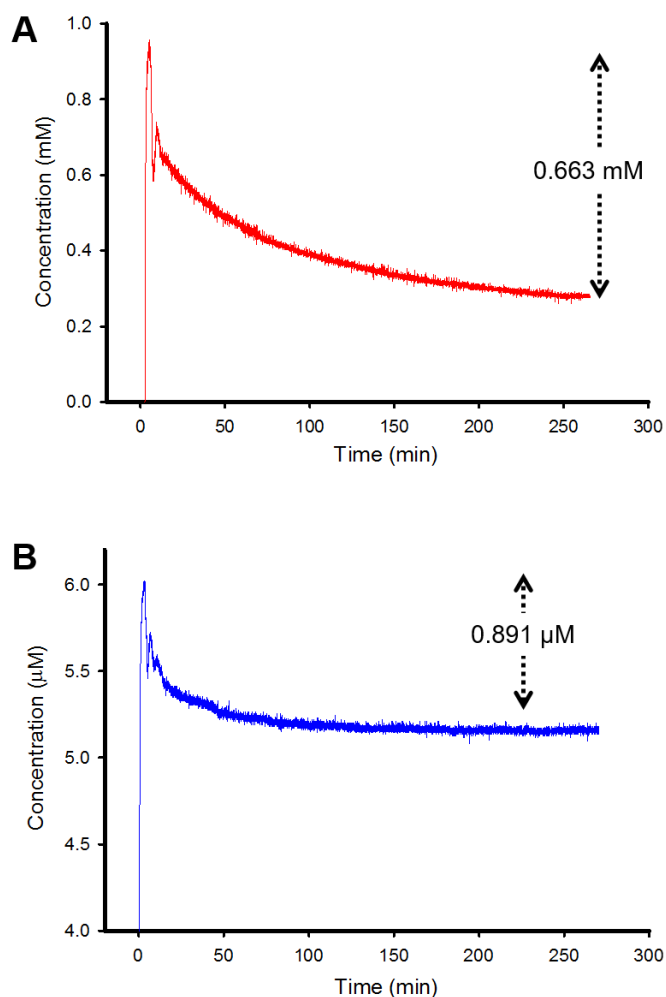


Figure 4.5. Loading curve of (A) LA on np-Au monolith and (B) Con A on SAM-modified np-Au monolith as recorded by a UV detector at 330 and 280 nm, respectively.

4.2.4. Characterization of selective capture of Ova using Con A-modified np-Au monoliths

Our chosen model glycoprotein is chicken egg white ovalbumin (Ova) with a molecular weight of 44.3 kDa. Ova is glycosylated mainly with high-mannose and hybrid structures [164], therefore it binds to Con A with high specificity. We used bovine serum albumin (BSA), a 66.4 kDa non-glycosylated

protein, as a negative control. The three estimated areas per molecule occupied by Ova provided that we assume adsorption of the solid state conformation on the surface oriented on a face of the unit cell are 45 nm², 53 nm² and 61 nm² based on the reported unit cell dimensions (PDB ID: 1 Ova) $a = 53.27 \text{ \AA}$, $b = 44.97 \text{ \AA}$, $c = 60.56 \text{ \AA}$ [165]. On the other hand, there are four BSA molecules per unit cell with reported unit cell dimensions (PDB ID: 4F5S) of $a = 217.80 \text{ \AA}$, $b = 44.99 \text{ \AA}$, $c = 143.06 \text{ \AA}$ [166]. The possible footprints of Ova and BSA molecules adsorbed onto modified np-Au surfaces will be affected by the conformational changes the proteins undergo in solution. Changes in proteins structure in solution are dependent on pH, ionic strength and temperature [167,168]. For example, in solution below pH 4, BSA has been described as a prolate ellipsoid (E-form) with dimensions of 4.0 nm \times 4.0 nm \times 14.0 nm; however, it adopts the N-form of dimensions 3.0 nm \times 8.0 nm \times 8.0 nm between pH 4.5 – 8.0 [169] and therefore in our experiments it is most likely the N-form that becomes surface bound. BSA dimensions on the surface are therefore likely to be those of the N-form however the orientation is not certain. The footprint of BSA on the surface could be estimated to range from as low as 24 nm² to as much as 64 nm². BSA is monomeric in solution but Ova has been reported to form dimers with a radius of gyration of 2.7 nm [170]. Moreover, proteins undergo conformational changes upon adsorption on solid surfaces [171,172]. These uncertainties in protein sizes in solution make it difficult to assign a size factor based on a clearly known difference in area occupied per adsorbed protein molecule; however, it appears plausible that the areas occupied by each of these proteins on the surface do not differ by more than a factor of two and could be closer.

We circulated 10 μM Ova solution in buffer for 1 h through a Con A-modified np-Au monolith. A mass loss of 0.64% accounted for an additional mass of 0.3098 mg m^{-2} to the mass loss from Con A-modified np-Au monolith due to the captured Ova molecules (Figure 4.6). This resulted in a surface coverage of 4.21×10^{15} Ova molecules m^{-2} and Ova:Con A ratio of 2.3 (Table 4.4). On the other hand, circulation of the 10 μM BSA solution for 1 h through the Con A-modified np-Au resulted in an additional mass loss of 0.2899 mg m^{-2} and a weight change of 0.63% that corresponded to a surface coverage of 2.63×10^{15} BSA molecules m^{-2} on np-Au and BSA:Con A ratio of 1.4 (Table 4.4). The greater surface coverage of Ova than BSA to Con A-modified np-Au monolith suggests some selectivity of the substrate for the Ova molecules. The high BSA:Con A ratio and the partial coverage of Con A to the SAM-modified np-Au monolith led us to suspect that there could be some non-specific adsorption of BSA molecules onto the “unused” activated esters still available for protein immobilization.

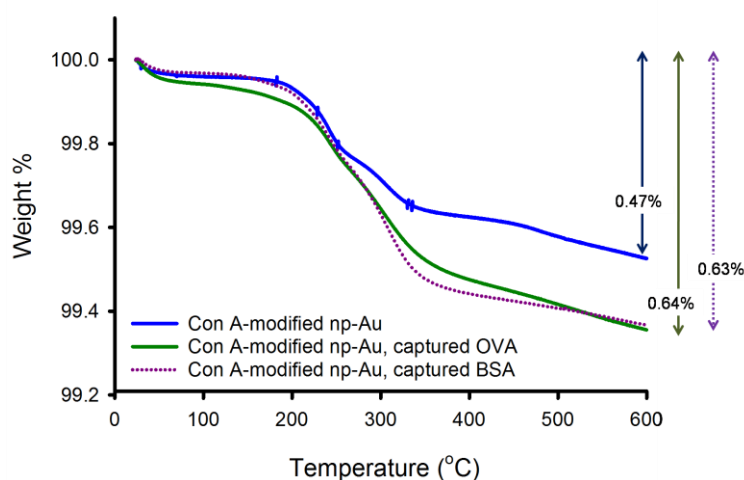


Figure 4.6. TGA thermograms showing the capture of Ova and BSA using Con A-modified np-Au monolith without the capping procedure. The temperature was ramped at $20 \text{ }^\circ\text{C min}^{-1}$.

Table 4.4. TGA analysis data from pyrolysis of Con A-modified np-Au monoliths with captured Ova or BSA without capping procedure.

	Wt. Change (%)	Mass loss (mg m ⁻²)
Con A-modified np-Au	0.47	0.7098 ± 0.0580
Con A-modified np-Au, captured Ova	0.64	0.9680 ± 0.0791
Con A-modified np-Au, captured BSA	0.63	0.9514 ± 0.0777
Molecules Ova captured per m ² np-Au	4.21 × 10 ¹⁵	
Ova :Con A	2.3	
Molecules BSA captured per m ² np-Au	2.63 × 10 ¹⁵	
BSA:Con A	1.4	

To minimize this non-specific adsorption caused by “free” activated esters, we circulated a 1% (v/v) ethanolamine solution prior to the capture of Ova or BSA to “cap” the “unused” reactive esters and convert them to hydroxyls that were not capable of covalently immobilizing proteins. We initially tested the effectivity of the capping procedure by circulating ethanolamine solution over the activated SAM prior to Con A circulation. TGA showed an insignificant amount of Con A added to the mass loss of SAM-modified np-Au monolith capped and suggests that immobilization by non-specific adsorption was restricted (Figure 4.7A). Employing the capping procedure to the Con A modified monolith prior to the capture of Ova gave a weight change of 0.59% or a surface coverage of 3.51 × 10¹⁵ molecules m⁻² np-Au and Ova:Con A ratio of 2.19 (Table 4.5). The capping procedure allowed only a weight change of 0.48% for BSA or a surface coverage of 0.533 × 10¹⁵ molecules m⁻² np-Au and BSA:Con A ratio of 0.33 (Figure 4.7B). Therefore, the capping procedure

enhanced selectivity by greatly reducing the non-specific adsorption of BSA. The disordered structure of the lipic acid SAMs and their likely incomplete coverage of the Au surface may allow for a degree of non-specific adsorption onto the np-Au monolith, and thus optimization of the SAM structure and coverage could be a strategy for improving the selectivity. A possible strategy for improving the selectivity would be to introduce a spacer chain onto the LA based on oligo (ethylene glycol) that is terminated in a carboxylic acid group, as such a LA derivative would better resist non-specific protein adsorption to regions of the SAM that are between immobilized Con A proteins.

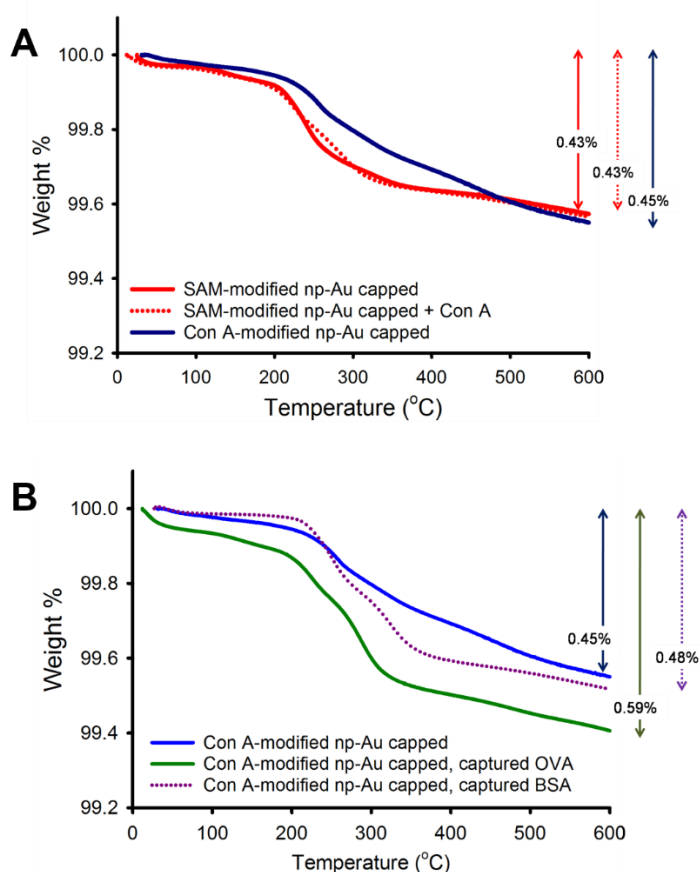


Figure 4.7. TGA thermograms showing the (A) effect of adding the capping procedure, i.e., immobilization of Con A to the esters of SAM-modified np-Au monolith was restricted by the capping procedure, (B) capture of Ova and BSA

using Con A-modified np-Au monolith with capping procedure. The temperature was ramped at 20 °C min⁻¹.

Table 4.5. TGA analysis data from pyrolysis of Con A-modified np-Au monoliths with captured Ova or BSA with capping procedure.

	Wt. Change (%)	Mass loss (mg m ⁻²)
SAM-modified np-Au capped	0.43	0.6401 ± 0.0523
SAM-modified np-Au capped + Con A	0.43	0.6501 ± 0.0531
Con A-modified np-Au capped	0.45	0.6745 ± 0.0551
Con A-modified np-Au capped, captured Ova	0.59	0.8895 ± 0.0727
Con A-modified np-Au capped, captured BSA	0.48	0.7235 ± 0.0591
Molecules Ova captured per m ² np-Au	3.51 × 10 ¹⁵	
Ova :Con A	2.19	
Molecules BSA captured per m ² np-Au	0.533 × 10 ¹⁵	
BSA:Con A	0.33	

4.2.5. Extraction of Ova from a mixture using Con A-modified np-Au monolith

To demonstrate the application of Con A-modified np-Au monolith in extracting and isolating Ova from a mixture, we prepared a mixture of 5 µM Ova and 15 µM BSA, circulated it through the Con A-modified np-Au monoliths and observed how the concentrations of these proteins depleted over time. We initially prepared a batch of Con A-modified np-Au monoliths. The 1:3 Ova:BSA mixtures were circulated for 30 min per cycle, and at the start of each cycle a new set of Con A-modified np-Au monoliths were added and an aliquot of the circulating solution was obtained at the end of each cycle and kept (Figure 4.8A). Ova and BSA, having molar masses of 66.4 kDa and 44.3 kDa,

respectively, appeared at different positions on 4–20% polyacrylamide gel run through SDS-PAGE and stained by Coomassie blue (Figure 4.8B). The size and intensity of protein bands in the gel were analyzed using ImageJ (Figure 4.8B). The size and intensity of the band of BSA aliquot 4 (after the cycles) was 74.58% of aliquot 0 (before the cycles). The initial 2 mL 15 μ M BSA solution contained 1.81×10^{16} molecules. Therefore, after the cycles, it could be estimated that 1.35×10^{16} BSA molecules were remaining in the solution and that 4.56×10^{15} molecules have been depleted. On the other hand, the size and intensity of the band of Ova aliquot 4 was 11.74% of the initial solution. The initial 2 mL of 5 μ M Ova solution contained 6.02×10^{15} molecules. There were thus approximately 0.707×10^{15} molecules left in the solution and 5.31×10^{15} molecules were depleted. Thus, the Con A-modified np-Au monoliths were able to capture a significant amount of Ova molecules in the presence of an excess of BSA. The captured BSA molecules could be washed off after the cycles, and so the captured Ova could be isolated. This demonstrated the affinity of the Con A-modified np-Au monoliths for Ova, and thus these glycoproteins can be extracted from a mixture using the developed substrates.

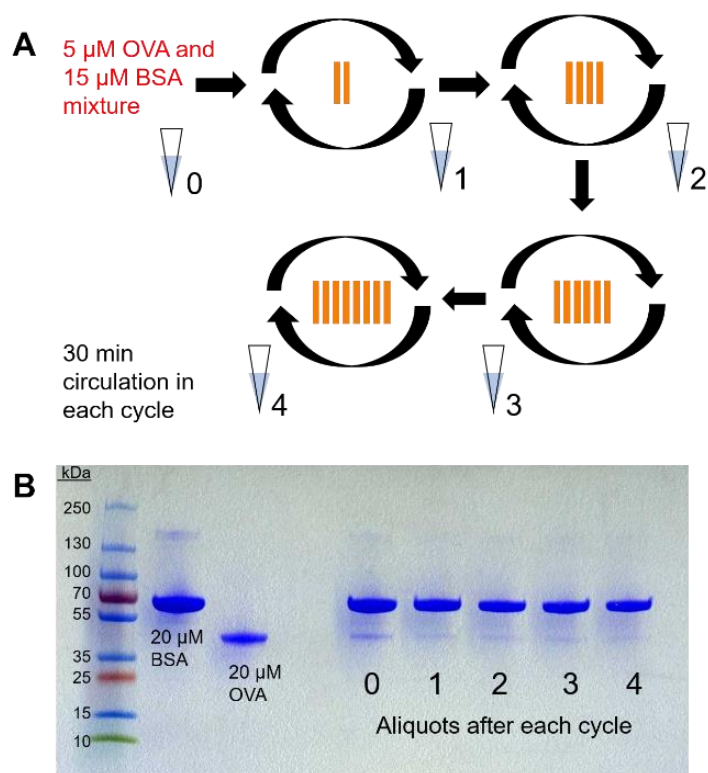


Figure 4.8. Characterization of extraction of Ova from a mixture with BSA using Con A-modified np-Au monoliths. (A) Schematic diagram of the procedure, (B) SDS-PAGE of 20 μM BSA (66.4 kDa) and 20 μM Ova (44.3 kDa) and of the aliquots obtained at the end of each 30 min cycle of circulation of 1:3 molar mixture of Ova and BSA through an increasing number of Con A-modified np-Au monoliths.

4.2.6. Elution of captured Ova

The captured Ova molecules by Con A-modified np-Au monoliths were eluted using a solution of a high concentration of ligand α -methylmannopyranoside in buffer. Lectin-carbohydrate interactions are reversible and therefore the binding would be able to be undone by a competitive ligand. We established a chromatogram using a UV detector by recording the A_{280} at 1 Hz. Flowing 1 μM Ova into the flow cell without the Con A-modified np-Au

monolith established a peak with AUC of 1.898 ± 0.073 ($n = 3$) (Figure 4.9A). This represented the amount of Ova molecules in a 2 mL 1 μ M solution, which was 1.20×10^{15} molecules. When this solution flowed through the developed substrate, the AUC decreased to 1.330 (Figure 4.9B). The difference of 0.568 represented the amount of Ova (approximately 0.36×10^{15} molecules) being captured by the Con A-modified monolith. When free ligand AMMP solution was flowed through the substrate after the washing, a peak was established with AUC of 0.4696 (Figure 4.9B). This represented the amount of Ova being eluted. The eluted amount was 83% of the amount of captured Ova.

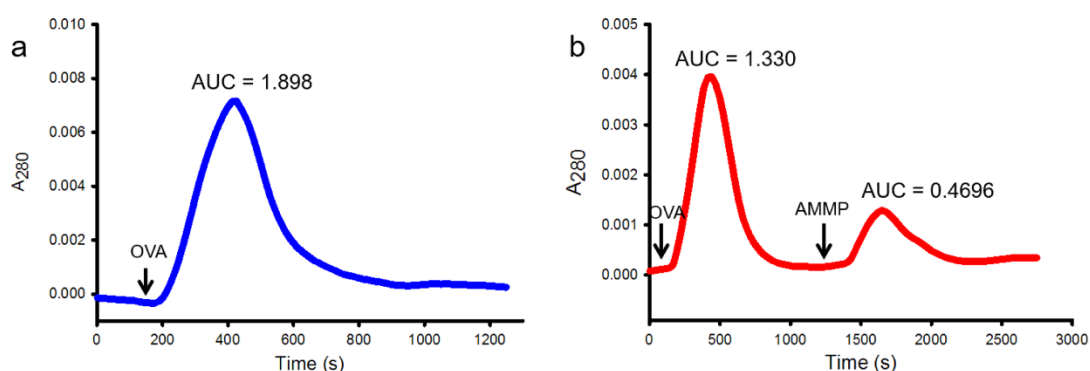


Figure 4.9. Chromatogram generated by flowing 2 mL 1 μ M Ova solution through the flow cell monitored at 280 nm (A) without np-Au monolith and (B) with Con A-modified np-Au monolith followed by elution using 2 mL 0.1 M α -methyl mannopyranoside (AMMP).

4.3. Conclusion

In this work, np-Au monolith surface modified with affinity ligands Con A were developed to create a stationary phase used in chromatographic separation and extraction of intact glycoproteins. Np-Au can be prepared by a fairly straightforward acid dealloying step followed by proceeding directly to

surface modification. The capture of target glycoproteins in the mobile phase was due to the reversible affinity of the carbohydrate residues of glycoproteins to the carbohydrate-binding domain of the immobilized lectins. TGA and a UV-detected in situ solution depletion method were used to determine the surface coverage of LA molecules forming SAMs. These SAMs were further utilized in covalent immobilization of Con A molecules that were found to have partial surface coverage. The function of the immobilized Con A was preserved as shown by the demonstrated selectivity of the substrate to high mannose-containing Ova versus non-glycosylated BSA. The selectivity was enhanced by reducing non-specific adsorption of proteins to the unutilized activated functional esters on the surface after Con A immobilization by using a capping reaction. The high surface area-to-volume ratio, robustness, chemical stability and biocompatibility of np-Au monoliths in addition to the wide range of available surface modification are the potential advantages of this developed lectin-modified np-Au monoliths for separation of intact glycoproteins and glycopeptides. The results of this work can be used as framework for further developments that may focus on optimizing monolayer structure to limit non-specific adsorption, tuning of experimental parameters, and use of other lectins and possibly other ligands in chromatographic separations of biomolecules by a variety of interaction modes.

CHAPTER V. Boronic acid-modified nanoporous gold monolith for extraction of glycopeptides from trypsin-digested glycoprotein

5.1 Introduction

Glycoproteins, due to their relative low efficiency of ionization and fragmentation like all other proteins, usually need to be digested into smaller peptides prior to MS analysis. Furthermore, release of glycans from digested peptides is also necessary if glycosylation sites are sought in the analysis. Peptide digestion is mostly done by enzymatic digestion using proteases like trypsin. For procedures in proteomics aimed at identification of protein, deglycosylation prior to trypsin digestion can increase the confidence of protein identification, and increase MS signal intensities. However in glycoproteomics, deglycosylation prior to protease digestion can improve the quality of proteome analysis [173]. Release of glycans from peptides uses endoglycosidases such as peptide N-glycosidase F (PNGase F). PNGase F hydrolyzes and cleaves the linkage between asparagines and N-acetylglucosamine liberating N-glycans from the peptides and resulting in conversion of the asparagine to aspartic acid by deamidation [174]. PNGase F will not remove glycans containing a (1-3)-linked core fucose [175]. The conventional enzymatic in-solution digestion and deglycosylation takes several hours or even overnight to complete the process. This is because a low concentration of trypsin should be maintained to avoid autolysis that produces digests of the enzymes that affect the purity of the sample, and so the efficiency of the process. An efficient and alternative method is to immobilize trypsin on a solid support to create flow-

through reactors that can speed up the process. In addition to flow-through reactors, it is also possible for flow of protein solution to be paused in a reactor to allow for digestion with the flow then resumed [176,177]. Autolysis is minimized when the enzymes are immobilized in enzyme reactors [178]. High density enzyme immobilized to these reactors increases the enzyme-to-substrate ratio, therefore capable even with samples of low concentration [179-181]. Moreover, enzymes like PNGase F are very expensive such that the use of solid support could be relatively economical. Immobilization of trypsin into beads and channels of microfluidic devices [182] and capillaries [183] were reported. Monolithic enzyme reactors can be coupled to MS and separation columns, an opportunity for automated, on-line multidimensional systems. Monolithic enzyme reactors that showed enhanced enzyme activity, *i.e.*, faster, higher loading density of enzymes and economical were showcased in recent research works (Table 4.1). Reactors that showed poor performance due to slow enzymatic reactions and low density of immobilized enzymes were aided by optimized immobilization conditions and addition of organic solvent, e.g., acetonitrile (ACN) in buffer to prevent non-specific adsorption. Enzyme immobilization is greatly influenced by the protein dynamics and substrate accessibility. Digestion efficiency, which is maximized when trypsin acts on all of the available cleavage sites, can be enhanced by denaturation of the target protein by use of aqueous-organic solvent systems containing methanol, isopropanol or ACN. Such enhanced digestion efficiency can improve sequence coverage [183,184].

Table 5.1. Monolithic enzyme reactor columns used in digestion and deglycosylation of glycoproteins and glycopeptides.

Column	Application	Amount of Enzyme Used *		Reaction Time and Temperature		Stability
		In-solution	Monolithic reactor	In-solution	Monolithic reactor	
Trypsin reactor [185]	Digestion of hIgG	Substrate-to-enzyme ratio of 50:1 (w/w) with 1.25 mg/mL protein	2.5 mg/mL	24 h; 37 °C	4 min; 22 °C	6 mos
LysC reactor [185]	Digestion of hIgG		0.5 mg/mL	24 h; 37 °C	6.2 min; 22 °C	
PNGase F reactor [186]	Deglycosylation of hIgG integrated on-line with HILIC mode separation and ESI-MS	0.5 µL	0.1 µL/min for 2.5 h	24 h; 37 °C	5.5 min; room temperature (RT)	2 mos
PNGase F reactor [187]	Simultaneous on-line release and analysis of acidic and neutral N-glycans from 0.1 µL human serum	NS **	NS **	Over-night; 37 °C	few min; RT	NS **
PNGase F micro-reactor [188]	Small scale deglycosylation of N-linked glycoproteins	5 µL of 1 mg/mL	1 µL of 1 mg/mL	10 h; 37 °C	3.5 min; 21–23 °C	8 wks
PNGase F reactor [189]	More efficient deglycosylation of hIgG	1 mg/mL ***	1 mg/mL	2 h; 37 °C ***	15 s; RT	5 mos

* Amount of enzyme used as mentioned in methods of the cited literature (concentration of enzyme is that of the prepared enzyme solution to which the monolith was exposed during preparation; volume of enzyme is that of the prepared enzyme solution used with a certain activity. ** Not specified. *** Enzyme was also immobilized in monolithic reactor but not in an oriented manner as described.

The importance of glycoproteins in biological process poses the need of the analysis of their glyco-structures and concentration levels. Recently, the use of boronic acids as affinity ligands in separation, detection and immobilization of glycoproteins and glycopeptides has been increasing (Table

5.2). Boronic acids recognize *cis-diol* moieties by covalently binding and form five- or six-membered cyclic esters. The recognition of boronic acids to glycans of glycoproteins may not be as selective as lectins, but it could capture all glycans due to its unique pH-dependent chemistry with *cis-diols* i.e., it binds in an alkaline aqueous solutions and dissociate when the medium is changed into acidic pH. Boronate-functionalized polymer monoliths can be prepared by copolymerization or post-polymerization synthesis and were determined to have good peak capacity [190].

Table 5.2. Summary of research works that use monolithic materials modified with boronic acids used in separation, enrichment and analysis of glycans, glycoproteins and glycopeptides.

Capture and Release Conditions	Applications	Year & Ref.
pH 8.5 → pH 2.7	Specific capture of Ova from fresh egg white	2011 [191]
pH 8.5 → pH 2.7	Selective capture of glycoproteins Ovotransferrin and Ova from fresh egg white sample	
pH 8.5 → pH 2.7	Capture of glycoproteins HRP and lactoferrin from a mixture with non-glycosylated proteins BSA, lactoglobulin, myoglobin, and cythchrome C	2009 [192]
pH 10.0 ↔ pH 7.4	Extraction of sialylated glycoprotein EPO from a mixture with non-sialylated glycoprotein HRP and non-glycoprotein BSA	2013 [193]
pH 10.0 ↔ pH 7.4	Extraction of spiked sialylated glycoprotein EPO from a human serum mixture with non-sialylated glycoprotein RNase B	
pH 8.0 → pH 3.6	Selective capture of glycoproteins HRP, Ova from a mixture with non-glycoproteins BSA, bovine hemoglobin, cyt C, lysozyme and myoglobin	2011 [194]
	Selective capture of glycoproteins OVT and Ova from fresh egg white sample	
pH 7.2 → 1% TFA	Identification of glycoproteins Ova, OVT and Ovomuroid	2013 [195]

pH 7.4→pH 2.7	Selective capture of <i>cis-diol</i> containing glycoprotein RNase B and Ova from a mixture with non <i>cis-diol</i> containing glycoprotein RNase A at neutral pH	2011 [196]
pH 7.4→pH 2.7	2D separation of HRP and 2D separation of lactoferrin (showed 2 peaks)	
pH 8.5→pH 2.7	Separation of glycoproteins HRP, RNase B and lactoferrin from a mixture with non-glycoproteins myoglobin and BSA	2013 [197]
pH 7.0→pH 2.7	Specific capture of glycoproteins RNase B, HRP, anti-AFP monoclonal antibody, anti-CEA polyclonal antibody, anti-PSA monoclonal antibody, from a mixture with RNase A, cyt C and β -lactoglobulin (possible capture at pH 5.0 was suggested)	2012 [198]
pH 9.2 → pH 3.6	Enrichment of glycopeptides in trypsin digest of HRP Extraction of HRP from a mixture with non-glycosylated bovine serum albumin (BSA) via polymer monolith microextraction (PMME)	2009 [199]
pH 8.5→0.2 M HAc	Selective capture of glycoproteins HRP and transferrin from a mixture with non-glycoproteins BSA and cyt C	2011 [200]
pH 8.6→pH 3.6	Selective extraction of HRP and enrichment of human serum that contains human serum albumin, IgG, transferrin and spiked HRP	2013 [201]
pH 7.0→0.2 M HAc	Selective capture of glycoproteins Ova and OVT from fresh egg white	2013 [202]
pH 7.0 → pH 2.7	Rapid selection of HRP-binding DNA aptamers	2013 [203]
pH 7.0 → pH 2.7	Potential alternative to Protein A in affinity chromatography of glycan-containing antibodies	2012 [204]
pH 7.2 → pH2.3	Rapid separation of hlgG in human serum	2002 [205]
(1a) isoc. elu. GlcNAc	(1a) Capture of glycoproteins AGP and k-Casein	2009 [206]
(1b) isoc. elu. Methyl- α -D-mannopyranoside	(1b) Capture of glycoproteins Ova and transferrin	
(2) isoc. elu. 75% ACN with small amount of modifiers β -CD	(2) Polar (CN-OH) based separation of N-glycans derived from AGP and Ova	
grad. elu. Increasing ACN content (20-40 %) in mobile phase with counter-ion	Separation of iron-binding glycoprotein transferrin from a mixture with non-glycoproteins cyt C and myoglobin	2013 [207]

(trifluoroacetate anions, TFA)		
--------------------------------	--	--

In this chapter, np-Au monoliths were used to display boronic acid groups on the surface by covalent immobilization and characterized its capability to capture compounds that contain *cis-diol* moiety e.g., adenosine. The developing substrate was tested to extract glycopeptides from trypsin digested Ovalbumin. The vision is to create a relatively simple method of trypsin digestion of glycoproteins followed by extraction of the glycopeptides by just incubating the one-piece substrate from the solutions containing the analytes. This study has the goal to demonstrate the advantage of easy handling of np-Au monoliths i.e., can be transferred from one place to another by using tweezers.

5.2. Results and discussion

5.2.1. Preparation of boronic acid-modified np-Au monoliths

The preparation of the substrate was done by continuous flow method with this series of steps: surface modification by LA, activation of the carboxylic acid functional group into an ester, immobilization of aminophenylboronic acid (APBA), and capping with ethanolamine (Figure 5.1). This method was based on the procedure that gave favorable amount of Con A covalently immobilized on np-Au monolith (Chapter 4). Variation in size i.e., Con A is a large and APBA is small molecule and the accessibility of the amino groups may require different experimental modification to optimize immobilization.

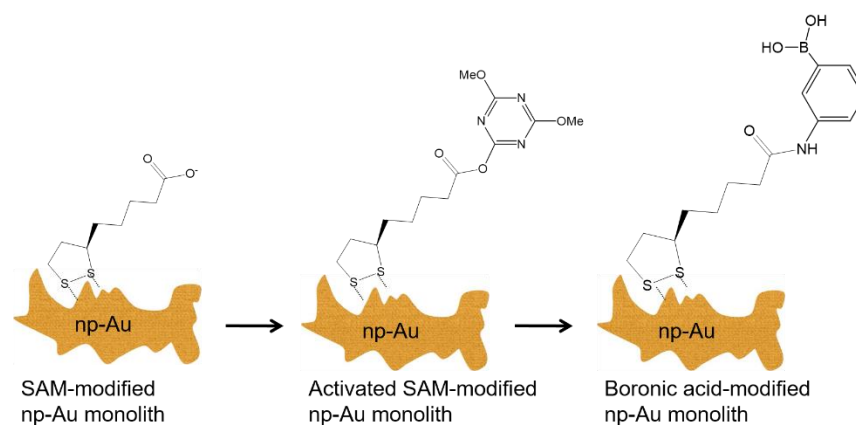


Figure 5.1. Schematic representation of the preparation of boronic acid-modified np-Au monolith.

The loading of APBA was monitored by the in situ solution depletion method described in the previous chapters. The time required for complete immobilization of APBA was determined by monitoring the A_{300} during the circulation. UV-vis scan showed APBA solution has maximum absorbance at 300 nm (Figure 5.2A). Loading APBA on LA SAM-modified np-Au monolith achieved a loading of 1.52×10^{15} molecules based on the change in concentration of 0.169 mM upon saturation (Figure 5.2B). The loading capacity of 70 mg np-Au is 3.15×10^{17} molecules APBA m^{-2} np-Au. This surface coverage is lower than what could be expected by looking at the loading curve of APBA on bare np-Au (Figure 5.2B). These data showed the presence of SAM on the np-Au surface to where the APBA specifically bind. The non-specific binding is another work to investigate.

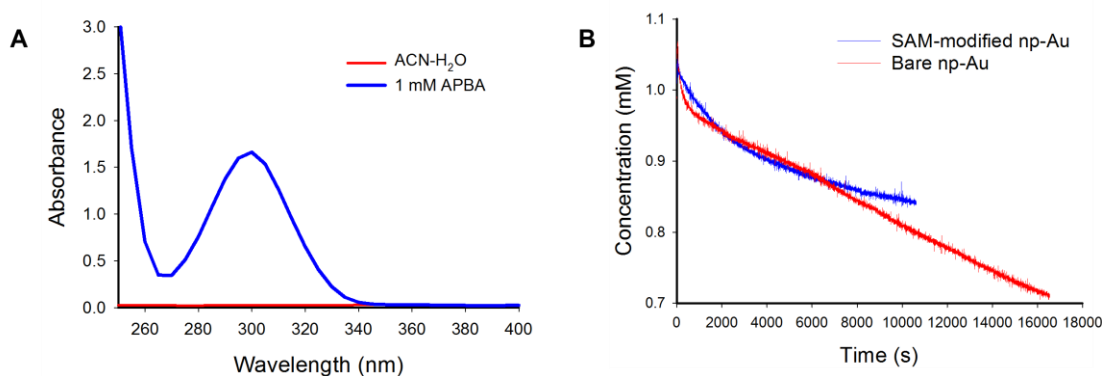


Figure 5.2. Characterization of loading of APBA on SAM-modified np-Au monolith using in situ solution depletion method. (A) UV-vis scan of 1 mM APBA in 60% acetonitrile solvent. (B) Loading curve of APBA on LA SAM-modified np-Au monolith monitored as recorded by a UV detector at 300 nm.

5.2.2. Characterization of pH-dependent capture and release by boronic acid-modified np-Au monolith of *cis-diol* containing compound

The structure of np-Au monolith as a free-standing one-piece macroporous substrate could have an advantage to design a simpler method of extracting target analytes from a mixture. A batch of boronic acid-modified np-Au monoliths were prepared. Afterwards, the prepared substrates were taken out from the flow tube and incubated in a 100 μ L adenosine and another in a 100 μ L deoxyadenosine for 1 h. Both used phosphate buffer pH 8.5 as solvent. Then substrates were placed back inside a flow tube, washed with phosphate buffer 8.5. Acetate buffer pH 2.7 was circulated through and the change in A_{260} was monitored. Both adenosine and deoxyadenosine have maximum absorbance at 260 nm (Figure 5.3A). More released amount of adenosine was observed than those of deoxyadenosine based on the increase

of the concentration of the circulating elution buffer (Figure 5.3B). This showed the capability of a “small” piece of in situ prepared boronic acid-modified np-Au monolith to preferentially capture *cis-diol* containing molecule from a little volume (100 μ L) of sample. The amount of non-specifically adsorbed deoxyadenosine could be reduced by optimizing the SAM composition.

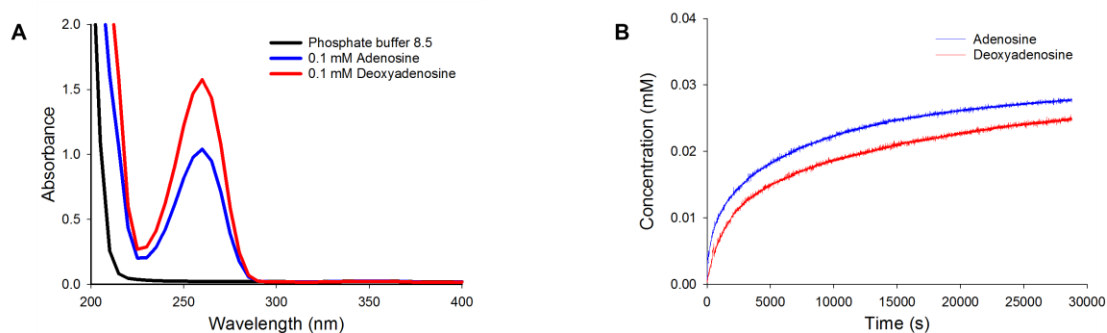


Figure 5.3. In situ characterization of release in acidic condition of captured adenosine and deoxyadenosine. (A) UV-vis scan of adenosine and deoxyadenosine in phosphate buffer 8.5. (B) Elution curve of adenosine and deoxyadenosine from boronic acid-modified np-Au monolith as recorded by a UV detector at 260 nm.

5.2.3. SDS-PAGE gel profile of trypsin digested Ova and characterization of its glycopeptide extraction using boronic acid modified np-Au monoliths

The selection of glycoprotein to use in this study was based on the SDS-PAGE gel band profile of Ova and HRP, two of the most commonly used glycoproteins in studying separation of glycoproteins. Band profiles of digested Ova produced more separated and distinct bands after digestion as compared to that of HRP even using twice the amount of trypsin (Figure 5.4A). Therefore,

Ova is used as the model glycoprotein in this experiment. The bands might represent the glycopeptides of Ova that can be observed the depletion after being circulated through boronic acid-modified np-Au monolith. Ova has 385 amino acids and a molar mass of 44,300 [208]. Based on a study of Ova glycopeptides obtained by proteolytic digestion, Ova contains only one oligosaccharide unit per molecule, linked to aspartic acid via N-acetylglucosamine, and this unit contains only the two sugars mannose and N-acetylglucosamine, i.e., high mannose [(Man)₅(GlcNAc)₂ and (Man)₆ (GlcNAc)₂] hybrid and bi- to penta-antennary structures [209]. Glycopeptides obtained from ovalbumin differ in the ratio of their mannose and hexosamine contents [210]. Comparing the band profiles of trypsin-digested Ova before and after circulation through boronic acid-modified np-Au monoliths, there was an observed decrease in intensity of the separated bands. This could represent the glycopeptides being captured by the substrate during the circulation. Eluted peptides, however, failed to show bands possibly due to very dilute concentration of the eluted peptides in a 1.5 mL circulating acetate buffer pH 2.7 (Figure 5.4B). This experiments could be further improved by sending the eluted sample for MALDI-MS analysis for identification of the captured and eluted glycopeptides.

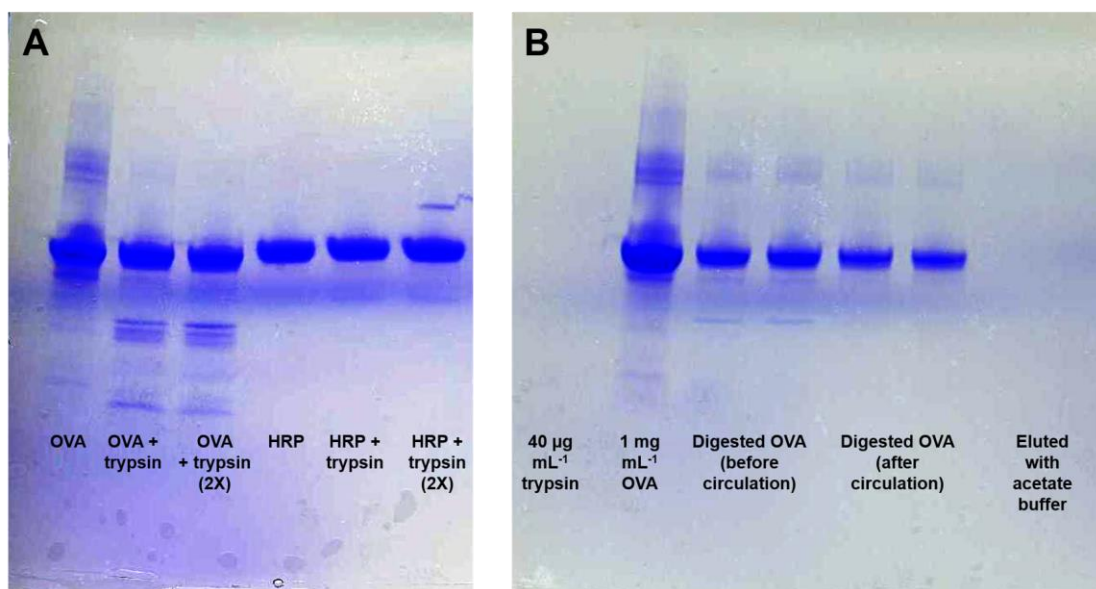


Figure 5.4. SDS-PAGE of (A) intact 1 mg mL^{-1} Ova and HRP and digested with 40 and $80 \text{ } \mu\text{g mL}^{-1}$ trypsin, (B) trypsin digested Ova before and after circulation through boronic acid modified np-Au monoliths and elution buffer acetate buffer 2.7.

5.3. Conclusion

This study was motivated by the increasing reported use of boronic acid as ligands in capture of glycoproteins and glycopeptides. The pH-dependent reversible but covalent binding of boronic acid to *cis-diols* make this ligand applicable to all kinds of glycans. The preparation method presented in this chapter showed significant amount of boronic acid immobilized on lipoic acid SAM-modified np-Au monolith. However, further optimization is necessary due to the non-specific adsorption of non *cis-diol* containing compound. The observed higher non-specific adsorption in this boronic acid-carbohydrate system compared to lectin-carbohydrate could be due to the conditions employed in capture and release. Changing the pH of the environment from

alkaline to acidic condition could have an effect not only to the dissociation process but also to protonation of some functional groups that may have contributed to electrostatic attraction or repulsion that favors immobilization during the loading step or dissociation during the elution step.

This study aimed to use np-Au monolith as a one-piece material that can be easily handled and transferred from one container to another. This allow the use of a small piece of a substrate that could extract analyte from a little amount of sample. Extracting an analyte from a limited amount of biological sample is one of the challenges in glycomics as described above. The dense porosity of np-Au monolith could be a tool in response to this challenge. Furthermore, the study of np-Au monolith in capturing trypsin has already been started in our lab. A simple kinetic study of immobilized trypsin either by physical adsorption or covalent immobilization was compared. Immobilized trypsin was used for cleavage of substrate *N*_α-Benzoyl-L-arginine ethyl ester hydrochloride (BAEE) to produce the product *N*_α-Benzoyl-L-arginine. The accumulation of the product was observed by measuring A_{253} through time. Preliminary results showed the capability of immobilized trypsin to do its function, and repeated use of the material showed significant production of the product. Though, the less activity of the immobilized trypsin was observed compared to the in-solution trypsin digestion, it should be noted that the amount of trypsin used to prepare trypsin-modified np-Au monoliths are much less than what was consumed in the in-solution method. These results combined with the presented results in this chapter could lead to a procedure of combined digestion of glycoproteins and extraction of glycopeptides using pieces of modified np-Au monoliths that can

be handled and transferred easily by tweezers into desired container of analytes, washing and eluting solutions.

CHAPTER VI. Methods in electroless deposition of Au and Au-Ag alloy

6.1. Introduction

SAM of alkanethiols that are very useful in biological assays can be formed on thin films of metal supported on silicon wafers, glass, mica, or plastic substrates. These thin films can be prepared by physical vapor deposition methods, *e.g.* thermal or electron beam evaporation, electrodeposition or electroless deposition. The last is the simplest and most economical method, wherein the rate of deposition and the structure of the plated metal depends on the deposition time and temperature [211]. The deposition of metal is due to the chemical reduction of metal salts to metals at the surfaces. Electroless deposition method has the following advantages [212]:

- Simplicity of the operation and no elaborate equipment, does not require an external electrical potential
- More cohesive particles with smaller particle size distributions than conventional top-down metal deposition, such as evaporation or sputtering that has weak bonding between metal film and structures
- Strong attachment of the gold to the substrate upon extreme thermal, solvent and electromagnetic exposure

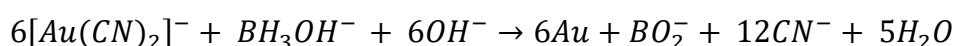
The limitations of the electroless method are the following [213]:

- Plating rates are low
- Necessary to control plating conditions carefully

- Plating baths tend to have relatively short lives
- Baths contain free cyanide

A recipe for depositing gold electrolessly onto a metal substrate has been proposed [94]. There are three suggested mechanisms of non-electrolytic process of deposition of metals and alloys: (1) galvanic displacement plating (also called immersion plating), (2) substrate-catalyzed plating, and (3) autocatalytic plating. Galvanic displacement method differs from the latter two by not requiring a reducing agent for the redox reaction to occur. Spontaneous redox reaction occurs due to the electrochemical potential difference between the elemental metal substrate and solution of cationic metal precursors leading to coating the metal substrate surface [214]. While galvanic displacement is deposition on the more active metals, substrate-catalyzed plating is onto the surface of more noble metals. This requires a chemical reducing agent that is present in the bath and serves as the electron donor and the process is catalyzed by the deposited noble metal. This method becomes autocatalytic if the substrate is of the same metal of the metal cation in the plating solution; thus, it is plating of gold on gold [94].

The suggested autocatalytic over-all plating reduction-oxidation reaction is:



Electroless deposition is advantageous in the way that it can deposit thin films on nanostructures such as colloids and nanopores that have internal surfaces by just immersing them into the plating solution [215]. The deposited gold on

glass substrates through electroless deposition has greater roughness than that prepared by thermal evaporation [211].

6.2. Results and discussion

6.2.1. Electroless deposition of Au

The autocatalytic electroless deposition that has successfully been done in the lab was based on the recipe of Okinaka using $\text{KAu}(\text{CN})_2$ as gold precursor, NaBH_4 as the reducing agent, NaOH to make the plating solution highly basic and NaCN to improve ductility of the deposit [94] (Table 6.1). These ingredients were mixed together in a proper order using water as a solvent. The plating was done using the set-up we built that enabled us to heat the solution while plating onto the immersed glass substrate, and has a thermometer to monitor the desired plating temperature (Figure 6.1A). The glass substrates were cleaned first with piranha solution and rinsed thoroughly with water then with ethanol. Then, sputtering of gold was done to create a gold surface that autocatalyzed the subsequent plating through electroless deposition (Figure 6.1B).

Table 6.1. Recipe in preparing borohydride bath for electroless deposition of Au [94].

	Concentration (M)	Function
$\text{KAu}(\text{CN})_2$	0.003	Gold precursor
NaCN	0.01	Improve the ductility of the deposit
KOH	0.20 M	Required high pH condition (10-14)
NaBH_4	0.20 M	Reducing agent

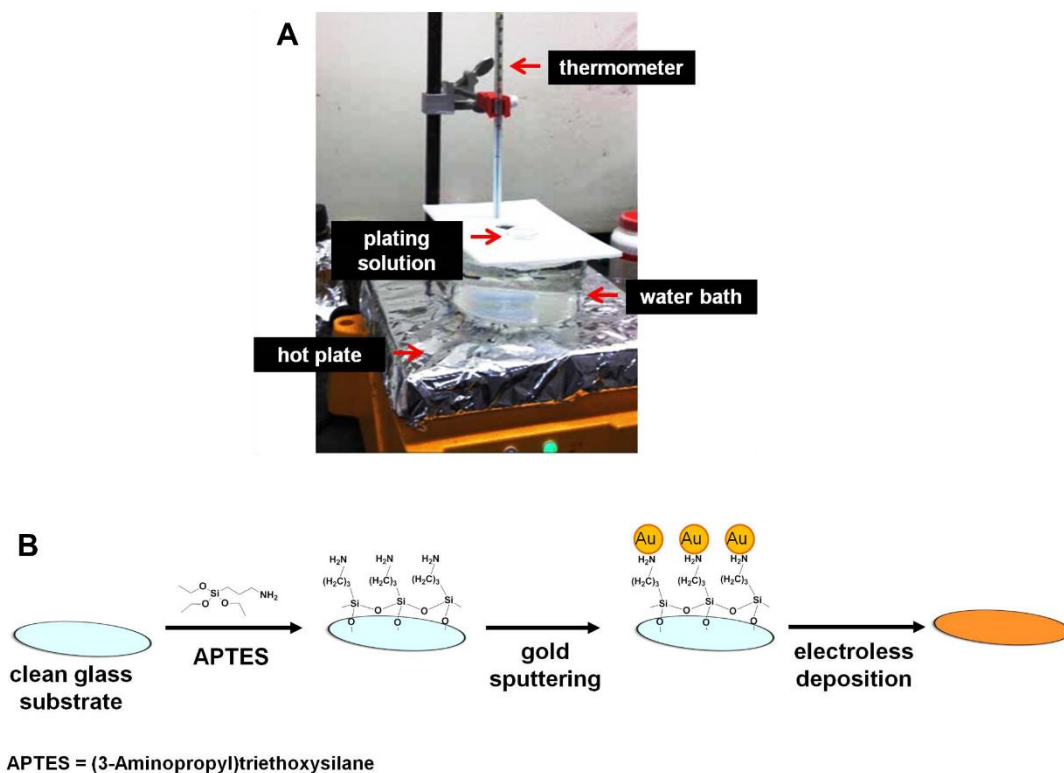


Figure 6.1. (A) Electroless plating set-up. (B) Schematic representation of the preparation of gold sputtered substrate for autocatalytic electroless deposition.

The conditions first varied was the plating temperature. It was observed in SEM images that the gold plated on the glass substrate at 97 °C for 5 minutes was already porous with a continuous ligament structure. Porosity was developed as the plating temperature was raised to 97 °C, pore size was not usual in the structure at 60 °C and 80 °C (Figure 6.2). It has been previously observed and reported that the deposit formed though autocatalytic electroless plating using dilute $\text{KAu}(\text{CN})_2$ without agitation was porous [216].

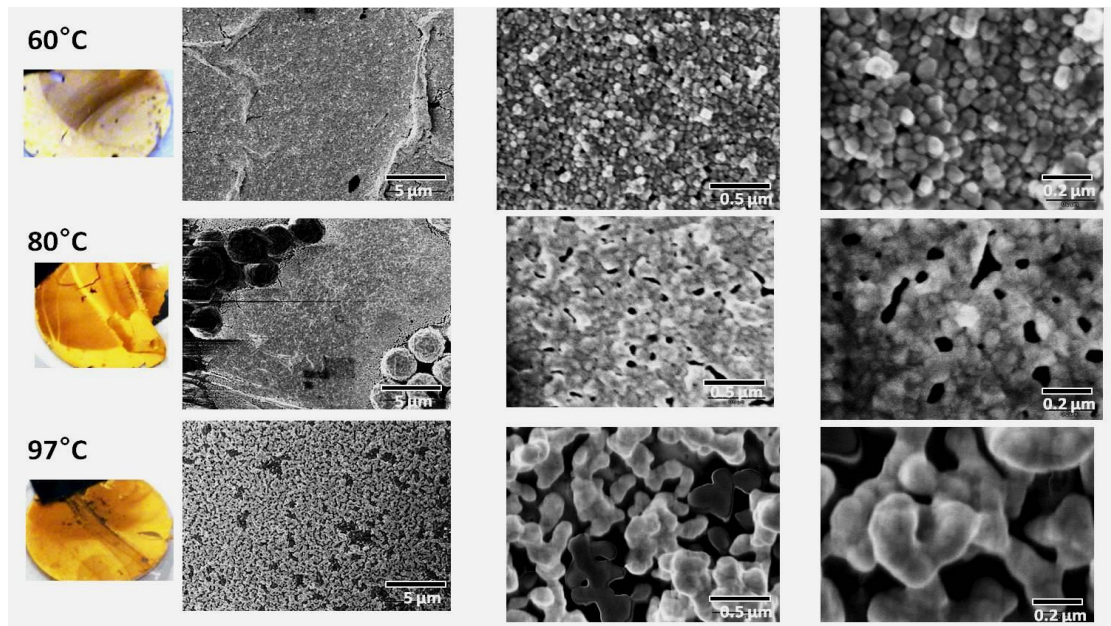


Figure 6.2. SEM images of electrolessly plated Au with different plating temperature. Scale bars are 5 μm, 0.5 μm and 0.2 μm in the first, second and last column panels, respectively.

The plating time at 80 °C was also varied from 5 min and 10 min. It was observed that plating at 97 °C longer than 5 min using the borohydride bath described above started to peel out from the substrate. At 80 °C, prolonging the deposition time created a thicker film (Figure 6.3).

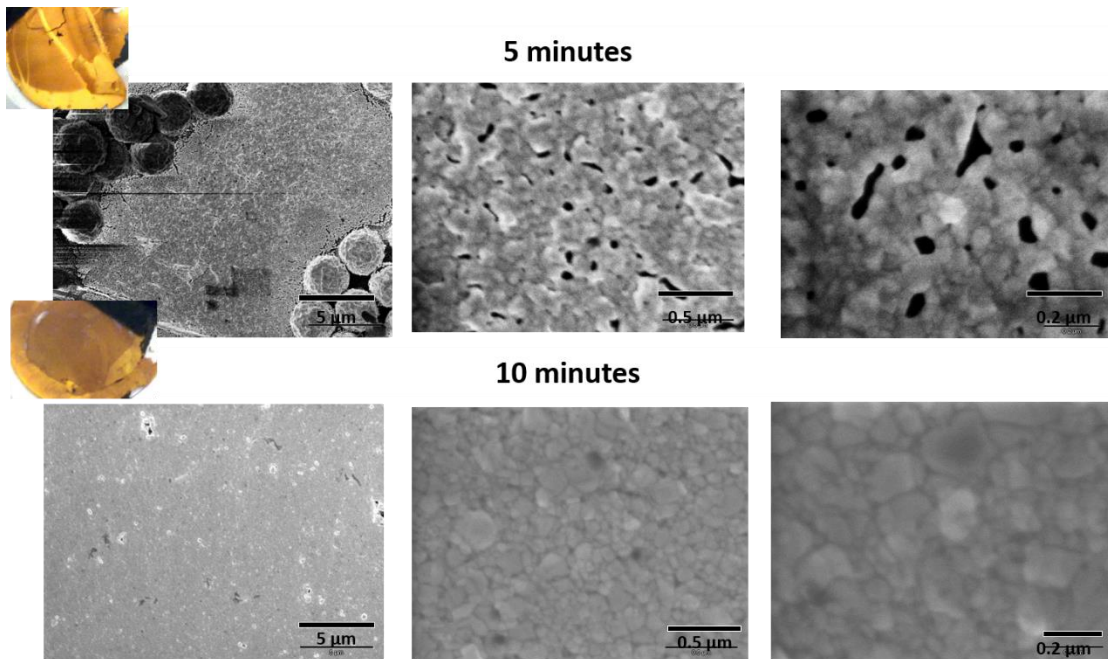


Figure 6.3. SEM images of electrolessly plated Au with different plating time at 80 °C. Scale bars are 5 μm , 0.5 μm and 0.2 μm in the first, second and last column panels, respectively.

It was next decided to investigate the effect of reducing the ratio of each component from the others in the deposited structure. Reducing the KOH in the borohydride bath composition resulted to a decrease in porosity of those plate at 97 80 °C for 5 min (Figure 6.4). At lower pH, the acid-catalyzed hydrolysis reaction proceed more rapidly. Therefore, the rate of electroless deposition of gold increases with decreasing KOH concentration. But it should be noted that the KOH concentration must be above 0.1 M to avoid spontaneous decomposition.

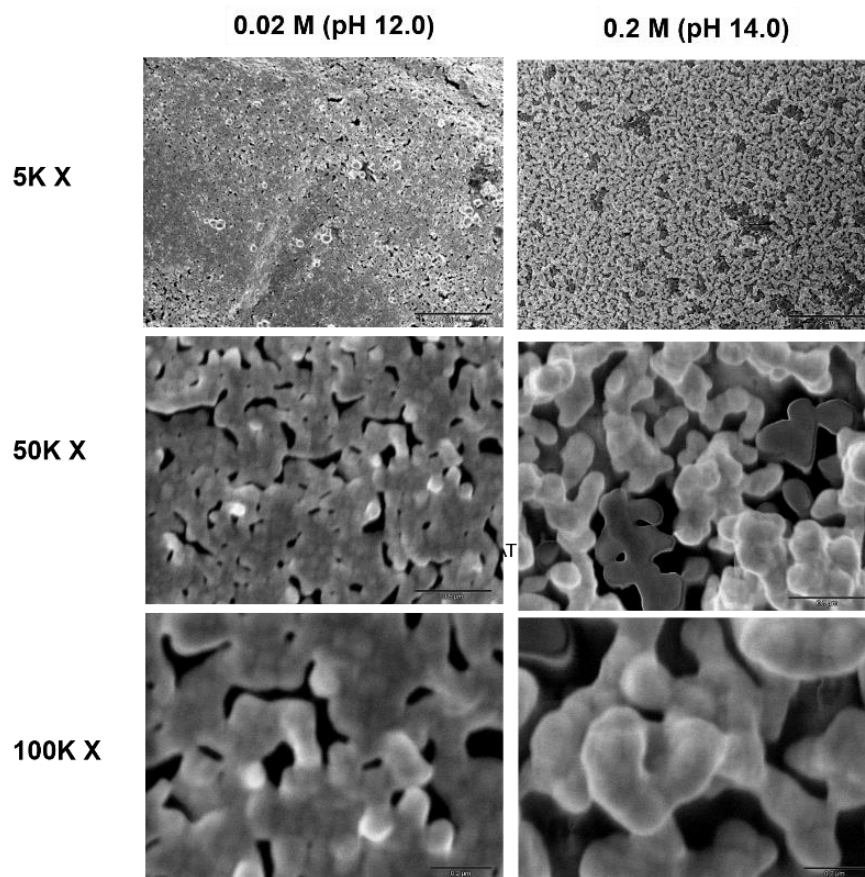


Figure 6.4. SEM images of electrolessly plated gold at 97 °C for 5 min with reduced KOH concentration. Scale bars are 5 μm, 0.5 μm and 0.2 μm in the first, second and last row panels, respectively.

Next was to reduce the reducing agent concentration from 0.2 M to 0.02 M. The plating at lower reducing agent concentration was not successful and no plating was observed. The stability of the plated film in solvents such as PBS, ethanol and acetonitrile was tested by incubating the plated gold film for 24 h. There were no peeling out from the substrate was observed and confirmed the stability of the plated film.

6.2.2. Electroless deposition of Au-Ag alloy

The electroless formation of np-Au could be achieved by depositing a Au-Ag alloy followed by dealloying. A recipe was also suggested to make Au-Ag alloy deposit [94] (Table 6.2). A silver complex, $\text{KAg}(\text{CN})_2$ is much more readily reducible than the gold complex, $\text{KAu}(\text{CN})_2$. ($E^\circ_{\text{Ag}^+} = +0.80$; $E^\circ_{\text{Au}^{3+}} = +1.40$). The deposition was done at 80 °C for 5 min. A collection of islands structures of different size were observed on the electrolessly deposited Au-Ag (Figure 6.5).

Table 6.2. Recipe in preparing borohydride bath for electroless deposition of Au-Ag alloy [94].

Composition	Concentration (M)
$\text{KAu}(\text{CN})_2$	0.026 M
$\text{KAg}(\text{CN})_2$	0.007 M
NaCN	0.01 M
KOH	0.2 M
NaBH_4	0.2 M

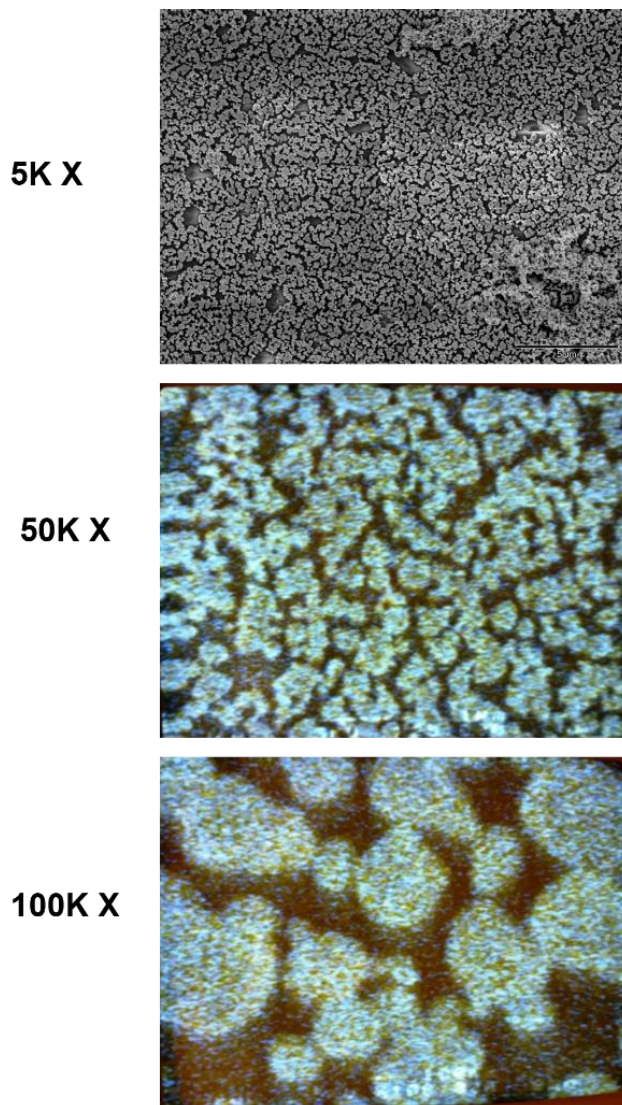


Figure 6.5. SEM images of electrolessly plated Au-Ag alloy at 80 °C for 5 min. Scale bars are 5 μm, 0.5 μm and 0.2 μm in the first, second and last row panels, respectively.

The ratio of Au and Ag in borohydride bath was varied and variation of sizes of structures were observed and not homogeneous (Figure 6.6). The elemental composition of the plated Au-Ag film was estimated by EDS spectroscopy (Figure 6.6). The ratio of the composition of Au-Ag in the plated

structure showed unmatched from the composition of the borohydride bath used except for the 30:70 ratio.

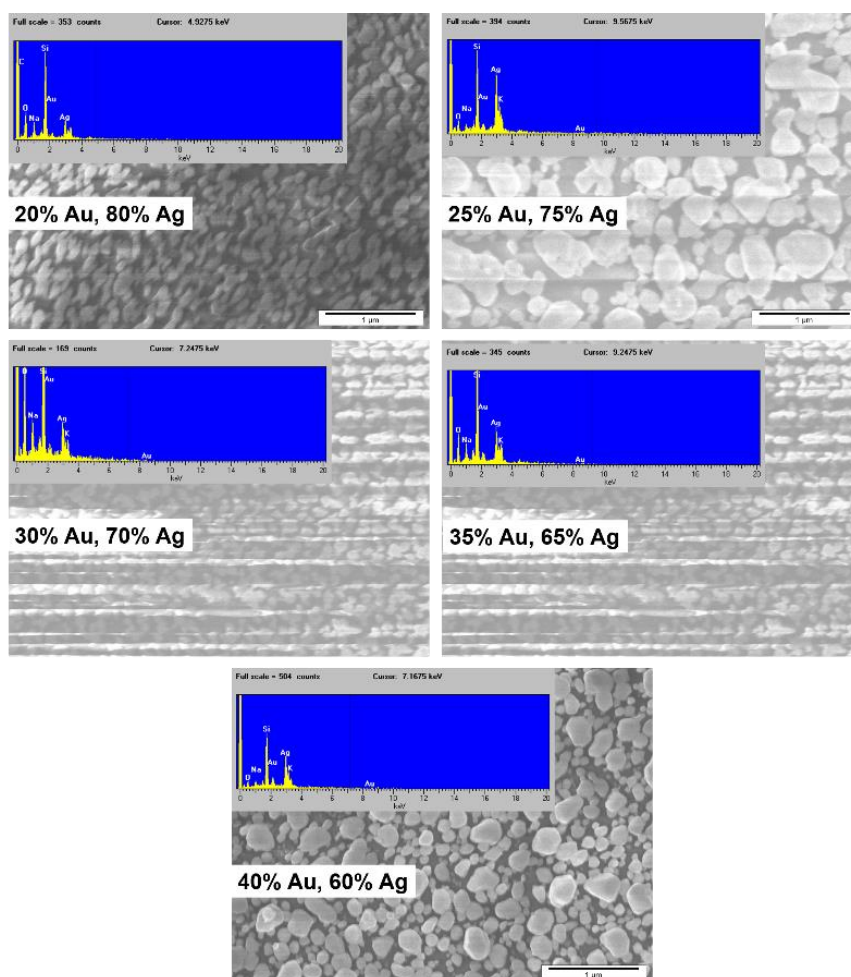


Figure 6.6. SEM images and EDS spectra (insets) of electrolessly plated Au-Ag alloy with varying Au:Ag composition ratio at 80 °C for 5 min. Scale bars are in 1 μm.

Homogeneous Au-Ag alloys of any composition can be plated using the same bath composition as above with continuous addition of $\text{KAg}(\text{CN})_2$ and excess free cyanide [217]. Another approach that could be done is through galvanic displacement, a one step process that utilizes the differences in the standard electrode potentials of various metals that causes deposition of the more noble element and dissolution of the less noble component. The galvanic displacement method for depositing metal onto surface has the potential to produce a hollow or porous deposit [218].

6.3. Conclusion

The data presented in this chapter could serve as preliminary results for optimization procedures in attaining the desirable electrolessly formed np-Au structures. In fact, electroless deposition methods described herein are now being used in our lab to attempt making a np-Au structure with multimodal pore size distribution using np-Au monolith as the catalytic substrate. The different pore sizes of porous noble metals have different functions i.e., larger sized pores could increase permeability therefore useful in microfluidic flow control, while very small pores enhanced the surface area that are useful for sensor applications [219]. In these porous materials, larger pore size is at 100s of nm, smaller pore size on the other hand is at 10s of nm. In one study, np-Au architecture with two pore sizes was achieved by thermal annealing of an np-Au gold leaf. The annealed pores were filled with silver followed by dealloying to create a porous membrane with large pores, but highly porous channel walls [219]. In another study, a np-Au ribbons was fabricated that has large-sized

channels with highly porous channel walls. The structure of the large-sized channels were controlled by the alloy composition. The structure of small ligaments/channels were controlled by changing the dealloying solution [220]. Thermal annealing of np-Au monolith within 200 to 300 °C for 30 to 120 min [221] produced large channels that is currently being used in electroless deposition of Au-Ag alloy in an attempt to create multimodal microstructure.

REFERENCES

- [1] B. Hammer and J.K. Norskov, Why gold is the noblest of all the metals, *Nature* 376 (1995) 238-240.
- [2] Y. Lu, Q. Wang, J. Sun and J. Shen, Selective dissolution of the silver component in colloidal Au and Ag multilayers: A facile way to prepare nanoporous gold film materials, *Langmuir* 21 (2005) 5179-5184.
- [3] M.D. Scanlon, U. Salaj-Kosla, S. Belochapkine, D. MacAodha, D. Leech, Y. Ding and E. Magner, Characterization of nanoporous gold electrodes for bioelectrochemical applications, *Langmuir* 28 (2012) 2251-61.
- [4] C.J. Dotzler, B. Ingham, B.N. Illy, K. Wallwork, M.P. Ryan and M.F. Toney, In situ observation of strain development and porosity evolution in nanoporous gold foils, *Adv. Funct. Mater.* 21 (2011) 3938-3946.
- [5] J.F. Huang and I.W. Sun, Fabrication and surface functionalization of nanoporous gold by electrochemical alloying/dealloying of Au-Zn in an ionic liquid, and the self-assembly of L-cysteine monolayers, *Adv. Funct. Mater.* 15 (2005) 989-994.
- [6] B. Pandey, A.V. Demchenko and K.J. Stine, Nanoporous gold as a solid support for protein immobilization and development of an electrochemical immunoassay for prostate specific antigen and carcinoembryonic antigen, *Microchim. Acta* 179 (2012) 71-81.
- [7] P.N. Ciesielski, A.M. Scott, C.J. Faulkner, B.J. Berron, D.E. Cliffel and G.K. Jennings, Functionalized Nanoporous Gold Leaf Electrode Films for the Immobilization of Photosystem I, *ACS Nano* 2 (2008) 2465-2472.
- [8] T. Fujita, L. Qian, K. Inoke, J. Erlebacher and M. Chen, Three-dimensional morphology of nanoporous gold, *Appl. Phys. Lett.* 92 (2008) 251902.
- [9] Y.H. Tan, J.A. Davis, K. Fujikawa, N.V. Ganesh, A.V. Demchenko and K.J. Stine, Surface area and pore size characteristics of nanoporous gold subjected to thermal, mechanical, or surface modification studied using gas adsorption isotherms, cyclic voltammetry, thermogravimetric analysis, and scanning electron microscopy, *J. Mater. Chem.* 22 (2012) 6733-6745.
- [10] D. Wang, R. Ji, A. Albrecht and P. Schaaf, Ordered arrays of nanoporous gold nanoparticles, *Beilstein J. Nanotechnol.* 3 (2012) 651-657.
- [11] M.K. Khristosov, L. Bloch, M. Burghammer, Y. Kauffmann, A. Katsman and B. Pokroy, Sponge-like nanoporous single crystals of gold, *Nat. Commun.* 6 (2015).
- [12] H.W. Pickering and P.R. Swann, Electron metallography of chemical attack upon some alloys susceptible to stress corrosion cracking, *Corrosion* 19 (1963) 373t-389t.
- [13] A.J. Forty and G. Rowlands, A possible model for corrosion pitting and tunneling in noble-metal alloys, *Philos. Mag. A* 43 (1981) 171-188.
- [14] A.J. Forty and P. Durkin, A micromorphological study of the dissolution of silver-gold alloys in nitric acid, *Philos. Mag. A* 42 (1980) 295-318.
- [15] A.J. Forty, Corrosion micromorphology of noble metal alloys and depletion gilding, *Nature* 282 (1979) 597-598.

- [16] J. Erlebacher, M.J. Aziz, A. Karma, N. Dimitrov and K. Sieradzki, Evolution of nanoporosity in dealloying, *Nature* 410 (2001) 450-453.
- [17] O. Zinchenko, H.A. De Raedt, E. Detsi, P.R. Onck and J.T.M. De Hosson, Nanoporous gold formation by dealloying: A Metropolis Monte Carlo study, *Comput. Phys. Commun.* 184 (2013) 1562-1569.
- [18] J. Erlebacher and K. Sieradzki, Pattern formation during dealloying, *Scr. Mater.* 49 (2003) 991-996.
- [19] J. Erlebacher, An atomistic description of dealloying: Porosity evolution, the critical potential, and rate-limiting behavior, *J. Electrochem. Soc.* 151 (2004) C614-C626.
- [20] M. Philip, Nanostructured materials, *Rep. Prog. Phys.* 64 (2001) 297.
- [21] R. Narayanan and M.A. El-Sayed, Catalysis with transition metal nanoparticles in colloidal solution: Nanoparticle shape dependence and stability, *J. Phys. Chem. B* 109 (2005) 12663-12676.
- [22] M.C. Daniel and D. Astruc, Gold nanoparticles: Assembly, supramolecular chemistry, quantum-size-related properties, and applications toward biology, catalysis, and nanotechnology, *Chem. Rev.* 104 (2004) 293-346.
- [23] R. Elghanian, J.J. Storhoff, R.C. Mucic, R.L. Letsinger and C.A. Mirkin, Selective colorimetric detection of polynucleotides based on the distance-dependent optical properties of gold nanoparticles, *Science (New York, N.Y.)* 277 (1997) 1078-1081.
- [24] M. Hu, J. Chen, Z.Y. Li, L. Au, G.V. Hartland, X. Li, M. Marquez and Y. Xia, Gold nanostructures: engineering their plasmonic properties for biomedical applications, *Chem. Soc. Rev.* 35 (2006) 1084-1094.
- [25] A.N. Shipway, M. Lahav and I. Willner, Nanostructured gold colloid electrodes, *Adv. Mater.* 12 (2000) 993-998.
- [26] H. Dong and X. Cao, Nanoporous gold thin film: Fabrication, structure evolution, and electrocatalytic activity, *J. Phys. Chem. C* 113 (2009) 603-609.
- [27] J. Haber, Manual on catalyst characterization, *Pure & Appl. Chem.* 63 (1991) 1227-1246.
- [28] T.B. Tennikova, M. Bleha, F. Švec, T.V. Almazova and B.G. Belenkii, High-performance membrane chromatography of proteins, a novel method of protein separation, *J. Chromatogr. A* 555 (1991) 97-107.
- [29] S. Hjertén, J.L. Liao and R. Zhang, High-performance liquid chromatography on continuous polymer beds, *J. Chromatogr. A* 473 (1989) 273-275.
- [30] F. Svec and J.M.J. Frechet, Continuous rods of macroporous polymer as high-performance liquid chromatography separation media, *Anal. Chem.* 64 (1992) 820-822.
- [31] A. Varki, Biological roles of oligosaccharides: all of the theories are correct, *Glycobiology* 3 (1993) 97-130.
- [32] Y. Mechref, Y. Hu, A. Garcia and A. Hussein, Identifying cancer biomarkers by mass spectrometry-based glycomics, *Electrophoresis* 33 (2012) 1755-67.
- [33] K. Hata, T. Tochigi, I. Sato, S. Kawamura, K. Shiozaki, T. Wada, K. Takahashi, S. Moriya, K. Yamaguchi, M. Hosono and T. Miyagi, Increased

- sialidase activity in serum of cancer patients: Identification of sialidase and inhibitor activities in human serum, *Cancer Sci.* 106 (2015) 383-9.
- [34] J.N. Arnold, R. Saldova, M.C. Galligan, T.B. Murphy, Y. Mimura-Kimura, J.E. Telford, A.K. Godwin and P.M. Rudd, Novel glycan biomarkers for the detection of lung cancer, *J. Proteome Res.* 10 (2011) 1755-64.
- [35] M.L. de Leoz, L.J. Young, H.J. An, S.R. Kronewitter, J. Kim, S. Miyamoto, A.D. Borowsky, H.K. Chew and C.B. Lebrilla, High-mannose glycans are elevated during breast cancer progression, *Mol. Cell Proteomics* 10 (2011) M110 002717.
- [36] H.Y. Tsai, K. Boonyapranai, S. Sriyam, C.J. Yu, S.W. Wu, K.H. Khoo, S. Phutrakul and S.T. Chen, Glycoproteomics analysis to identify a glycoform on haptoglobin associated with lung cancer, *Proteomics* 11 (2011) 2162-70.
- [37] C.B. Lebrilla and H.J. An, The prospects of glycan biomarkers for the diagnosis of diseases, *Mol. Biosyst.* 5 (2009) 17-20.
- [38] E. Meezan, H.C. Wu, P.H. Black and P.W. Robbins, Comparative studies on the carbohydrate-containing membrane components of normal and virus-transformed mouse fibroblasts. II. Separation of glycoproteins and glycopeptides by sephadex chromatography, *Biochemistry* 8 (1969) 2518-24.
- [39] C.B. Lebrilla and H.J. An, The prospects of glycan biomarkers for the diagnosis of diseases, *Mol. Biosyst.* 5 (2009) 17-20.
- [40] R.A. Dwek, *Glycobiology: Toward Understanding the Function of Sugars*, *Chem. Rev.* 96 (1996) 683-720.
- [41] M. Wuhler, A.M. Deelder and C.H. Hokke, Protein glycosylation analysis by liquid chromatography-mass spectrometry, *J. Chromatogr. B Analyt. Technol. Biomed. Life Sci.* 825 (2005) 124-33.
- [42] M. Wuhler and A.M. Deelder, Negative-mode MALDI-TOF/TOF-MS of oligosaccharides labeled with 2-aminobenzamide, *Anal. Chem.* 77 (2005) 6954-9.
- [43] D.J. Harvey, Derivatization of carbohydrates for analysis by chromatography; electrophoresis and mass spectrometry, *J. Chromatogr. B* 879 (2011) 1196-1225.
- [44] F. Higel, U. Demelbauer, A. Seidl, W. Friess and F. Sorgel, Reversed-phase liquid-chromatographic mass spectrometric N-glycan analysis of biopharmaceuticals, *Anal. Bioanal. Chem.* 405 (2013) 2481-93.
- [45] T. Ikegami, K. Horie, N. Saad, K. Hosoya, O. Fiehn and N. Tanaka, Highly efficient analysis of underivatized carbohydrates using monolithic-silica-based capillary hydrophilic interaction (HILIC) HPLC, *Anal. Bioanal. Chem.* 391 (2008) 2533-42.
- [46] E.F. Hilder, F. Svec and J.M.J. Fréchet, Latex-functionalized monolithic columns for the separation of carbohydrates by micro anion-exchange chromatography, *J. Chromatogr. A* 1053 (2004) 101-106.
- [47] N. Sharon, Lectins: Past, present and future, *Biochem. Soc. Trans.* 36 (2008) 1457-60.
- [48] M. Ambrosi, N.R. Cameron and B.G. Davis, Lectins: Tools for the molecular understanding of the glycode, *Org. & Biomol. Chem.* 3 (2005) 1593-608.

- [49] N. Sharon and H. Lis, Lectins: cell-agglutinating and sugar-specific proteins, *Science* 177 (1972) 949-59.
- [50]
- [51] H. Lis and N. Sharon, Lectins: Carbohydrate-specific proteins that mediate cellular recognition, *Chem. Rev.* 98 (1998) 637-674.
- [52] R. Loris, Principles of structures of animal and plant lectins, *Biochim. Biophys. Acta* 1572 (2002) 198-208.
- [53] W.I. Weis and K. Drickamer, Structural basis of lectin-carbohydrate recognition, *Annu. Rev. Biochem.* 65 (1996) 441-73.
- [54] H. Rudiger and H.J. Gabius, Plant lectins: occurrence, biochemistry, functions and applications, *Glycoconj. J.* 18 (2001) 589-613.
- [55] J. Hirabayashi, M. Yamada, A. Kuno and H. Tateno, Lectin microarrays: Concept, principle and applications, *Chem. Soc. Rev.* 42 (2013) 4443-58.
- [56] Z. Derewenda, J. Yariv, J.R. Helliwell, A.J. Kalb, E.J. Dodson, M.Z. Papiz, T. Wan and J. Campbell, The structure of the saccharide-binding site of concanavalin A, *EMBO J.* 8 (1989) 2189-2193.
- [57] T.K. Dam and C.F. Brewer, Thermodynamic studies of lectin-carbohydrate interactions by isothermal titration calorimetry, *Chem. Rev.* 102 (2002) 387-429.
- [58] J.H. Naismith and R.A. Field, Structural basis of trimannoside recognition by concanavalin A, *J. Biol. Chem.* 271 (1996) 972-6.
- [59] G.H. McKenzie and W.H. Sawyer, The binding properties of dimeric and tetrameric Concanavalin A: Binding of ligands to noninteracting macromolecular acceptors, *J. Biol. Chem.* 248 (1973) 549-556.
- [60] K.D. Hardman and C.F. Ainsworth, Structure of concanavalin A at 2.4-Ang resolution, *Biochemistry* 11 (1972) 4910-4919.
- [61] J.W. Becker, G.N. Reeke, B.A. Cunningham and G.M. Edelman, New evidence on the location of the saccharide-binding site of concanavalin A, *Nature* 259 (1976) 406-409.
- [62] R. Lotan, E. Skutelsky, D. Danon and N. Sharon, The purification, composition, and specificity of the anti-T lectin from peanut (*Arachis hypogaea*), *J. Biol. Chem.* 250 (1975) 8518-23.
- [63] N.M. Young, R.A. Johnston and D.C. Watson, The amino acid sequence of peanut agglutinin, *Eur. J. Biochem.* 196 (1991) 631-7.
- [64] D.A.R. Sanders, D.N. Moothoo, J. Raftery, A.J. Howard, J.R. Helliwell and J.H. Naismith, The 1.2 Å resolution structure of the con A-dimannose complex1, *J. Mol. Biol.* 310 (2001) 875-884.
- [65] S.K. Natchiar, O. Srinivas, N. Mitra, A. Surolia, N. Jayaraman and M. Vijayan, Structural studies on peanut lectin complexed with disaccharides involving different linkages: further insights into the structure and interactions of the lectin, *Acta Crystallogr. Sect. D* 62 (2006) 1413-1421.
- [66] Y. Mechref, M. Madera and M.V. Novotny, Glycoprotein enrichment through lectin affinity techniques, *Methods Mol. Biol.* 424 (2008) 373-96.
- [67] Z. Yang and W.S. Hancock, Approach to the comprehensive analysis of glycoproteins isolated from human serum using a multi-lectin affinity column, *J. Chromatogr. A* 1053 (2004) 79-88.

- [68] L.S.M. Ooi, H. Yu, C.-M. Chen, S.S.M. Sun and V.E.C. Ooi, Isolation and characterization of a bioactive mannose-binding protein from the chinese chive *Allium tuberosum*, *J. Agric. Food Chem.* 50 (2002) 696-700.
- [69] N.L. Andon, D. Eckert, J.R. Yates, 3rd and P.A. Haynes, High-throughput functional affinity purification of mannose binding proteins from *Oryza sativa*, *Proteomics* 3 (2003) 1270-8.
- [70] K.N. Suseelan, R. Mitra, R. Pandey, K.B. Sainis and T.G. Krishna, Purification and characterization of a lectin from wild sunflower (*Helianthus tuberosus* L.) tubers, *Arch. Biochem. Biophys.* 407 (2002) 241-7.
- [71] R.D. Cummings and S. Kornfeld, Fractionation of asparagine-linked oligosaccharides by serial lectin-Agarose affinity chromatography. A rapid, sensitive, and specific technique, *J. Biol. Chem.* 257 (1982) 11235-40.
- [72] T. Nishikawa, S. Kajii, C. Sato, Z. Yasukawa, K. Kitajima and M. Isobe, Alpha-C-mannosyltryptophan is not recognized by conventional mannose-binding lectins, *Bioorg. Med. Chem.* 12 (2004) 2343-8.
- [73] O.G. Potter, M.C. Breadmore and E.F. Hilder, Boronate functionalised polymer monoliths for microscale affinity chromatography, *Analyst* 131 (2006) 1094-1096.
- [74] L. Ren, Z. Liu, M. Dong, M. Ye and H. Zou, Synthesis and characterization of a new boronate affinity monolithic capillary for specific capture of cis-diol-containing compounds, *J. Chromatogr. A* 1216 (2009) 4768-4774.
- [75] L. Ren, Y. Liu, M. Dong and Z. Liu, Synthesis of hydrophilic boronate affinity monolithic capillary for specific capture of glycoproteins by capillary liquid chromatography, *J. Chromatogr. A* 1216 (2009) 8421-5.
- [76] Z.L. Hengye Li, advances in monolithic column-based boronate-affinity chromatography, *Trends Anal. Chem.* 37 (2012) 148–161.
- [77] B.P. Yih Horng Tan, Abeera Sharma, Jay Bhattarai, Keith J. Stine, Bioconjugation reactions for covalent coupling of proteins to gold surfaces, *Global J. Biochem.* 3 (2012).
- [78] J.C. Love, L.A. Estroff, J.K. Kriebel, R.G. Nuzzo and G.M. Whitesides, Self-assembled monolayers of thiolates on metals as a form of nanotechnology, *Chem. Rev.* 105 (2005) 1103-69.
- [79] R.A. Sperling and W.J. Parak, Surface modification, functionalization and bioconjugation of colloidal inorganic nanoparticles, *Phil. Trans. Royal Soc. A: Math., Phys. Eng. Sci.* 368 (2010) 1333-1383.
- [80] N.K. Chaki and K. Vijayamohanan, Self-assembled monolayers as a tunable platform for biosensor applications, *Biosens. Bioelectron.* 17 (2002) 1-12.
- [81] H. Qiu, Y. Li, G. Ji, G. Zhou, X. Huang, Y. Qu and P. Gao, Immobilization of lignin peroxidase on nanoporous gold: Enzymatic properties and in situ release of H₂O₂ by co-immobilized glucose oxidase, *Biores. Tech.* 100 (2009) 3837-3842.
- [82] D. Sykora, V. Kasicka, I. Miksik, P. Rezanka, K. Zaruba, P. Matejka and V. Kral, Application of gold nanoparticles in separation sciences, *J. Sep. Sci.* 33 (2010) 372-87.

- [83] Q.-S. Qu, X.-X. Zhang, Z.-Z. Zhao, X.-Y. Hu and C. Yan, Gold microspheres modified with octadecanethiol for capillary liquid chromatography, *J. Chromatogr. A* 1198–1199 (2008) 95-100.
- [84] J. Bundy and C. Fenselau, Lectin-based affinity capture for MALDI-MS analysis of bacteria, *Anal. Chem.* 71 (1999) 1460-1463.
- [85] M.D. Porter, T.B. Bright, D.L. Allara and C.E.D. Chidsey, Spontaneously organized molecular assemblies. 4. Structural characterization of n-alkyl thiol monolayers on gold by optical ellipsometry, infrared spectroscopy, and electrochemistry, *J. Amer. Chem. Soc.* 109 (1987) 3559-3568.
- [86] H. Alwael, D. Connolly, P. Clarke, R. Thompson, B. Twamley, B. O'Connor and B. Paull, Pipette-tip selective extraction of glycoproteins with lectin modified gold nano-particles on a polymer monolithic phase, *Analyst* 136 (2011) 2619-28.
- [87] G. Bucher, C. Lu and W. Sander, The photochemistry of lipoic acid: photoionization and observation of a triplet excited state of a disulfide, *Chemphyschem* 6 (2005) 2607-18.
- [88] T. Carofiglio, R. Fornasier, L. Jicsinszky, U. Tonellato and C. Turco, Synthesis, characterization and chemisorption on gold of a β -cyclodextrin–lipoic acid conjugate, *Tetrahedron Lett.* 42 (2001) 5241-5244.
- [89] J. Sharma, R. Chhabra, C.S. Andersen, K.V. Gothelf, H. Yan and Y. Liu, Toward reliable gold nanoparticle patterning on self-assembled DNA nanoscaffold, *J. Am. Chem. Soc.* 130 (2008) 7820-7821.
- [90] M. Kunishima, C. Kawachi, J. Monta, K. Terao, F. Iwasaki and S. Tani, 4-(4,6-dimethoxy-1,3,5-triazin-2-yl)-4-methyl-morpholinium chloride: an efficient condensing agent leading to the formation of amides and esters, *Tetrahedron* 55 (1999) 13159-13170.
- [91] Z.J. Kamiński, P. Paneth and J. Rudziński, A study on the activation of carboxylic acids by means of 2-chloro-4,6-dimethoxy-1,3,5-triazine and 2-chloro-4,6-diphenoxy-1,3,5-triazine, *J. Org. Chem.* 63 (1998) 4248-4255.
- [92] C.N. Pace, F. Vajdos, L. Fee, G. Grimsley and T. Gray, How to measure and predict the molar absorption coefficient of a protein, *Protein Sci.* 4 (1995) 2411-2423.
- [93] R.M. Stroud and C.H. Carlisle, A single-crystal structure determination of dl-6-thioctic acid, $C_8H_{14}O_2S_2$, *Acta Crystallogr. Sect. B* 28 (1972) 304-307.
- [94] Y. Okinaka, editors. Electroless plating of gold and gold alloys
- [95] R.D. Cummings, Use of lectins in analysis of glycoconjugates, *Methods in Enzymol.* 230 (1994) 66-86.
- [96] H.J. Issaq, The role of separation science in proteomics research, *Electrophoresis* 22 (2001) 3629-38.
- [97] S. Sasidharan, Y. Chen, D. Saravanan, K.M. Sundram and L. Yoga Latha, Extraction, isolation and characterization of bioactive compounds from plants' extracts, *African J. Trad., Complem., Alt. Med.: AJTCAM / African Networks on Ethnomedicines* 8 (2011) 1-10.
- [98] A. Kuno, N. Uchiyama, S. Koseki-Kuno, Y. Ebe, S. Takashima, M. Yamada and J. Hirabayashi, Evanescent-field fluorescence-assisted lectin microarray: a new strategy for glycan profiling, *Nat. Meth.* 2 (2005) 851-856.

- [99] P. Cuatrecasas, Protein Purification by Affinity Chromatography: Derivatives of agarose and polyacrylamide beads, *J. Biol. Chem.* 245 (1970) 3059-3065.
- [100] A. Namera, A. Nakamoto, T. Saito and S. Miyazaki, Monolith as a new sample preparation material: Recent devices and applications, *J. Sep. Sci.* 34 (2011) 901-924.
- [101] Z. Walsh, B. Paull and M. Macka, Inorganic monoliths in separation science: A review, *Anal. Chim. Acta* 750 (2012) 28-47.
- [102] F. Svec and J.M. Fréchet, New designs of macroporous polymers and supports: from separation to biocatalysis, *Science (New York, N.Y.)* 273 (1996) 205-11.
- [103] C. Viklund, F. Svec, J.M.J. Fréchet and K. Irgum, Monolithic, "molded", porous materials with high flow characteristics for separations, catalysis, or solid-phase chemistry: Control of porous properties during polymerization, *Chem. Mater.* 8 (1996) 744-750.
- [104] H. Korekane, T. Hasegawa, A. Matsumoto, N. Kinoshita, E. Miyoshi and N. Taniguchi, Development of an antibody-lectin enzyme immunoassay for fucosylated alpha-fetoprotein, *Biochim. Biophys. Acta* 1820 (2012) 1405-11.
- [105] L.T. Zheng, Y.L. Wei, H.Q. Gong and L. Qian, Application progress of nanoporous gold in analytical chemistry, *Chinese J. Anal. Chem.* 41 (2013) 137-144.
- [106] Y.H. Tan, J.R. Schallom, N.V. Ganesh, K. Fujikawa, A.V. Demchenko and K.J. Stine, Characterization of protein immobilization on nanoporous gold using atomic force microscopy and scanning electron microscopy, *Nanoscale* 3 (2011) 3395-407.
- [107] A. Sharma, J.K. Bhattarai, A.J. Alla, A.V. Demchenko and K.J. Stine, Electrochemical annealing of nanoporous gold by application of cyclic potential sweeps, *Nanotechnology* 26 (2015) 085602.
- [108] Y.H. Tan, K. Fujikawa, P. Pornsuriyasak, A.J. Alla, N.V. Ganesh, A.V. Demchenko and K.J. Stine, Lectin-carbohydrate interactions on nanoporous gold monoliths, *New J. Chem.* 37 (2013) 2150-2165.
- [109] G.M. Gross, D.A. Nelson, J.W. Grate and R.E. Synovec, Monolayer-protected gold nanoparticles as a stationary phase for open tubular gas chromatography, *Anal. Chem.* 75 (2003) 4558-4564.
- [110] Q.-S. Qu, F. Shen, M. Shen, X.-Y. Hu, G.-J. Yang, C.-Y. Wang, C. Yan and Y.-K. Zhang, Open-tubular gas chromatography using capillary coated with octadecylamine-capped gold nanoparticles, *Anal. Chim. Acta* 609 (2008) 76-81.
- [111] B.B. Agrawal and I.J. Goldstein, Protein-carbohydrate interaction. VII. Physical and chemical studies on concanavalin A, the hemagglutinin of the jack bean, *Arch. Biochem. Biophys.* 124 (1968) 218-29.
- [112] S. Matsugo, D. Han, H.J. Tritschler and L. Packer, Decomposition of alpha-lipoic acid derivatives by photoirradiation-formation of dihydrolipoic acid from alpha-lipoic acid, *Biochem. Mol. Biol. Int.* 38 (1996) 51-9.
- [113] Y. Wang and A.E. Kaifer, Interfacial molecular recognition. Binding of ferrocenecarboxylate to β -Aminocyclodextrin hosts electrostatically immobilized on a thioctic acid monolayer, *J. Phys. Chem. B* 102 (1998) 9922-9927.

- [114] J. Madoz, B.A. Kuznetsov, F.J. Medrano, J.L. Garcia and V.M. Fernandez, Functionalization of gold surfaces for specific and reversible attachment of a fused β -galactosidase and choline-receptor protein, *J. Am. Chem. Soc.* 119 (1997) 1043-1051.
- [115] L.S. Ooi, H. Yu, C.M. Chen, S.S. Sun and V.E. Ooi, Isolation and characterization of a bioactive mannose-binding protein from the Chinese chive *Allium tuberosum*, *J. Agric. Food Chem.* 50 (2002) 696-700.
- [116] R. Lotan, H.W. Siegelman, H. Lis and N. Sharon, Subunit Structure of Soybean Agglutinin, *J. Biol. Chem.* 249 (1974) 1219-1224.
- [117] M.E.A. Pereira, E.A. Kabat and N. Sharon, Immunochemical studies on the specificity of soybean agglutinin, *Carbohydr. Res.* 37 (1974) 89-102.
- [118] S. Sinha, N. Mitra, G. Kumar, K. Bajaj and A. Surolia, Unfolding studies on soybean agglutinin and Concanavalin A tetramers: A comparative account, *Biophys. J.* 88 (2005) 1300-1310.
- [119] A. Thakur, M. Rana, T.N. Lakhanpal, A. Ahmad and M.I. Khan, Purification and characterization of lectin from fruiting body of *Ganoderma lucidum*: Lectin from *Ganoderma lucidum*, *Biochim. Biophys. Acta* 1770 (2007) 1404-1412.
- [120] Z. Liu, J. Cao, Y. He, L. Qiao, C. Xu, H. Lu and P. Yang, Tandem 18O stable isotope labeling for quantification of N-glycoproteome, *J. Proteome Res.* 9 (2010) 227-36.
- [121] H.J. Wanebo, B. Rao, C.M. Pinsky, R.G. Hoffman, M. Stearns, M.K. Schwartz and H.F. Oettgen, Preoperative carcinoembryonic antigen level as a prognostic indicator in colorectal cancer, *N. Engl. J. Med.* 299 (1978) 448-51.
- [122] I.M. Thompson, D.K. Pauler, P.J. Goodman, C.M. Tangen, M.S. Lucia, H.L. Parnes, L.M. Minasian, L.G. Ford, S.M. Lippman, E.D. Crawford, J.J. Crowley and C.A. Coltman, Prevalence of prostate cancer among men with a prostate-specific antigen level ≤ 4.0 ng per milliliter, *N. Engl. J. Med.* 350 (2004) 2239-2246.
- [123] R.D. Cummings and J.M. Pierce, The challenge and promise of glycomics, *Chem. Biol.* 21 (2014) 1-15.
- [124] J. Zaia, Mass spectrometry and the emerging field of glycomics, *Chem. Biol.* 15 (2008) 881-92.
- [125] Y. Mechref and M.V. Novotny, Structural investigations of glycoconjugates at high sensitivity, *Chem. Rev.* 102 (2002) 321-69.
- [126] M. Wührer, Glycomics using mass spectrometry, *Glycoconj. J.* 30 (2013) 11-22.
- [127] J. Duus, C.H. Gotfredsen and K. Bock, Carbohydrate structural determination by NMR spectroscopy: Modern methods and limitations, *Chem. Rev.* 100 (2000) 4589-614.
- [128] T. Bertók, J. Katrík, P. Gemeiner and J. Tkac, Electrochemical lectin based biosensors as a label-free tool in glycomics, *Microchim. Acta* 180 (2013) 1-13.
- [129] Y. Liu, C. Shu and J.D. Lamb, High-performance capillary electrophoretic separation of carbohydrates with indirect UV detection using diethylamine and borate as electrolyte additives, *J. Capillary Electrophor.* 4 (1997) 97-103.

- [130] M. Sawa, T. Hsu, T. Itoh, M. Sugiyama, S.R. Hanson, P.K. Vogt and C. Wong, Glycoproteomic probes for fluorescent imaging of fucosylated glycans in vivo, *Proc. Nat. Acad. of Sci. U. S. A.* 103 (2006) 12371-12376.
- [131] A. Kuno, N. Uchiyama, S. Koseki-Kuno, Y. Ebe, S. Takashima, M. Yamada and J. Hirabayashi, Evanescent-field fluorescence-assisted lectin microarray: a new strategy for glycan profiling, *Nat. Methods* 2 (2005) 851-6.
- [132] S. Chen and B.B. Haab, Analysis of glycans on serum proteins using antibody microarrays, *Methods Mol. Biol.* 520 (2009) 39-58.
- [133] B. Kuster, S.F. Wheeler, A.P. Hunter, R.A. Dwek and D.J. Harvey, Sequencing of N-linked oligosaccharides directly from protein gels: in-gel deglycosylation followed by matrix-assisted laser desorption/ionization mass spectrometry and normal-phase high-performance liquid chromatography, *Anal. Biochem.* 250 (1997) 82-101.
- [134] Y. Mechref, Analysis of glycans derived from glycoconjugates by capillary electrophoresis-mass spectrometry, *Electrophoresis* 32 (2011) 3467-81.
- [135] M. Wuhler, A.M. Deelder and C.H. Hokke, Protein glycosylation analysis by liquid chromatography-mass spectrometry, *J. Chromatogr. B Analyt. Technol. Biomed. Life Sci.* 825 (2005) 124-33.
- [136] A.H. Que and M.V. Novotny, Structural characterization of neutral oligosaccharide mixtures through a combination of capillary electrochromatography and ion trap tandem mass spectrometry, *Anal. Bioanal. Chem.* 375 (2003) 599-608.
- [137] M. Bedair and R.D. Oleschuk, Lectin affinity chromatography using porous polymer monolith assisted nanoelectrospray MS/MS, *Analyst* 131 (2006) 1316-21.
- [138] Z. Yang and W.S. Hancock, Approach to the comprehensive analysis of glycoproteins isolated from human serum using a multi-lectin affinity column, *J. Chromatogr. A* 1053 (2004) 79-88.
- [139] S. Selvaraju and Z. El Rassi, Tandem lectin affinity chromatography monolithic columns with surface immobilised Concanavalin A, wheat germ agglutinin and Ricinus communis agglutinin-I for capturing sub-glycoproteomics from breast cancer and disease-free human sera, *J. Sep. Sci.* 35 (2012) 1785-95.
- [140] A.J. Alla and K.J. Stine, Development of monolithic column materials for the separation and analysis of glycans, *Chromatography* 2 (2015) 20-65.
- [141] Y. Xu, Q. Cao, F. Svec and J.M.J. Fréchet, Porous polymer monolithic column with surface-bound gold nanoparticles for the capture and separation of cysteine-containing peptides, *Anal. Chem.* 82 (2010) 3352-3358.
- [142] Q. Cao, Y. Xu, F. Liu, F. Svec and J.M.J. Fréchet, Polymer monoliths with exchangeable chemistries: Use of gold nanoparticles as intermediate ligands for capillary columns with varying surface functionalities, *Anal. Chem.* 82 (2010) 7416-7421.
- [143] D. Connolly, B. Twamley and B. Paull, High-capacity gold nanoparticle functionalised polymer monoliths, *Chem. Commun.* 46 (2010) 2109-2111.
- [144] Y. Lv, Z. Lin and F. Svec, Hypercrosslinked large surface area porous polymer monoliths for hydrophilic interaction liquid chromatography of small

- molecules featuring zwitterionic functionalities attached to gold nanoparticles held in layered structure, *Anal. Chem.* 84 (2012) 8457-60.
- [145] Y. Lv, F.M. Alejandro, J.M.J. Fréchet and F. Svec, Preparation of porous polymer monoliths featuring enhanced surface coverage with gold nanoparticles, *J. Chromatogr. A* 1261 (2012) 121-128.
- [146] M. Guerrouache, S. Mahouche-Chergui, M.M. Chehimi and B. Carbonnier, Site-specific immobilisation of gold nanoparticles on a porous monolith surface by using a thiol-yne click photopatterning approach, *Chem. Commun.* 48 (2012) 7486-7488.
- [147] S. Currivan, D. Connolly and B. Paull, Production of polymer monolithic capillary columns with integrated gold nano-particle modified segments for on-capillary extraction, *Microchem. J.* 111 (2013) 32-39.
- [148] L. Terborg, J.C. Masini, M. Lin, K. Lipponen, M.L. Riekolla and F. Svec, Porous polymer monolithic columns with gold nanoparticles as an intermediate ligand for the separation of proteins in reverse phase-ion exchange mixed mode, *J. Adv. Res.* 6 (2015) 441-448.
- [149] P. Floris, B. Twamley, P. Nesterenko, B. Paull and D. Connolly, Fabrication and characterisation of gold nano-particle modified polymer monoliths for flow-through catalytic reactions and their application in the reduction of hexacyanoferrate, *Microchim. Acta* 181 (2014) 249-256.
- [150] Y. Lv, Z. Lin, T. Tan and F. Svec, Preparation of reusable bioreactors using reversible immobilization of enzyme on monolithic porous polymer support with attached gold nanoparticles, *Biotechnol. Bioeng.* 111 (2014) 50-58.
- [151] A.J. Alla, D.A. FB, J.K. Bhattarai, J.A. Cooper, Y.H. Tan, A.V. Demchenko and K.J. Stine, Selective capture of glycoproteins using lectin-modified nanoporous gold monolith, *J. Chromatogr. A* 1423 (2015) 19-30.
- [152] Z. Derewenda, J. Yariv, J.R. Helliwell, A.J. Kalb, E.J. Dodson, M.Z. Papiz, T. Wan and J. Campbell, The structure of the saccharide-binding site of concanavalin A, *Embo. J.* 8 (1989) 2189-93.
- [153] D.K. Mandal, N. Kishore and C.F. Brewer, Thermodynamics of lectin-carbohydrate interactions. Titration microcalorimetry measurements of the binding of N-linked carbohydrates and ovalbumin to Concanavalin A, *Biochemistry* 33 (1994) 1149-1156.
- [154] J.H. Naismith and R.A. Field, Structural basis of trimannoside recognition by Concanavalin A, *J. Biol. Chem.* 271 (1996) 972-976.
- [155] Y. Xu, Q. Cao, F. Svec and J.M. Frechet, Porous polymer monolithic column with surface-bound gold nanoparticles for the capture and separation of cysteine-containing peptides, *Anal. Chem.* 82 (2010) 3352-8.
- [156] D. Connolly, B. Twamley and B. Paull, High-capacity gold nanoparticle functionalised polymer monoliths, *Chem. Commun.* 46 (2010) 2109-11.
- [157] J. Sun, L.R. Jordan, M. Forsyth and D.R. MacFarlane, Acid-organic base swollen polymer membranes, *Electrochim. Acta* 46 (2001) 1703-1708.
- [158] J.J. Kirkland, J.W. Henderson, J.J. DeStefano, M.A. van Straten and H.A. Claessens, Stability of silica-based, endcapped columns with pH 7 and 11 mobile phases for reversed-phase high-performance liquid chromatography, *J. Chromatogr. A* 762 (1997) 97-112.

- [159] A.R. Blackler, A.E. Speers and C.C. Wu, Chromatographic benefits of elevated temperature for the proteomic analysis of membrane proteins, *Proteomics* 8 (2008) 3956-3964.
- [160] M.N. Lee, M.A. Santiago-Cordoba, C.E. Hamilton, N.K. Subbaiyan, J.G. Duque and K.A.D. Obrey, Developing monolithic nanoporous gold with hierarchical bicontinuity using colloidal bijels, *J. Phys. Chem. Lett.* 5 (2014) 809-812.
- [161] G. Guiochon, Monolithic columns in high-performance liquid chromatography, *J. Chromatogr. A* 1168 (2007) 101-68; discussion 100.
- [162] K.D. Hardman and C.F. Ainsworth, Structure of concanavalin A at 2.4-Å resolution, *Biochemistry* 11 (1972) 4910-9.
- [163] M. Blanco, J. Coello, H. Iturriaga, S. MasPOCH and M. Redón, Principal component regression for mixture resolution in control analysis by UV-visible spectrophotometry, *Appl. Spectrosc.* 48 (1994) 37-43.
- [164] D.J. Harvey, Postsource decay fragmentation of N-linked carbohydrates from ovalbumin and related glycoproteins, *J. Am. Soc. Mass Spectrom.* 11 (2000) 572-577.
- [165] P.E. Stein, A.G. Leslie, J.T. Finch and R.W. Carrell, Crystal structure of uncleaved ovalbumin at 1.95 Å resolution, *J. Mol. Biol.* 221 (1991) 941-59.
- [166] A. Bujacz, Structures of bovine, equine and leporine serum albumin, *Acta Crystallogr. D Biol. Crystallogr.* 68 (2012) 1278-89.
- [167] Y. Mine, T. Noutomi and N. Haga, Emulsifying and structural properties of ovalbumin, *J. Agric. Food Chem.* 39 (1991) 443-446.
- [168] K. Monkos, Viscosity analysis of the temperature dependence of the solution conformation of ovalbumin, *Biophys. Chem.* 85 (2000) 7-16.
- [169] D.H. Tsai, F.W. DelRio, A.M. Keene, K.M. Tyner, R.I. MacCusprie, T.J. Cho, M.R. Zachariah and V.A. Hackley, Adsorption and conformation of serum albumin protein on gold nanoparticles investigated using dimensional measurements and in situ spectroscopic methods, *Langmuir* 27 (2011) 2464-2477.
- [170] L. Ianeselli, F. Zhang, M.W.A. Skoda, R.M.J. Jacobs, R.A. Martin, S. Callow, S. Prévost and F. Schreiber, Protein-protein interactions in ovalbumin solutions studied by small-angle scattering: Effect of ionic strength and the chemical nature of cations, *J. Phys. Chem. B* 114 (2010) 3776-3783.
- [171] A. Jungbauer, C. Machold and R. Hahn, Hydrophobic interaction chromatography of proteins: III. Unfolding of proteins upon adsorption, *J. Chromatogr. A* 1079 (2005) 221-228.
- [172] A. Kondo, S. Oku and K. Higashitani, Structural changes in protein molecules adsorbed on ultrafine silica particles, *J. Colloid Interface Sci.* 143 (1991) 214-221.
- [173] U.M. Bailey and B.L. Schulz, Deglycosylation systematically improves N-glycoprotein identification in liquid chromatography-tandem mass spectrometry proteomics for analysis of cell wall stress responses in *Saccharomyces cerevisiae* lacking Alg3p, *J. Chromatogr. B Analyt. Technol. Biomed Life Sci.* 923-924 (2013) 16-21.

- [174] A.L. Tarentino, C.M. Gomez and T.H. Plummer, Deglycosylation of asparagine-linked glycans by peptide:N-glycosidase F, *Biochemistry* 24 (1985) 4665-4671.
- [175] V. Tretter, F. Altmann and L. Marz, Peptide-N4-(N-acetyl-beta-glucosaminy)asparagine amidase F cannot release glycans with fucose attached alpha 1----3 to the asparagine-linked N-acetylglucosamine residue, *Eur. J. Biochem.* 199 (1991) 647-52.
- [176] A. Cingoz, F. Hugon-Chapuis and V. Pichon, Total on-line analysis of a target protein from plasma by immunoextraction, digestion and liquid chromatography-mass spectrometry, *J. Chromatogr. B Analyt Technol Biomed Life Sci* 878 (2010) 213-21.
- [177] B. Bruyneel, J.S. Hoos, M.T. Smoluch, H. Lingeman, W.M. Niessen and H. Irth, Trace analysis of proteins using postseparation solution-phase digestion and electrospray mass spectrometric detection of marker peptides, *Anal. Chem.* 79 (2007) 1591-8.
- [178] J. Duan, L. Sun, Z. Liang, J. Zhang, H. Wang, L. Zhang, W. Zhang and Y. Zhang, Rapid protein digestion and identification using monolithic enzymatic microreactor coupled with nano-liquid chromatography-electrospray ionization mass spectrometry, *J. Chromatogr. A* 1106 (2006) 165-174.
- [179] B. Kuster, T.J. Naven and D.J. Harvey, Rapid approach for sequencing neutral oligosaccharides by exoglycosidase digestion and matrix-assisted laser desorption/ionization time-of-flight mass spectrometry, *J. Mass Spectrom.* 31 (1996) 1131-40.
- [180] A.K. Palm and M.V. Novotny, Analytical characterization of a facile porous polymer monolithic trypsin microreactor enabling peptide mass mapping using mass spectrometry, *Rapid Commun. Mass Spectrom.* 18 (2004) 1374-82.
- [181] D.S. Peterson, T. Rohr, F. Svec and J.M. Frechet, High-throughput peptide mass mapping using a microdevice containing trypsin immobilized on a porous polymer monolith coupled to MALDI TOF and ESI TOF mass spectrometers, *J. Proteome Res.* 1 (2002) 563-8.
- [182] L.J. Jin, J. Ferrance, J.C. Sanders and J.P. Landers, A microchip-based proteolytic digestion system driven by electroosmotic pumping, *Lab Chip* 3 (2003) 11-8.
- [183] G.W. Slysz and D.C. Schriemer, On-column digestion of proteins in aqueous-organic solvents, *Rapid Commun. Mass Spectrom.* 17 (2003) 1044-50.
- [184] M.B. Strader, D.L. Tabb, W.J. Hervey, C. Pan and G.B. Hurst, Efficient and specific trypsin digestion of microgram to nanogram quantities of proteins in organic-aqueous solvent systems, *Anal. Chem.* 78 (2006) 125-34.
- [185] J. Krenkova, N.A. Lacher and F. Svec, Highly efficient enzyme reactors containing trypsin and endoproteinase LysC immobilized on porous polymer monolith coupled to MS suitable for analysis of antibodies, *Anal. Chem.* 81 (2009) 2004-12.
- [186] J. Krenkova, N.A. Lacher and F. Svec, Multidimensional system enabling deglycosylation of proteins using a capillary reactor with peptide-N-glycosidase F immobilized on a porous polymer monolith and hydrophilic interaction liquid

- chromatography-mass spectrometry of glycans, *J. Chromatogr. A* 1216 (2009) 3252-9.
- [187] Y. Jmeian, L.A. Hammad and Y. Mechref, Fast and efficient online release of N-glycans from glycoproteins facilitating liquid chromatography-tandem mass spectrometry glycomic profiling, *Anal. Chem.* 84 (2012) 8790-6.
- [188] A.K. Palm and M.V. Novotny, A monolithic PNGase F enzyme microreactor enabling glycan mass mapping of glycoproteins by mass spectrometry, *Rapid Commun. Mass Spectrom.* 19 (2005) 1730-8.
- [189] J. Krenkova, A. Szekrenyes, Z. Keresztessy, F. Foret and A. Guttman, Oriented immobilization of peptide-N-glycosidase F on a monolithic support for glycosylation analysis, *J. Chromatogr. A* 1322 (2013) 54-61.
- [190] X. Wang, N. Xia and L. Liu, Boronic Acid-based approach for separation and immobilization of glycoproteins and its application in sensing, *Int. J. Mol. Sci.* 14 (2013) 20890-912.
- [191] Z.A. Lin, J.L. Pang, Y. Lin, H. Huang, Z.W. Cai, L. Zhang and G.N. Chen, Preparation and evaluation of a phenylboronate affinity monolith for selective capture of glycoproteins by capillary liquid chromatography, *Analyst* 136 (2011) 3281-8.
- [192] L. Ren, Y. Liu, M. Dong and Z. Liu, Synthesis of hydrophilic boronate affinity monolithic capillary for specific capture of glycoproteins by capillary liquid chromatography, *J. Chromatogr. A* 1216 (2009) 8421-8425.
- [193] Y. Lu, Z. Bie, Y. Liu and Z. Liu, Fine-tuning the specificity of boronate affinity monoliths toward glycoproteins through pH manipulation, *Analyst* 138 (2013) 290-8.
- [194] Z. Lin, J. Pang, H. Yang, Z. Cai, L. Zhang and G. Chen, One-pot synthesis of an organic-inorganic hybrid affinity monolithic column for specific capture of glycoproteins, *Chem. Commun.* 47 (2011) 9675-7.
- [195] X. Qin, Q. Chen, C. Sun, C. Wang, Q. Peng, L. Xie, Y. Liu and S. Li, High-throughput screening of tumor metastatic-related differential glycoprotein in hepatocellular carcinoma by iTRAQ combines lectin-related techniques, *Med. Oncol.* 30 (2013) 420.
- [196] Y. Liu, L. Ren and Z. Liu, A unique boronic acid functionalized monolithic capillary for specific capture, separation and immobilization of cis-diol biomolecules, *Chem Commun (Camb)* 47 (2011) 5067-9.
- [197] X. Wang, Y. Liu, L. Ren, H. Li and Z. Liu, Development of poly((3-acrylamidophenyl)boronic acid-co-N,N-methylenebisacrylamide) monolithic capillary for the selective capture of cis-diol biomolecules, *Analytical Methods* 5 (2013) 5444-5449.
- [198] H. Li, H. Wang, Y. Liu and Z. Liu, A benzoboroxole-functionalized monolithic column for the selective enrichment and separation of cis-diol containing biomolecules, *Chem. Commun.* 48 (2012) 4115-7.
- [199] M. Chen, Y. Lu, Q. Ma, L. Guo and Y.Q. Feng, Boronate affinity monolith for highly selective enrichment of glycopeptides and glycoproteins, *Analyst* 134 (2009) 2158-64.
- [200] F. Yang, Z. Lin, X. He, L. Chen and Y. Zhang, Synthesis and application of a macroporous boronate affinity monolithic column using a metal-organic gel as a

- porogenic template for the specific capture of glycoproteins, *J. Chromatogr. A* 1218 (2011) 9194-201.
- [201] Z. Lin, J. Wang, X. Tan, L. Sun, R. Yu, H. Yang and G. Chen, Preparation of boronate-functionalized molecularly imprinted monolithic column with polydopamine coating for glycoprotein recognition and enrichment, *J. Chromatogr. A* 1319 (2013) 141-7.
- [202] F. Yang, J. Mao, X.W. He, L.X. Chen and Y.K. Zhang, Preparation of a boronate-functionalized affinity hybrid monolith for specific capture of glycoproteins, *Anal. Bioanal. Chem.* 405 (2013) 5321-31.
- [203] H. Nie, Y. Chen, C. Lu and Z. Liu, Efficient selection of glycoprotein-binding DNA aptamers via boronate affinity monolithic capillary, *Anal. Chem.* 85 (2013) 8277-83.
- [204] Y. Liu, Y. Lu and Z. Liu, Restricted access boronate affinity porous monolith as a protein A mimetic for the specific capture of immunoglobulin G, *Chem. Sci.* 3 (2012) 1467-1471.
- [205] Z. Pan, H. Zou, W. Mo, X. Huang and R. Wu, Protein A immobilized monolithic capillary column for affinity chromatography, *Anal. Chim. Acta* 466 (2002) 141-150.
- [206] H. Zhong and Z. El Rassi, Monolithic silica capillary columns having immobilized lectins and surface bound polar functionalities for lectin affinity and normal phase nano-LC and CEC of glycoconjugates, respectively, *J. Sep. Sci.* 32 (2009) 1642-53.
- [207] C. Aydođan, F. Yılmaz and A. Denizli, Cation exchange/hydrophobic interaction monolithic chromatography of small molecules and proteins by nano liquid chromatography†, *J. Sep. Sci.* 36 (2013) 1685-1692.
- [208] D.J. Harvey, D.R. Wing, B. Küster and I.B.H. Wilson, Composition of N-linked carbohydrates from ovalbumin and co-purified glycoproteins, *J. Am. Soc. Mass Spectrom.* 11 (2000) 564-571.
- [209] J. Conchie, A.J. Hay, I. Strachan and G.A. Levvy, The enzymic degradation of ovalbumin and its glycopeptides, *Biochem. J.* 115 (1969) 717-23.
- [210] T. Tai, K. Yamashita, M. Ogata-Arakawa, N. Koide, T. Muramatsu, S. Iwashita, Y. Inoue and A. Kobata, Structural studies of two ovalbumin glycopeptides in relation to the endo-beta-N-acetylglucosaminidase specificity, *J. Biol. Chem.* 250 (1975) 8569-75.
- [211] Z. Hou, N.L. Abbott and P. Stroeve, Electroless Gold as a Substrate for Self-Assembled Monolayers, *Langmuir* 14 (1998) 3287-3297.
- [212] W. Ahn and D.K. Roper, Periodic nanotemplating by selective deposition of electroless gold island films on particle-lithographed dimethyldichlorosilane layers, *ACS Nano* 4 (2010) 4181-4189.
- [213] H.O. Ali and I.R.A. Christie, A review of electroless gold deposition processes, *Gold Bulletin* 17 118-127.
- [214] C.K. Srikanth and P. Jeevanandam, Comparison of galvanic displacement and electroless methods for deposition of gold nanoparticles on synthetic calcite, *Bull. Mater. Sci.* 35 (2012) 939-946.

- [215] T. Pham, J.B. Jackson, N.J. Halas and T.R. Lee, Preparation and characterization of gold nanoshells coated with self-assembled monolayers, *Langmuir* 18 (2002) 4915-4920.
- [216] Y. Okinaka, R. Sard, C. Wolowodiuk, W.H. Craft and T.F. Retajczyk, Some practical aspects of electroless gold plating, *J. Electrochem. Soc.* 121 (1974) 56-62.
- [217] Y. Okinaka, R. Sard, C. Wolowodiuk, W.H. Craft and T.F. Retajczyk, Some practical aspects of electroless gold plating, *J. Electrochem. Soc.* 121 (1974) 56-62.
- [218] V. Bansal, H. Jani, J. Du Plessis, P.J. Coloe and S.K. Bhargava, Galvanic replacement reaction on metal films: A one-step approach to create nanoporous surfaces for catalysis, *Adv. Mater.* 20 (2008) 717-723.
- [219] Y. Ding and J. Erlebacher, Nanoporous metals with controlled multimodal pore size distribution, *J. Amer. Chem. Soc.* 125 (2003) 7772-7773.
- [220] Z. Zhang, Y. Wang, Z. Qi, J. Lin and X. Bian, Nanoporous gold ribbons with bimodal channel size distributions by chemical dealloying of Al–Au alloys, *J. Phys. Chem. C* 113 (2009) 1308-1314.
- [221] Y.H. Tan, J.A. Davis, K. Fujikawa, N.V. Ganesh, A.V. Demchenko and K.J. Stine, Surface area and pore size characteristics of nanoporous gold subjected to thermal, mechanical, or surface modification studied using gas adsorption isotherms, cyclic voltammetry, thermogravimetric analysis, and scanning electron microscopy, *J. Mater. Chem.* 22 (2012) 6733-6745.